2003

A novel hydrogen and oxygen generation system

Zhiyong Peng
Louisiana State University and Agricultural and Mechanical College

A NOVEL HYDROGEN AND OXYGEN GENERATION SYSTEM

A Thesis
Submitted to the Graduate Faculty of the
Louisiana State University and
Agricultural and Mechanical College
In partial fulfillment of the
requirements for the degree of
Master of Science in Chemical Engineering

In

The Gorden A. and Mary Cain
Department of Chemical Engineering

By

Zhiyong Peng
B.E., Tianjin University, 1995
December, 2003

ACKNOWLEDGEMENTS

I would like to express my deep gratitude to my advisor, Dr. Douglas P. Harrison, for guiding me through the research project and thesis composition with his great patience and meticulous corrections. My thanks are also due to Dr. Armando B. Corripio, for directing me on Aspen simulation, and Dr. Karsten E. Thompson, for serving as members of examining committee.

The grant received from TDA Research Inc. is gratefully acknowledged. I would also like to thank the Department of Chemical Engineering for their financial support during my first year at LSU.

I would like to thank my fellow graduate students Kwangbok Yi, and Ya Liang for their assistance and support throughout this project. The help from student worker Jennifer Bailey, and Stevens Chan are also greatly appreciated.

Finally, I would like to extend my gratitude to my family who are always encouraging and motivating me.

TABLE OF CONTENTS

LIST OF TABLES

LIST OF FIGURES

ABSTRACT

This study examined the three phases of the sorption-enhanced SMR process for H_2 production: production of low-CO hydrogen using the standard Ni-based reforming catalyst and high purity CaO sorbent precursor, evaluation of combined reforming catalyst-sorbent samples supplied by TDA, and an Aspen simulation study of the process for simultaneous production of H_2 and O_2.

The production of low-CO (<20ppmv) hydrogen was studied using the single-step sorption-enhanced steam methane reforming process. The effects of temperature, volumetric feed rate, and feed gas composition on the purity of H_2 and the content of CO were investigated. The feasibility of producing 95+% H_2 with CO content of less than 20ppmv was experimentally proven in a test at 480°C and 5 atm using a commercial Ni-based catalyst and the calcium-based CO_2 sorbent. The feed gas contained 20% CH_4 and 80% H_2O, while the product gas contained 97.8% H_2 and 17 ppmv CO. With this low CO concentration, the product can be used in a proton exchange membrane (PEM) fuel cell without further purification.

The catalyst-sorbent samples from TDA Research Inc. were extensively studied and evaluated with respect to their performance in the steam-reforming reaction using both the fixed-bed reactor system and TGA. The activity of the catalyst samples having different compositions was examined and compared at different temperatures and space velocities using a feed gas containing 11.1% CH_4 with a steam-to-carbon (S/C) ratio of 3.0. The sorption activity and durability was also examined in the TGA system.

The overall hydrogen and oxygen co-production process was studied and evaluated using the Aspen Plus simulator. Material and energy balance calculations showed that

this system can produce 99+% purity hydrogen and oxygen simultaneously with efficient energy integration. This process is balanced on power consumption and generation, so no external power is required.

CHAPTER 1

INTRODUCTION

1.1 Overview of the Importance and Demand for Hydrogen

Hydrogen is a commonly used feedstock for the chemical and petroleum industries. Its early use in the petroleum industry mainly involved hydrotreating of naphtha before it was processed in catalytic reforming. With environmental regulations becoming tightened, there are more strict tailpipe emission controls for automobiles, requiring less benzene and sulfur compounds in gasoline. Therefore more hydrogen is needed in refineries for further processing of heavy hydrocarbons and desurfurization to meet petroleum products quality. Refineries have now changed their role from primary producers of H_2 to major consumers of H_2 (Armor, 1999). In the chemical industry, large amounts of hydrogen are consumed in ammonia synthesis, which accounts for about 40% of the world's consumption of H_2 (Scholz, 1993). Smaller amounts of hydrogen are consumed in methanol synthesis, food processing and electronic industries.

Hydrogen is a great source of clean energy since no CO_2 or NO_x is produced during combustion. Hydrogen has the highest energy-to-weight ratio of any fuel since hydrogen is composed solely of the lightest element without heavy carbon atoms appearing in its structure. For a given weight of fuel, the heat liberated from combustion of hydrogen (131KJ/g) is more than 2.5 times that liberated from combustion of common hydrocarbon fuels, such as gasoline (46KJ/g) and diesel (Lanz, 2001). Owing to this merit, hydrogen has been used extensively in the space program where weight is crucial. Hydrogen is also an ideal transitional fuel and feedstock to extend the useful life of those traditional fuels such as coal, natural gas and petroleum. Coal, for instance, when gasified to produce

hydrogen, becomes more usable and environmentally acceptable. Oil supplies can be extended with hydrogen-enhanced processing of heavy hydrocarbons.

Fuel cells are getting more and more attention from scientific researchers because of their great potential to generate pollution-free electricity. Recently, the U.S. government proposed a program to support research and commercialization of fuel cell technologies with an investment of as much as 1.2 billion dollars. Hydrogen is the basic feedstock to fuel cells. Combustion of fossil fuels contributes a large part of the CO_2 emission on the earth. Borgwardt (1998) indicated that roughly 30% of U.S. total CO_2 emissions comes from production and use of transportation fuels. Development and widespread use of cars and mass transit vehicles powered by hydrogen-based fuel cell engines or hydrogen fueled internal combustion engines will improve our environment and help to mitigate climate change due to greenhouse gas emissions.

In the future, hydrogen could also join electricity as a premier energy carrier, capable of storing, moving, and delivering energy in a usable form to consumers when needed. Widespread use of hydrogen in transportation and utility power generation will have a dramatic and lasting positive impact on our environment.

Some experts predict that hydrogen will eventually change the basic energy infrastructure that powers future societies, replacing today's natural gas, oil, coal, and electricity infrastructures, although that probably won't happen until far in the future.

The space industry is another field where hydrogen is used. Hydrogen is the major propellant used in space flight. NASA has used liquid hydrogen since the 1970s to propel the space shuttle and other rockets into orbit. Hydrogen fuel cells onboard the space shuttle generate electricity to power life support systems and computers while producing a clean byproduct--pure water--which the crew drinks.

1.2 Control of Carbon Dioxide Emissions

With the rapid development of industry, more and more waste gases are emitted to the atmosphere. Some gases, like nitrogen oxides and sulfur oxides, are harmful to people's health, while others, like freon and CO_2, may adversely influence the composition of the atmosphere and eventually destroy its balance.

In terms of total air emissions, CO_2 is emitted in the greatest quantity, accounting for 99wt% of the total air emissions (Spath and Mann, 2001). Unrestricted emission of CO_2 leads to its accumulation in the atmosphere, and contributes to global warming, the so-called greenhouse effect. The recovery and disposal of CO_2 from flue gas is currently the subject of great international interest.

Most of the CO_2 comes from the combustion of fossil fuels in power generation, industrial boilers, residential and commercial heating, and transportation sectors. Widespread use of low emission fuels will become increasingly important to our environment. Hydrogen, as a clean energy source, could play a crucial role in the world's energy future.

1.3 Technologies of Hydrogen Production

Though one of the most plentiful elements in the universe, hydrogen does not exist naturally as a gas on the earth—it is always combined with other elements. In addition to water (H_2O), hydrogen is also found in many organic compounds, notably the "hydrocarbons" that make up many of our fuels, such as natural gas, oil and coal.

There are various commercial technologies for hydrogen production, including steam reforming of light hydrocarbons, partial oxidation of oil and electrolysis of water.

Steam reforming is a thermal process, typically carried out over a nickel-based catalyst at high temperature and pressure, which involves reacting methane and other light hydrocarbons with steam by applying heat. Currently in the US, approximately 95% of the hydrogen is produced via steam reforming (U.S. Department of Energy, 2002).

Partial oxidation (POX) is another thermal process for hydrogen production, which mainly deals with heavier petroleum feedstocks. Fuel, steam and air are reacted with or without a catalyst, depending on the type of feedstock and process chosen. High purity oxygen is used in many situations to enhance this process. POX can handle more flexible feedstocks ranging from light hydrocarbons to heavy oils as well as hydrocarbon solids. Compared to the steam reforming process, the POX reactor is less expensive than the steam reformer, while the investment in the oxygen plant and addition of a desulfurization process make it capital intensive.

Autothermal reforming (AR) is a process that combines both steam reforming and partial oxidation. In an autothermal reformer, fuel, steam and air (or oxygen) pass through a mixed catalyst bed that supports both partial oxidation and steam reforming reactions. The heat produced from the exothermic partial oxidation reaction supplies the heat required by the endothermic steam reforming reaction. Therefore an external burner or heat source is not needed. Heat balance and temperature matching between the two reactions have to be controlled strictly by careful thermal integration.

Hydrogen can also be produced through gasification of coal. The mechanism is similar to that of POX, except it handles solid fuels. Solid coals are pulverized and then partially oxidized with steam and oxygen. The product gas contains CO, CO_2, H_2, H_2O and H_2S, which is removed in purification. The gas mixture is quenched by water to

remove ash particles, then fed to a shift reactor to further convert CO to CO_2 and produce additional H_2. The effluent gas is purified through a pressure swing adsorption (PSA) or scrubbing process to obtain high purity hydrogen. Hydrogen production via coal gasification is the least economic among the three processes, because it needs a gasification plant which requires a huge investment and the energy efficiency in this process is very low.

Electrolysis of water is a simple yet costly approach to produce hydrogen that is applied in some special circumstances. Electricity is consumed to decompose water directly into its components of oxygen and hydrogen. Due to the high cost of electric energy, this process is practical only where electricity can be economically generated from nuclear, solar energy, or hydropower.

Hydrogen can also be produced by thermal cracking of natural gas. Gaudernack (1998) and Shah (2001) studied the production of H_2 using high temperature pyrolysis of natural gas to avoid formation of CO_2. Hydrogen is obtained from the direct cracking of methane and carbon black, the primary byproduct, can be subsequently used in rubber industry.

Another potential way to produce hydrogen is biogenic production. Some algae and bacteria, when exposed to sunlight above some threshold intensity, will give off hydrogen. Water vapor reforming of biomass also has good prospects in an energy economy requiring CO_2 emission limitations.

Currently on a commercial basis, the catalytic steam reforming of natural gas is the most economical process for producing hydrogen because it has the highest thermal efficiency and lowest capital investment. Within decades, hydrogen produced from

biomass, wind and solar sources are predicted to be the ultimate, abundant, renewable energy currency.

1.4 Project Objectives

This project is sponsored by NASA under subcontract from TDA Research Inc. NASA requires efficient production of rocket fuel, primarily liquid hydrogen and oxygen, to achieve affordable access to space. Therefore, the overall project examines a novel method of hydrogen and oxygen co-production to achieve higher efficiency and improved economics.

In this phase of the project, newly developed combined reforming catalysts and sorbents from TDA have been evaluated experimentally using a laboratory-scaled fixed-bed reactor system. In addition, the overall process for co-production of liquid hydrogen and oxygen has been simulated on the commonly used commercial simulator, ASPEN PLUS, with its economic aspects evaluated.

Finally, prior work from this laboratory has been extended to examine the sorption-enhanced steam reforming process to produce low CO hydrogen with target CO levels of 20 ppm or less.

CHAPTER 2

LITERATURE REVIEW

2.1 Overview of the Steam Reforming Process

Steam reforming has been in use for several decades as a means of effectively producing hydrogen. A process for the conversion of hydrocarbons into hydrogen in the presence of steam was first described by Tessie du Motay and Marechal in 1868 (Adris and Pruden, 1996). The first industrial application of steam reforming was implemented in 1930. The feedstock for this process includes methane, naphtha and No. 2 fuel oil (Minet and Desai, 1983). When methane (CH_4) is used as the feedstock 50% of H_2 produced comes from steam. This number increases to 69% when heavy oil is used and 89% when coal is used (Steinberg, 1989). More steam consumption means higher energy cost. Methane is naturally stored in the earth, hence relatively low cost compared to production of steam. Therefore, Steam Methane Reforming (SMR) is mainly adopted in the U.S. where natural gas is abundant and readily available as feedstock.

The conventional SMR process includes steam reforming, water-gas shift and H_2 purification. A schematic flowsheet for a conventional SMR process is shown in Figure 2-1.

2.1.1 Steam-Reforming

Natural gas (pretreated and desulphurized) and superheated steam are fed into the reformer furnace, where the following reforming reaction occurs.

$$CH_4(g) + H_2O(g) \Leftrightarrow CO(g) + 3H_2(g) \quad (\Delta H = 49.31 \text{ kcal/mol})$$

This reaction is typically carried out at a temperature of 800-1000 °C and a pressure

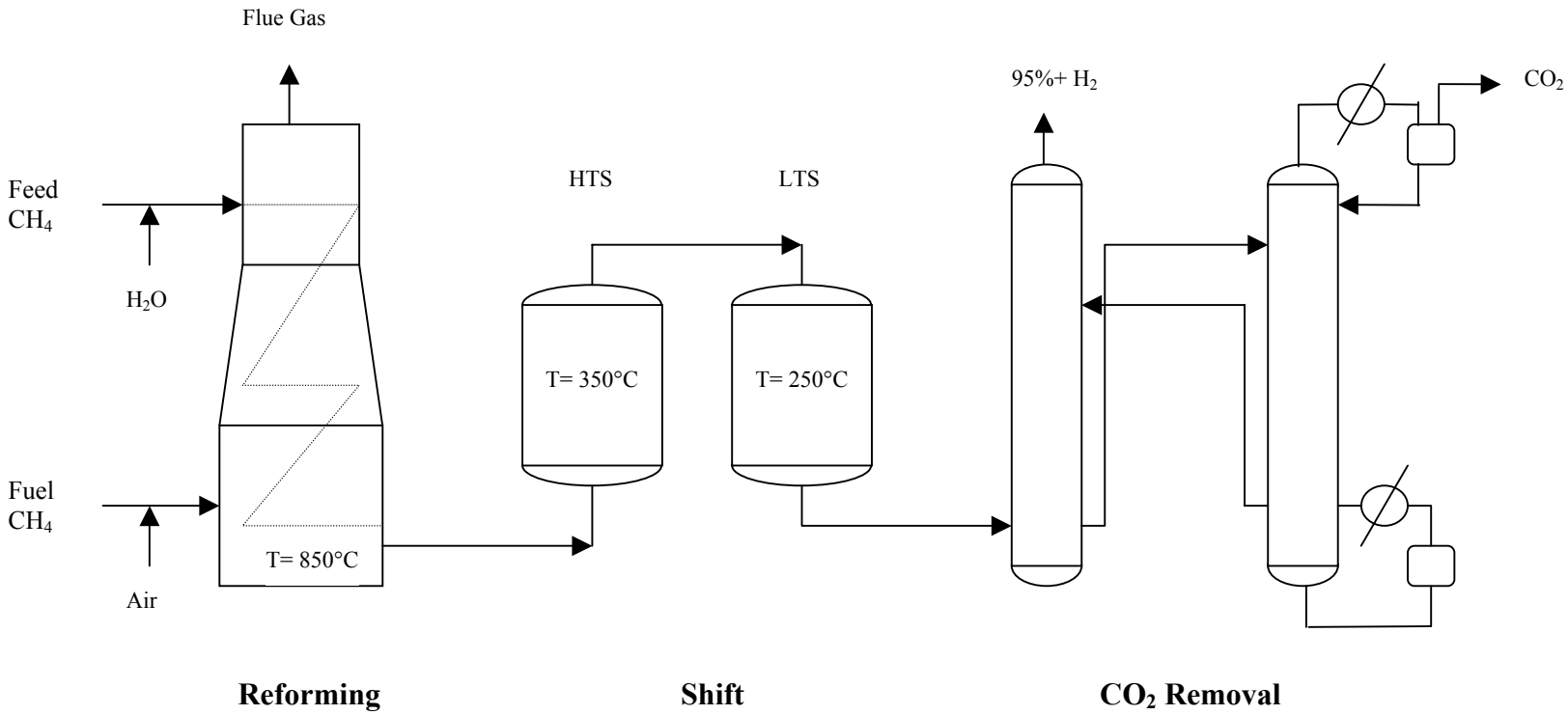

Figure 2-1 A Schematic Diagram for the Conventional Steam-Methane Reforming Process

of 14-20 atm over a nickel-based catalyst. In the reformer up to 95% CH_4 is converted to H_2 and CO at steam to methane ratios in the range of 3.5-4.5 (Lopez, 2000). This reaction is highly endothermic and a large amount of heat is provided by feeding supplemental natural gas to the furnace in a feed to fuel ratio of 1.27~2 (Baade et al., 1993). The effluent gas from the reformer contains about 76% H_2 (mol%), 1.3% CH_4, 12% CO and 10% CO_2 on a dry basis (Kirk-Othmer, 1999).

2.1.2 Water-Gas-Shift

This reformer product is then fed to a shift reactor where the following reaction occurs.

$$CO(g) + H_2O(g) \Leftrightarrow CO_2(g) + H_2(g) \qquad (\Delta H = -9.85 \text{ kcal/mol})$$

This reaction is weakly exothermic and conducted in a fixed-bed adiabatic reactor. Due to its exothermic nature, dual catalyst beds with interbed cooling are normally employed to prevent overheating and to promote complete conversion of CO. The first bed is loaded with a high temperature shift catalyst of chromium promoted iron oxide, which operates at near 350°C. The second bed is loaded with a low-temperature shift catalyst of copper promoted zinc oxide, which operates at approximately 250°C. The shift reactor effluent typically contains about 86%H_2, 12%CO_2, 0.25%CO and 1.3% CH_4 on a dry basis (Kirk-Othmer, 1999).

2.1.3 Hydrogen Purification

To acquire high purity H_2, CO, CO_2 and other impurities must be removed from the product gas.

There are several techniques for separation of CO_2 from mixtures with other gases.

Chemical scrubbing (e.g. absorption in a monoethanol amine solution) and physical scrubbing (e.g. absorption in Selexol or in water at elevated pressure) are commonly practiced methods in industry (Gaudernack, 1998). When the effluent gas stream from the shift reactor passes through a circulating amine or hot potassium carbonate solution, CO_2 is selectively adsorbed and removed by the chemical scrubbing. The scrubbed gas contains about 98.2% H_2, 0.3% CO, 0.01% CO_2, and 1.5% CH_4 (Kirk-Othmer, 1999). The scrubbing solution is regenerated for cyclic use by depressurizing and steam-stripping. Though low in concentration, CO may still act as a catalyst poison and must be removed for many applications. This can be implemented in two ways.

First, both CO and CO_2 can also be removed simultaneously by a process called methanation, which is the reverse of reforming and carried out in the presence of a nickel catalyst. These reactions are listed as follows:

$$CO(g) + 3H_2(g) \rightarrow CH_4(g) + H_2O(g)$$

$$CO_2(g) + 4H_2(g) \rightarrow CH_4(g) + 2H_2O(g)$$

After the methanation step, the carbon oxides are decreased to ppm levels.

In addition to the scrubbing and methanation process referred to above, pressure swing adsorption (PSA) is another important technology to remove CO, CO_2 and other impurities in H_2 product gas. This process consists of a series of beds filled with molecular sieves or active carbon where all components except H_2 are preferentially adsorbed. The purity of H_2 after this step can reach as high as 99+%. The adsorbent is regenerated by depressurization of the sorbent bed followed by purge of H_2. The

disadvantage of PSA is that approximately 20% of the H_2 is lost with impurities during column purge and blowdown.

Hydrogen can also be separated from the gas mixture by the use of membranes. Air Products Inc. (Sircar et al., 2000) recently developed a novel membrane, called selective surface flow (SSF) membrane. This membrane can be integrated into the PSA process to increase the overall H_2 recovery. When the exit gas from the PSA unit passes through the high pressure side of the SSF membrane, the larger and more polar molecules (CO, CO_2, hydrocarbons) are selectively adsorbed on the membrane, then diffuse toward the low pressure side of the membrane where they desorbed into the permeate stream. The H_2 enriched effluent gas is thus produced from the high pressure side of the membrane.

In PEM type (polymer electrolyte membrane) fuel cells, the content of CO in the H_2 feed is critical. The anode catalyst is readily poisoned by CO, even at very low levels. Therefore, the CO content in the H_2 feed gas must be controlled stringently. CO is usually removed via preferential oxidation (PROX), which uses O_2 to convert CO to CO_2 over a catalyst, typically Pt, while minimizing the oxidation of H_2. Cole et al. (2002) reported a similar method which selectively oxidizes carbon monoxide in the presence of hydrogen gas while leave the hydrogen substantially intact. This method applied a catalyst which is easily reduced by carbon monoxide and which is easily oxidized by air. H_2 containing CO impurity and air are alternately contacted with the catalytic material, such that the CO is selectively oxidized while the catalytic material is regenerated. The method produced high purity hydrogen for fuel cell use.

Among the conventional approaches of hydrogen production, steam methane reforming (SMR) is the most economical, because it has the highest thermal efficiency

and lowest capital investment and also has a moderate steam by-product. Other hydrogen production technologies such as coal gasification and electrolysis of water are 2 to 3 times more expensive than the SMR process (Steinberg and Cheng, 1989). Therefore, SMR is the most widely applied process today. It is projected (Scott, 1987) that SMR will dominate in the production of hydrogen for at least three decades and be important for more than fifty years. Finally, the hydrogen produced by SMR will set the reference price for hydrogen.

2.2 Attempts to Improve Steam Reforming Performance

2.2.1 Problems in Conventional Steam Reforming

Heat transfer is a major problem in the operation of the steam reformer. To maintain the high temperature required by the strongly endothermic steam reforming reaction, heat is supplied by burning supplemental fuel gas in the furnace chamber. Gas is a poor thermal conductor and heat transfer from the gas phase to the catalyst pellets is a slow process. When heat is transferred from the combustion chamber to the catalyst, the outermost sections of the packed bed tend to insulate the inner sections. To provide an adequate heat transfer rate, the catalyst has to be packed in long narrow tubes made of superalloy, which are very costly.

In the H_2 production process, there are also concerns with regard to the formation of carbon deposits, or coking. Carbon formation may cause deactivation of catalyst, reduce conversion of methane, block the packed bed, increase pressure drop, cause overheating of tube metal due to formation of hotspots, and eventually lead the plant to shut down.

Carbon deposition may occur according to the following reactions:

$$2CO(g) \rightarrow C(s) + CO_2(g)$$

$$CO(g) + H_2(g) \leftrightarrow C(s) + H_2O(g)$$

$$CH_4(g) \rightarrow C(s) + 2H_2(g)$$

Carbon formation can be reduced either by improvement of the catalyst or by controlling the operational parameters. The commercial process usually applies nickel based catalyst supported on α-alumina ceramic. The alumina is acidic and readily results in cracking of hydrocarbon and formation of coke. Therefore an alkali promoter, such as some form of potash (KOH), is added to the catalyst to increase its resistance to coking. In addition to the use of alkalized catalyst, carbon deposit formed on the catalyst can be oxidized by steam through the following reversible reaction:

$$C(s) + H_2O(g) \leftrightarrow CO(g) + H_2(g)$$

Therefore increasing the steam-to-carbon ratio helps to reduce the risk of carbon deposit. The formation and consumption of carbon is a competitive process and the most suitable steam-to-carbon ratio is usually obtained in operation through attempts to eliminate carbon deposit while achieving the best economics.

2.2.2 Improvement of Conventional Steam Reforming

Current research efforts to improve the steam reforming process are proceeding in several ways. The first approach is to improve catalyst performance to provide higher activity, higher mechanical strength, better resistance to carbon formation and sulfur poisoning, and better catalyst effectiveness by improving the pellet configuration (Adris et al., 1996). The second approach is to enhance the properties of the reactor tube

material to be able to withstand higher stresses at high temperature and thermal flux. The third research line, which emerged around 1970 and has intensified over the past decade, addresses the reforming reactor configuration. Three major areas are being developed: (1) transferring from a fixed-bed reactor to a fluidized-bed reactor; (2) adoption of membrane technology to drive the reaction beyond the thermodynamic equilibrium limit; and (3) changing from external firing to internal heat supply.

Aitani (1996) and Abrardo (1995) reported the application of pre-reforming before the hydrocarbon enters the main reformer. The pre-reformer was loaded with high activity and high surface area nickel reforming catalyst that can function at lower temperature. The catalyst has more flexibility in feedstock ranging from natural gas to heavy naphtha. The pre-reformer can reduce heat duty of the main reformer by 5-10%. Aitani (1996) and Abrardo (1995) also reported the addition of an oxygen-fed secondary reformer to an existing steam reforming process, which may expand the hydrogen capacity up to 50%. The secondary reformer is located right after the main reformer and shifts a portion of the load of the primary reformer. Unconverted methane leaving the primary reformer is combusted in the secondary reformer by injecting oxygen. Towler et al. (2001) included a pre-reforming unit in their steam reforming process to generate high purity hydrogen for fuel cell applications.

2.3 Membrane Enhanced Steam Reforming

The application of membranes in the steam reforming process results in simultaneous separation of hydrogen with the reforming and shift reactions. Membranes made of palladium and its alloys have the property that allows only hydrogen to pass through while keeping other gas components blocked. When the gas mixture in the reaction zone

contacts the membrane, hydrogen is recovered as the only permeate stream while other components are retained by the membrane. According to Le Chatelier's principle, when one of the reaction products is selectively removed from the reaction zone, the conversion of reactants to products, and the rate of the forward reaction in an equilibrium controlled reaction can be increased. If H_2 is removed from the reacting gas mixture as soon as it is produced, the overall reforming and shift reaction will be pushed forward and overcome the thermodynamic equilibrium limitation. A higher conversion of methane is thus made possible. A common disadvantage in membrane application is that feed impurities can irreversibly damage the membrane. Therefore purification of the feed gas is usually required before it enters the reactor.

Nagamoto (1985) designed a hydrogenation reactor with Pd walls that are selectively permeable to H_2. The H_2 permeation rate restricts the overall reaction rate and can be controlled by changing the pressure difference between the two sides of the membrane. Itoh (1987) proposed that application of membranes can also drive the dehydrogenation of cyclohexane to benzene beyond its thermodynamic limit. A conversion of 99.7% was obtained as compared to 18.7% using an ordinary catalytic reactor.

Theoretical studies of the membrane steam reforming reactor have been conducted by Adris (1991, 1996), Kim (1999) and Madia (1999). In Adris's study (1991), a novel fluidized bed membrane reactor was designed with membranes installed in the reactor in the configuration of parallel tubes. The reforming reaction occurred inside the tubes and the H_2 gas was selectively permeated through the walls of the tubes thus avoiding further separation. This design also included integrated sodium heat pipes to transit thermal flux in a more efficient way to the strongly endothermic reforming reaction. Kim (1999) considered heat transfer at the reactor wall in a modelling study and results provided

better agreement with experimental results. Madia (1999) also considered the non-isothermal behavior occurring inside the membrane reforming reactor and determined a temperature profile for the packed-bed in his theoretical study. Roy et al. (1998) presented a simulation model of the Fluidized Bed Membrane Reforming (FBMR) process and evaluated its economics. The conversion rate of methane to hydrogen was increased up to 35% over the conventional steam methane reforming process at comparable reaction conditions when hydrogen was efficiently removed from the reaction zone.

2.4 Sorption Enhanced Reaction Process

Addition of a CO_2 acceptor is another approach to improving the conventional SMR process. According to Le Chatelier's principle referred to above, if CO_2 is removed as soon as it is formed, then the reforming and water-gas shift reactions can proceed beyond the conventional thermodynamic limits and more methane will be converted.

The addition of a solid CO_2 acceptor for H_2 production using SMR was first described by Gluud et al. (1931) in a patent on a process incorporating the combined reactions. Gorin and Retallick (1963) received a patent for a continuous process involving a fluidized-bed reactor containing both catalyst and a carbon dioxide acceptor.

2.4.1 Process Description

The CO_2 removal reaction in the presence of a calcium oxide based adsorbent is:

$$CaO(s) + CO_2(g) \Leftrightarrow CaCO_3(s) \qquad (\Delta H = -42.55 \text{ kcal/mol})$$

The net result of the reforming, shift and CO_2 sorption reactions is:

$$CH_4(g) + 2H_2O(g) + CaO(s) \Leftrightarrow CaCO_3(s) + 4H_2(g) \qquad (\Delta H = -3.09 \text{ kcal/mol})$$

A schematic diagram for this alternate SMR process operating in a circulating fluidized-bed mode is shown in Figure 2-2.

CH_4 and H_2O are fed to the primary reactor, where steam methane reforming, water-gas shift and CO_2 removal occur simultaneously. The primary reactor contains a mixture of Ni-based reforming catalyst and Ca-based CO_2 sorbent. Freshly regenerated particles of sorbent are fed to the primary reactor countercurrently to the reactant-gas flow. Large sorbent particles may be used so that they travel under gravity through the fluidized catalyst particles toward the gas end of the bed. The size and density differences of the catalyst and sorbent particles allow complete separation at the gas inlet end. The sorbent particles are then pneumatically carried to the secondary reactor (a thermal regenerator) for desorption of CO_2. Supplement fuel is added to supply the energy needed for regeneration.

Brun-Tsekhovoi et al. (1986) studied the process above experimentally. A fluidized-bed reactor loaded with catalyst and CO_2 acceptor was used and limited data were presented showing that combined reforming, shift and CO_2 removal equilibrium could be closely approached at 800°C, 2 MPa, and space velocities as high as 12,000 hr^{-1}. A significant enhancement of CH_4 conversion to H_2 (compared to that achieved by catalyst only) was achieved at pressure levels of 10-100 atm and at a reaction temperature of 627°C. The product gas leaving the fluidized-bed reactor contained 92-96% H_2.

2.4.2 Advantages of Sorption Enhanced Process

The sorption enhanced reforming process (SERP) for the production of H_2 has several potential advantages over the conventional reforming process. First, high purity (95+%)

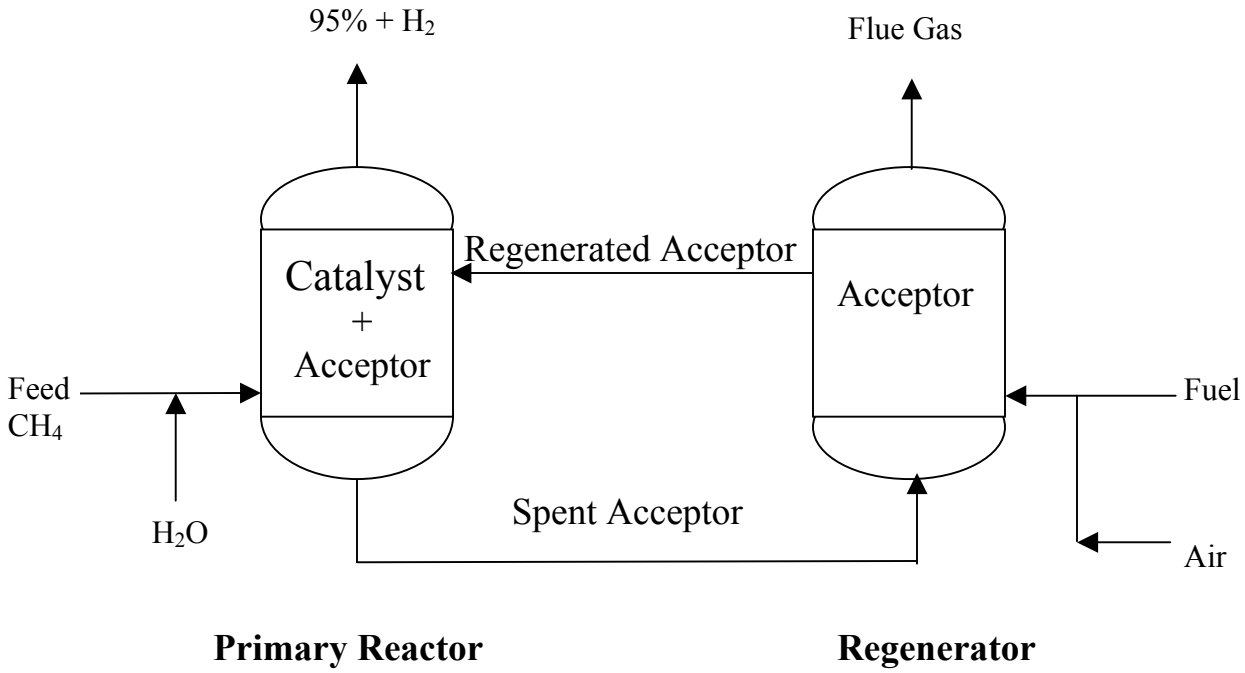

Figure 2.2 A Schematic Diagram of the Sorption-Enhanced Steam-Methane Reforming Process

hydrogen can be produced in a single-step in SERP over a wide range of temperatures without further purification. The five steps – reforming, two shift stages, CO_2 absorption and steam stripping – required in conventional steam reforming are integrated in one reaction step plus one sorbent regeneration step. No separate CO_2 absorber and stripper (or PSA unit) are required. Process simplification has the potential to lower the cost of hydrogen production. Secondly, a shift catalyst is not required at the anticipated primary reactor temperature (Han and Harrison, 1994). Thirdly, the shift and carbonation reactions are exothermic and the amount of heat released from these two reactions almost compensates for the heat required by the endothermic reforming reaction. The overall reactions are nearly thermal neutral. Hence no supplemental energy is needed for the primary reactor and requirements for heat exchangers are greatly reduced. Fourthly, the primary reactor operating temperature may be reduced from about 850°C to around 600°C or even lower and pressure may also be decreased. Lower reaction pressure allows less expensive stainless steel as the construction material of the reactor. The regenerator may be operated so that pure CO_2, suitable for use or sequestration, is produced during sorbent regeneration. Supplemental energy needed for regeneration is estimated to be 20-25% less than supplemental energy to the reformer in the standard process. The bulk CO_2 separated from SERP can be disposed to exhausted natural gas fields, deep ocean or underground to eliminate its negative impact on the atmosphere (Gaudernack, 1998). Another advantage worthy of mention is that conversion of CO is almost complete at low temperature, which is very important in fuel cell applications.

2.4.3 Recent Research in the Sorption Enhanced Process

Han (1994) studied the simultaneous shift and carbonation reactions for the direct production of H_2 from synthesis gas. In his study, no shift catalysts were employed in the temperature range of 500-600°C at 15 atm, while equilibrium CO conversion and CO_2 removal were closely approached. Greater than 99.5% removal of CO_2 was achieved over a range of reaction conditions.

Balasubramanian (1999) studied the combined reforming, water-gas shift and carbonation reactions using methane as feed. He used a solid mixture of calcined $CaCO_3$ and a commercial nickel-based reforming catalyst in a laboratory scale fixed-bed reactor. The feasibility of the single-step process of steam methane reforming was proved in his experimental studies. The reforming, shift and CO_2 sorption reactions were sufficiently fast that combined equilibrium was closely approached at 15 atm and temperatures above 550°C. The effects of temperature, steam-to-methane ratio, feed gas flow rate and methane content in the feed gas were investigated.

Lopez (2000) examined a low-cost commercial dolomite as the CO_2 acceptor in the combined reactions. He showed that the dolomite can be utilized as a CO_2 acceptor precursor after proper pretreatment for sulfur removal. He also investigated the durability of the sorbent through multicycle tests consisting of as many as twenty-five cycles in a fixed-bed reactor and 150 cycles in an electrobalance reactor. In a typical twenty-five-cycle test, there was no decrease in maximum H_2 concentration.

Air Products and Chemicals, Inc. has been actively involved in research on the sorption enhanced steam reforming process for the production of H_2 in recent years (Carvill, 1996; Anand, 1996; Mayorga, 1997; Hufton, 1998, 1999; Waldron, 2001). A

bench-scale experimental installation was used to demonstrate the concept, which used an electrically heated fixed-bed tubular reactor packed with catalyst and CO_2 sorbent. The combined reaction was carried out in the temperature range of 300-500°C compared to the temperature range of 800-1100°C in the conventional process. 95+% purity hydrogen was produced directly from the reactor with trace quantities of carbon oxides (~50ppm) compared to only 75% hydrogen with a large amount of carbon oxides (~20mol%) from the conventional process. The sorbent was regenerated periodically in the same reactor by pressure-swing adsorption (PSA) or thermal-swing adsorption (TSA). They tested the cyclic behavior of the sorption enhanced reaction process on a pilot-scale apparatus and reported that the process was capable of producing 88-95% hydrogen with carbon oxide content controlled below 40 ppm at 490°C, 66 psi and a steam-to-carbon ration of 6:1. A proprietary CO_2 sorbent, containing potassium carbonate promoted hydrocalcite worked well in the temperature range of 300-500°C with the presence of excess steam.

2.5 Unmixed Steam Reforming

Energy and Environmental Research Corp. (EERC) has reported a similar research effort to improve the traditional steam reforming process. Lyon et al. (2000) described a novel technology called Unmixed Combustion (UMC), which is significantly different from flame combustion in that fuel and air are not mixed during combustion. In the UMC process, fuel and air are alternately passed through a metal catalyst, such as Ni or Cu which is readily oxidized by air from its elemental state and reduced by fuel from its oxidized state. The metal is supported on a high surface area material like alumina. The heat of combustion is released and deposited on the catalyst support when the metal is oxidized and additional energy is released when the metal oxide is reduced back to its oxide state by fuel. The heat thus generated in-situ can be utilized to supply the strongly

endothermic steam reforming reactions. In UMC, the fuel is converted to CO_2 and water, and the air is depleted of O_2. The function of the catalyst is not to increase chemical reaction rates but to facilitate mass transfer. It stores O_2 during the oxidation of metal and releases it during the reduction of metal oxide, which avoids the need to mix fuel and air. Jin et al. (1998) proposed the similar concept, which was called Chemical Looping Combustion. They examined several looping material candidates and found that the CoO-NiO/YSZ (8mol% yttria-stabilized zirconia) combination was the most suitable one for application of chemical-looping combustion. This material was reported to have high reactivity, complete avoidance of carbon deposition, as well as good durability. Kumar et al. (1999) applied the unmixed combustion concept to the steam methane reforming process, which was called Unmixed Reforming (UMR).

The primary reactions occurring in this process are as follows:

(1) Reforming $CH_4(g) + H_2O(g) \Leftrightarrow CO(g) + 3H_2(g)$ (Endothermic)

$CO(g) + H_2O(g) \Leftrightarrow CO_2(g) + H_2(g)$ (Exothermic)

$CaO(s) + CO_2(g) \Leftrightarrow CaCO_3(s)$ (Exothermic)

(2) Air Regeneration $2Ni(s) + O_2(g) \Leftrightarrow 2NiO(s)$ (Exothermic)

$CaCO_3(s) \Leftrightarrow CaO(s) + CO_2(g)$ (Endothermic)

$C(s) + O_2(g) \Rightarrow CO_2(g)$ (Exothermic)

(3) Fuel Regeneration

$CH_4(g) + 4NiO(s) \Leftrightarrow CO_2(g) + 2H_2O(g) + 4Ni(s)$ (Exothermic)

Nickel was used as the catalyst in the steam reforming process. During the reforming step, methane and steam react over the catalyst to produce hydrogen. Calcium oxide is used as sorbent to capture CO_2 formed by the reforming reactions, which improves the purity of hydrogen and keeps the reactions nearly thermally neutral. In the air regeneration step, air is passed through the reactor bed to oxidize the catalyst. The temperature of the bed is raised by the heat released from the oxidation reaction. Thus calcium carbonate is decomposed back to calcium oxide that may be used cyclically. In the fuel regeneration step, methane is passed through the reactor bed to reduce the nickel oxide back to its catalytic metallic state.

Unmixed reforming has several advantages over the conventional steam reforming process. Firstly, UMR can be operated autothermally without the need of an external heat supply. In conventional steam reforming, supplying the heat consumed by the endothermic reaction is awkward because the gas-solid heat transfer coefficients are relatively low. However, in unmixed reforming, heat is liberated from the oxidation of nickel and delivered uniformly throughout the solid phase of the packed beds, which is more efficient than an external heat supply. When the ratio of nickel to calcium is 1 to 1.35, the heat released from the oxidation of nickel was claimed to be sufficient to fully decompose the $CaCO_3$ back to CaO. Also, in conventional steam reforming, coke may be formed when hydrogen is generated not from light hydrocarbons but from logistics fuel, such as diesel/jet fuel. The coke will accumulate in the packed beds and plug the reactor without proper post-treatment. This is a particular problem in some military applications. In UMR, any coke formed is burned off by O_2 during the air regeneration step. Finally, in conventional steam reforming, any sulfur present in heavier feedstock fuel will poison the

catalyst by forming nickel sulfide. In UMR, the nickel sulfide formed during the reforming reaction will be rejected as SO_2 during the air regeneration step and the activity of the catalyst is restored. EERC has established both bench scale and pilot scale experimental systems to evaluate the feasibility of this process.

The pilot scale system used to perform the experiments is illustrated in Figure 2-3. This system consists of dual packed bed reactors, which makes it possible to shift the process between reforming and regeneration without interrupting the continuous process between reforming and regeneration without interrupting the continuous production of H_2. Switching valves are installed to control the alternate delivery of fuel and steam, air and finally fuel to the packed bed for the three steps of the UMR process. The packing consists of a blended mixture of the catalyst and CO_2 sorbent. The catalyst is nickel supported on calcium aluminate and the CO_2 sorbent is dolomite. The particle sizes of the catalyst and dolomite are 1 to 7 mm. A back pressure regulator is used downstream of the beds to maintain the pressure in the reactor, which is 2-7 bar for the reforming reaction, and 1-2 bar for the regeneration step. The reformate (reformer product) stream was analyzed by online infrared gas analyzers with the readings verified by a gas chromatography.

Hydrogen product with an average purity of above 70 percent was reported when diesel fuel was used in UMR. When sulfur was added to diesel fuel at a concentration of 2000 ppm by weight, the sulfur concentration in the reformate stream was around 12 ppm. The content of CO was typically less than 10 ppm.

UMR is claimed to be an economically suitable process for small scale production of H_2, typically for fuel cell applications. Lyon et al. (2000) also studied UMR using

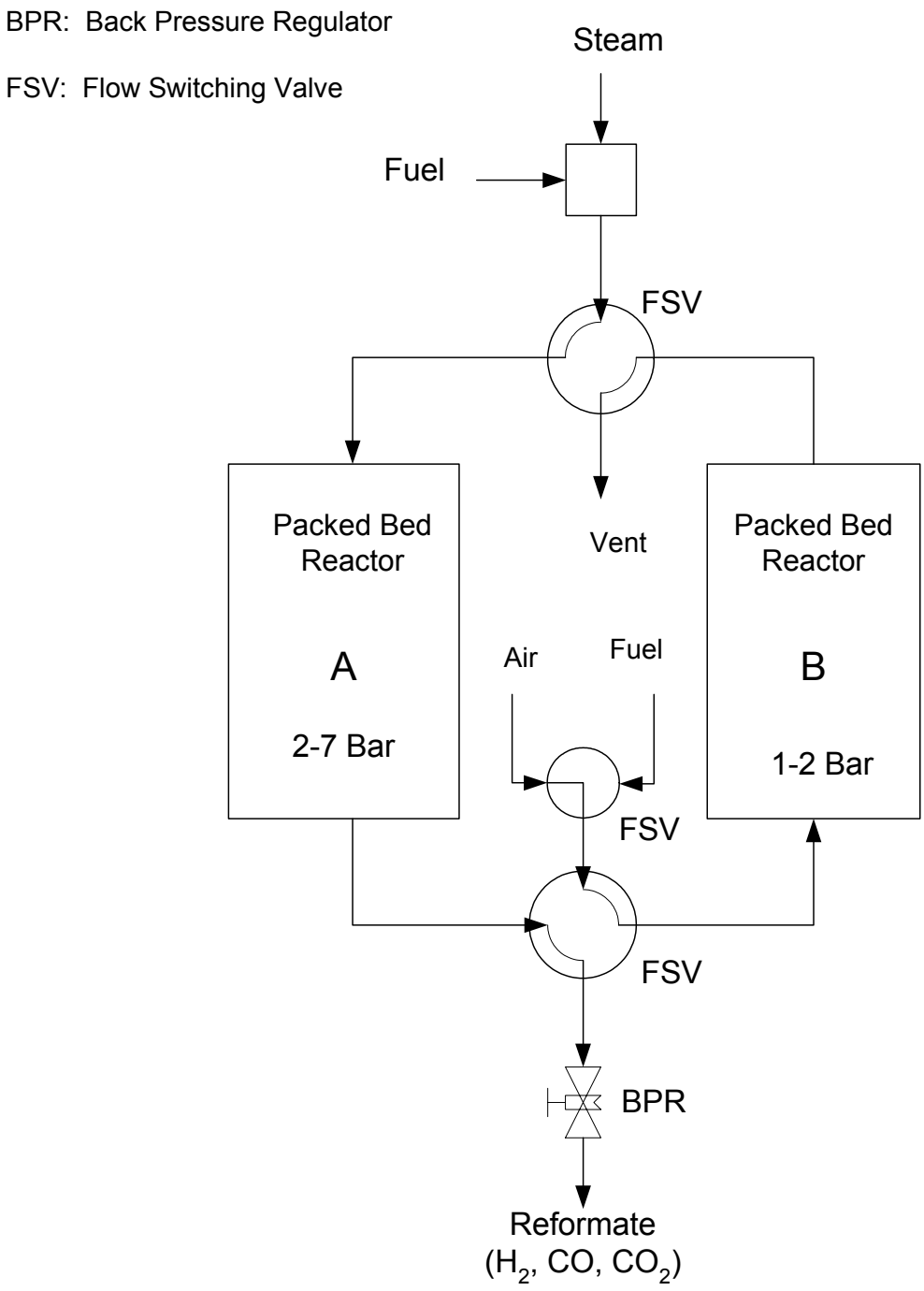

Figure 2-3 A Schematic Diagram of Experimental System of Unmixed Reforming

biomass (wood chips and switch grass), which is considerably less expensive than natural gas, as feed. Bench scale experimental tests produced 95% pure H_2 at a rate sufficient to power a 1.4 KW fuel cell, which is suitable for farms and rural users of electricity.

CHAPTER 3

THERMODYNAMIC ANALYSIS

This chapter presents a thermodynamic comparison of the conventional and sorption-enhanced SMR processes based upon HSC (Roine,1999) software. In the thermodynamic calculations, the initial components of the reaction system, their amounts and phase state as well as temperature and pressure of the system are initially input. Possible components of the equilibrium product are chosen from a database of approximately 15,000 chemical species. The gas phase is assumed to be ideal gas and the condensed species are assumed to be pure phases with an activity coefficient of 1.0. The equilibrium composition of the mixture is then calculated based on the free energy minimization approach, which determines the equilibrium composition by minimizing the Gibbs energy of the system. HSC serves as a useful tool in determining suitable experimental conditions such as temperature, pressure, and steam-to-carbon ratio for the SMR process.

The sorption-enhanced SMR reactions appear as follows when Ca-based CO_2 adsorbent is present in the reactor.

(1) Reforming $CH_4(g) + H_2O(g) \Leftrightarrow CO(g) + 3H_2(g)$ (endothermic)

(2) Shift $CO(g) + H_2O(g) \Leftrightarrow CO_2(g) + H_2(g)$ (exothermic)

(3) Carbonation $CaO(s) + CO_2(g) \Leftrightarrow CaCO_3(s)$ (exothermic)

(4) Overall Reaction $CH_4(g) + 2H_2O(g) + CaO(s) \Leftrightarrow CaCO_3(s) + 4H_2(g)$

(approximately thermally neutral)

The calculated results of the overall reaction from HSC are discussed in the following sections.

3.1 Comparison of Conventional and Sorption-Enhanced Processes

Figure 3-1 compares the equilibrium mole fraction of H_2 , y_{H_2} , in the dry product gas from the conventional SMR process and sorption-enhanced process as a function of temperature at 5 atm and steam-to-carbon ratio of 4.0. In the conventional process, y_{H_2} increases as the temperature is increased and reaches a maximum of 0.77 at 800°C. In the sorption-enhanced process, the y_{H_2} curve is bifurcated when the temperature is lower than 575°C. In the upper branch of the curve, $CaCO_3$ is the only solid reaction product allowed. y_{H_2} increases slightly with increasing temperature and reaches a maximum of about 0.98 at 580°C. In the lower branch of the curve, $Ca(OH)_2$ is also considered as a possible reaction product. Formation of $Ca(OH)_2$ is thermodynamically possible when the temperature is below 575°C. Since $Ca(OH)_2$ decomposes when the temperature is higher than 575°C, the two branches merge into one line above 575°C. From Figure 3-1, it is evident that the sorption-enhanced process is superior to the conventional process in that it has a higher equilibrium content of H_2 in the product gas. In the conventional process, y_{H_2} is equal to 0.75 at 700°C, while in the alternate process, y_{H_2} is 0.96 at that temperature. Above 820°C, reaction between CO_2 and CaO is impossible, and the conventional and the alternate processes become equal.

In both the conventional and sorption-enhanced processes at lower temperature, unreacted CH_4 is the main impurity, while the content of carbon oxides (CO and CO_2) is

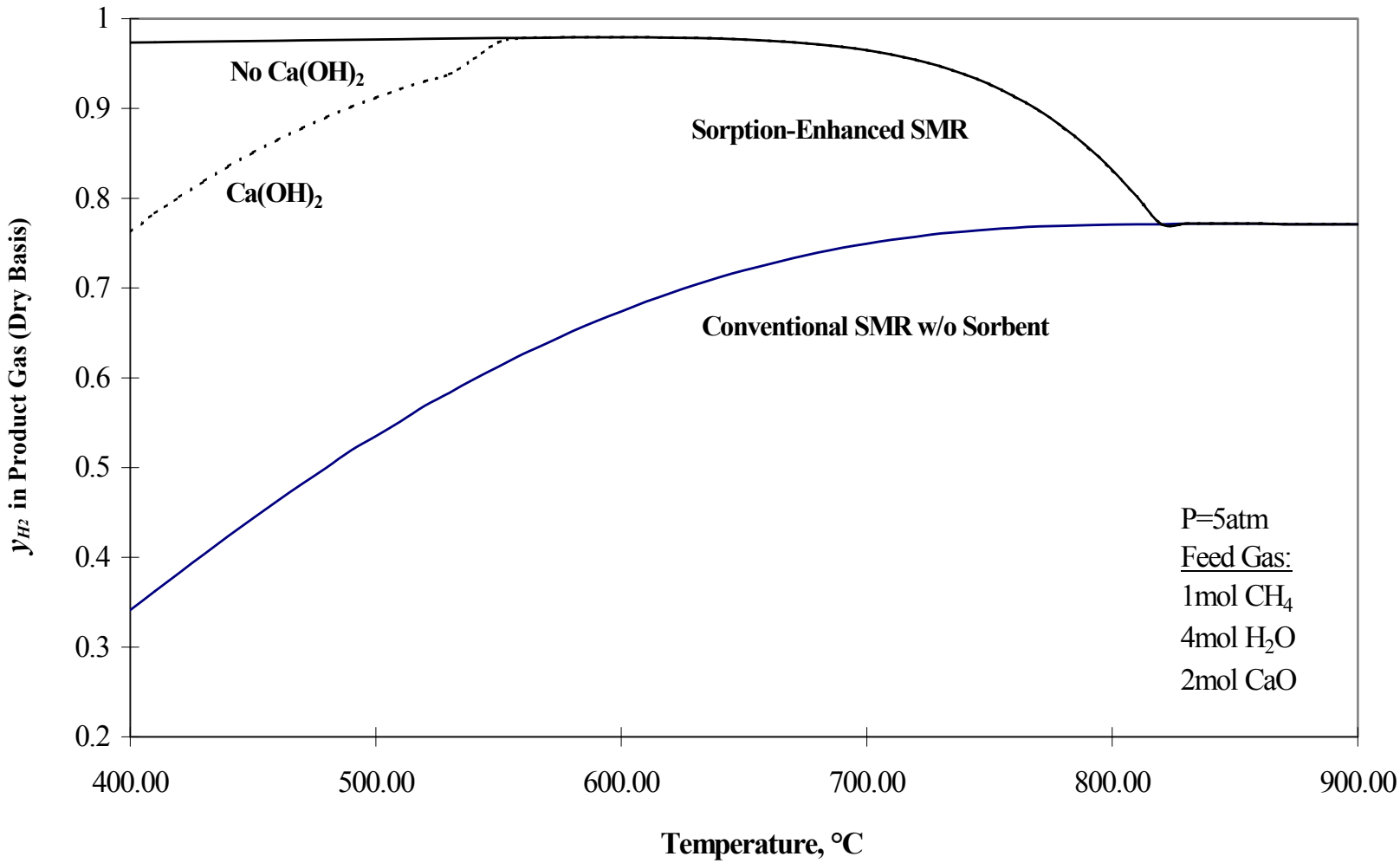

Figure 3-1 Comparison of Equilibrium H_2 Content at 5 atm for SMR with and without CO_2 Acceptor

very small and almost negligible. At higher temperature, the endothermic reforming reaction is enhanced, while the exothermic shift and carbonation reactions are inhibited. Therefore CO and CO_2 become the main impurities at high temperature. This is shown in Figure 3-2 and Figure 3-3.

From Figure 3-2 and Figure 3-3, it is also seen that the sorption-enhanced process is superior to the conventional process in that in the low temperature range, the CH_4 content from the sorption-enhanced process is much lower than that from the conventional process. For example, in the conventional process, the CH_4 content is 14.9% at 450°C, while in the sorption-enhanced process it is only 2.5% at that temperature. This suggests that production of high purity H_2 may be possible using sorption-enhanced SMR at low temperature.

3.2 Effect of Temperature and Pressure

Figure 3-4 shows the dry basis equilibrium mol fraction of H_2 as a function of temperature and pressure for the sorption-enhanced process. At a fixed pressure, the equilibrium content of H_2, y_{H_2}, initially increases with increasing temperature and reaches a maximum near the temperature where $Ca(OH)_2$ cannot be formed. y_{H_2} then decreases slightly with further increase in temperature until the $CaCO_3$ decomposition temperature is approached. Then y_{H_2} decreases significantly. For example, at 10 atm, y_{H_2} increases with increasing temperature and is approximately constant at 0.96 between 580°C and 650°C, and then decreases rapidly. At 860°C, y_{H_2} drops to 0.78.

This thermodynamic response of y_{H_2} with temperature can be interpreted from the nature of the reforming, shift and carbonation reactions. The reforming reaction is

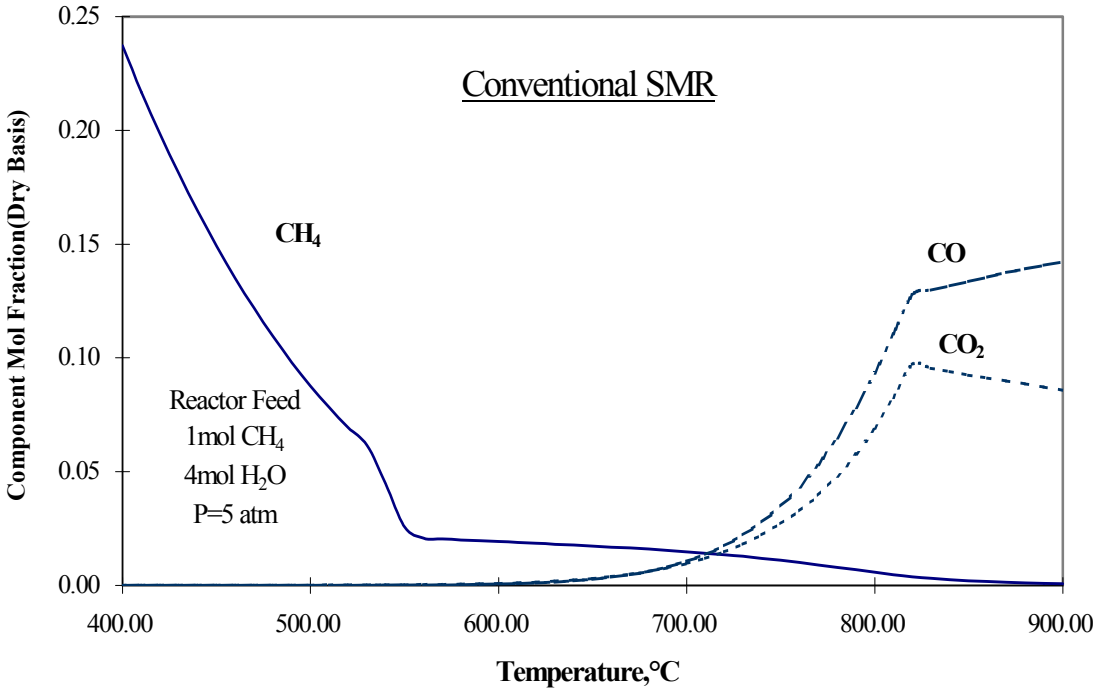

Figure 3-2 Equilibrium Composition of Impurities(CH_4 and COx) as a Function of Temperature at 5atm for the Conventional SMR

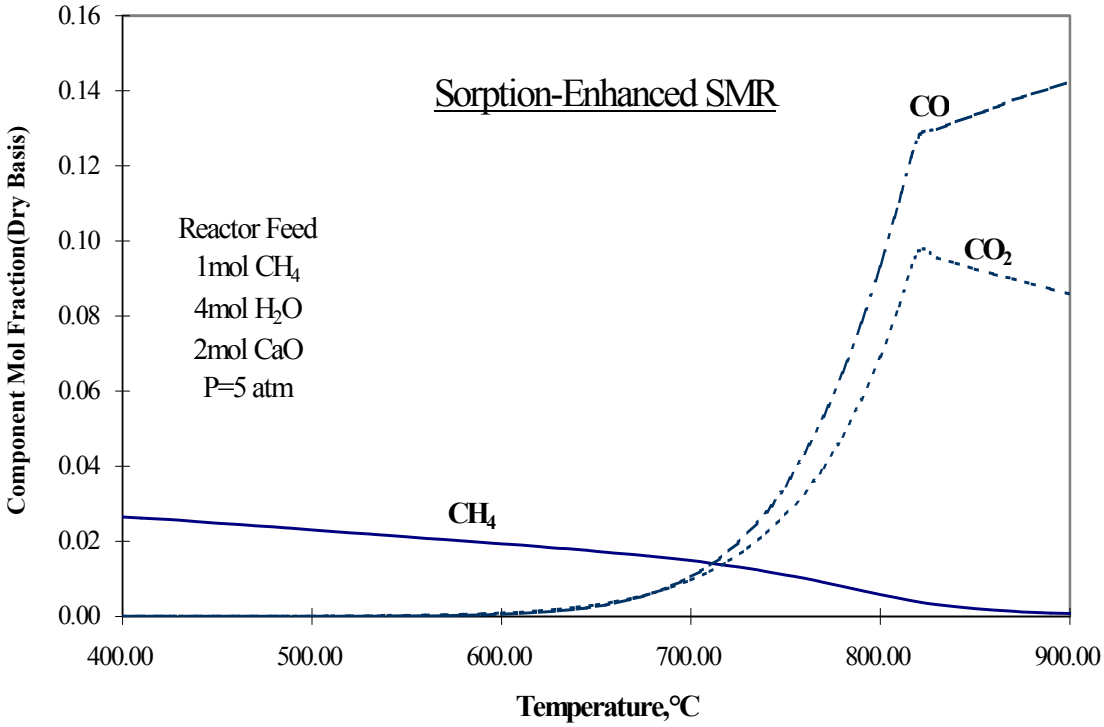

Figure 3-3 Equilibrium Composition of Impurities(CH_4 and COx) as a Function of Temperature at 5atm for the Sorption-Enhanced SMR

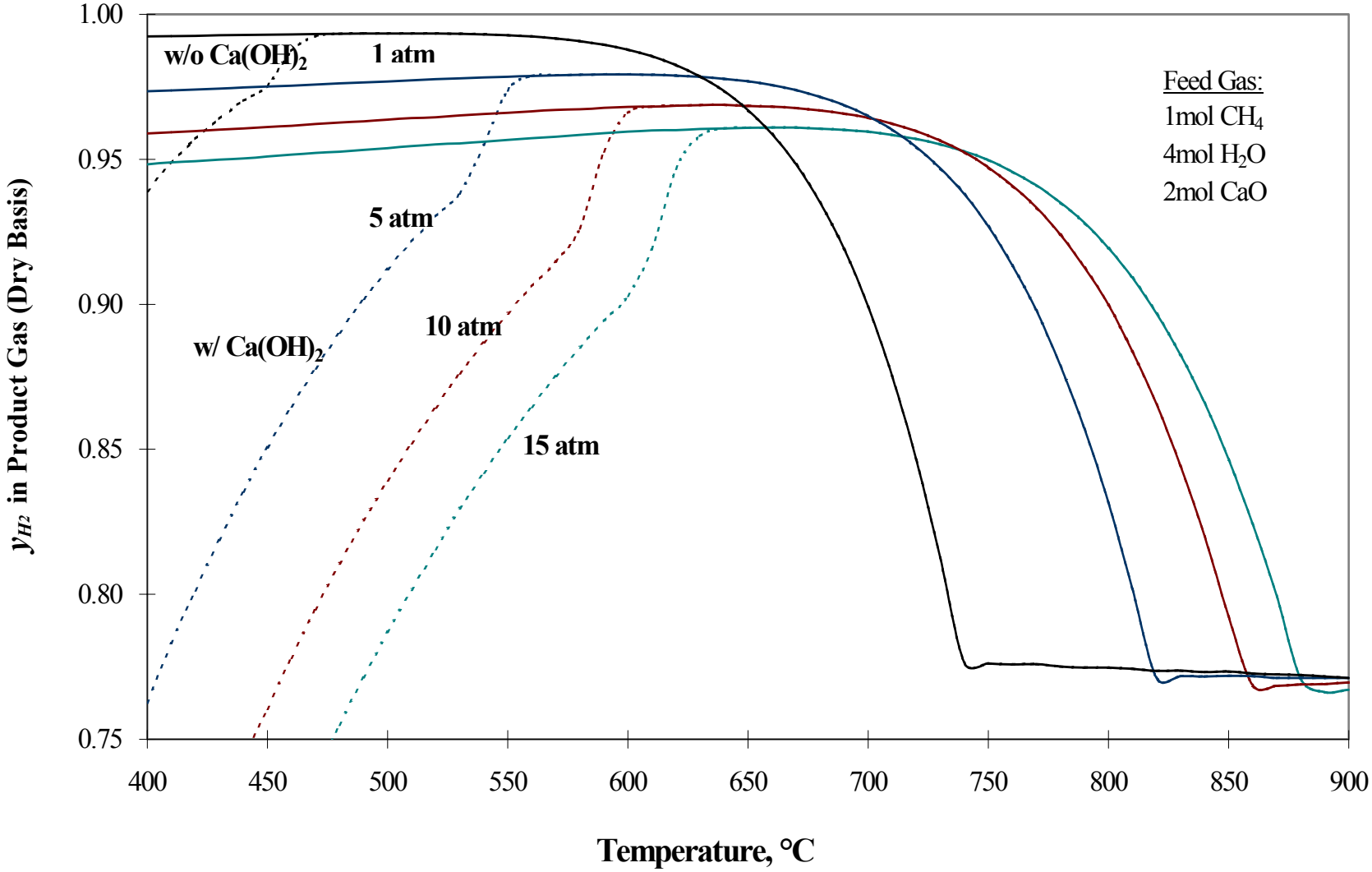

Figure 3-4 Equilibrium Mol Fraction of H_2 as a Function of Temperature and Pressure for the Sorption-Enhanced SMR Process

endothermic and favored by higher temperature. When the combined reactions are carried out in low temperature range, the reforming reaction is dominant. Higher temperature pushes the reforming reaction forward and leads to a higher CH_4 conversion; therefore y_{H_2} increases when the temperature is increased. In the high temperature range, the exothermic shift and carbonation reactions govern the overall process. Carbonation becomes very sensitive to temperature, and y_{H_2} decreases abruptly with increasing temperature until above a certain temperature carbonation will not occur. At this point the conventional and sorption enhanced processes are identical.

From the thermodynamic equilibrium point of view, lower pressure favors the production of H_2. This is shown from the equation of the overall reaction (4), which involves an increase in the total number of gas phase moles. In Figure 3-4, it is clear that the maximum y_{H_2} decreases with increased system pressure. At 1 atm, the maximum y_{H_2} is about 0.99, while at 5 atm the maximum value falls to 0.97. For most conventional H_2 applications, economics requires the process to be operated under high pressure (15~20 atm) even though it leads to lower equilibrium content of H_2. However for some emerging applications, such as fuel cells, such high pressure may not be optimal. It is thus necessary to make a further study on this process at low pressures.

Another concern in the steam reforming process for the production of H_2 is the content of CO in the dry product gas. High concentrations of CO will poison the catalyst when the H_2 is utilized in some areas such as ammonia synthesis or in fuel cells. Therefore the CO content is always an important index of the quality of H_2. In low temperature PEM fuel cells, CO is more easily adsorbed on the Pt catalyst than H_2, which greatly reduces the power density produced from the fuel cell. To maintain proper fuel

cell operation, the CO content in the H_2 feed must be strictly controlled at low levels. 20 ppm is the target in the subsequent experimental study.

The equilibrium concentration of CO, y_{CO}, in the product gas is influenced by both temperature and pressure. From Figure 3-5, it is seen that at a fixed pressure y_{CO} increases with increasing temperature. This can be interpreted from the viewpoint of the heat of the reactions. Higher temperature promotes the endothermic reforming reaction and inhibits the exothermic water gas shift reaction and carbonation reaction. The overall result is the increase of y_{CO}. An increase in pressure will result in lower y_{CO}. The primary reason for this is that the CO_2 removal, or carbonation reaction, involves elimination of gas phase moles and is favored by high pressure. The steam reforming reaction leads to an increase in the total mols in the gas phase. Therefore higher pressure limits the formation of CO, which is in the product side of this reaction. The water gas shift reaction is not affected by pressure because there is no change in the total moles in the gas phase. The net result is a decrease of y_{CO} with increasing pressure. From Figure 3-5, it is seen that at 1 atm the CO content is limited to 20 ppm at temperature below about 470°C. At 15 atm the upper limit of the temperature is increased to 540°C. The purity of H_2 is 99% and 95%, respectively, under these conditions.

3.3 Effect of Steam to Carbon Ratio (S/C) and Temperature

Steam-to-methane or steam-to-carbon (S/C) ratio in the feed gas is another important process index as well as an economic index in steam reforming. Figures 3-6 and 3-7 show the effect of S/C ratio in the feed gas, in the range of 2.0 to 6.0, on y_{H_2} in the temperature

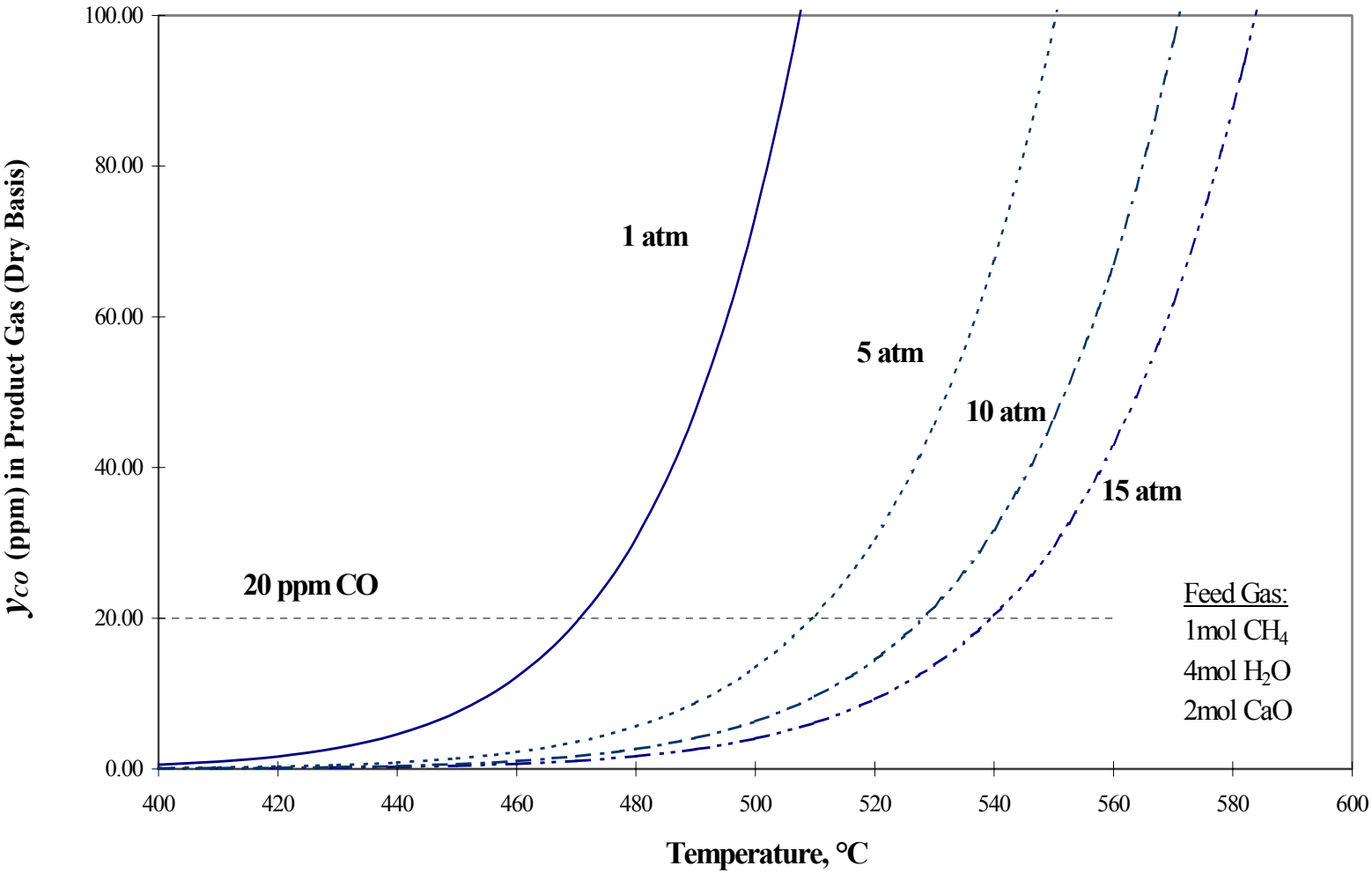

Figure 3-5 Equilibrium Mol Fraction of CO as a Function of Temperature and Pressure for the Sorption-Enhanced SMR Process

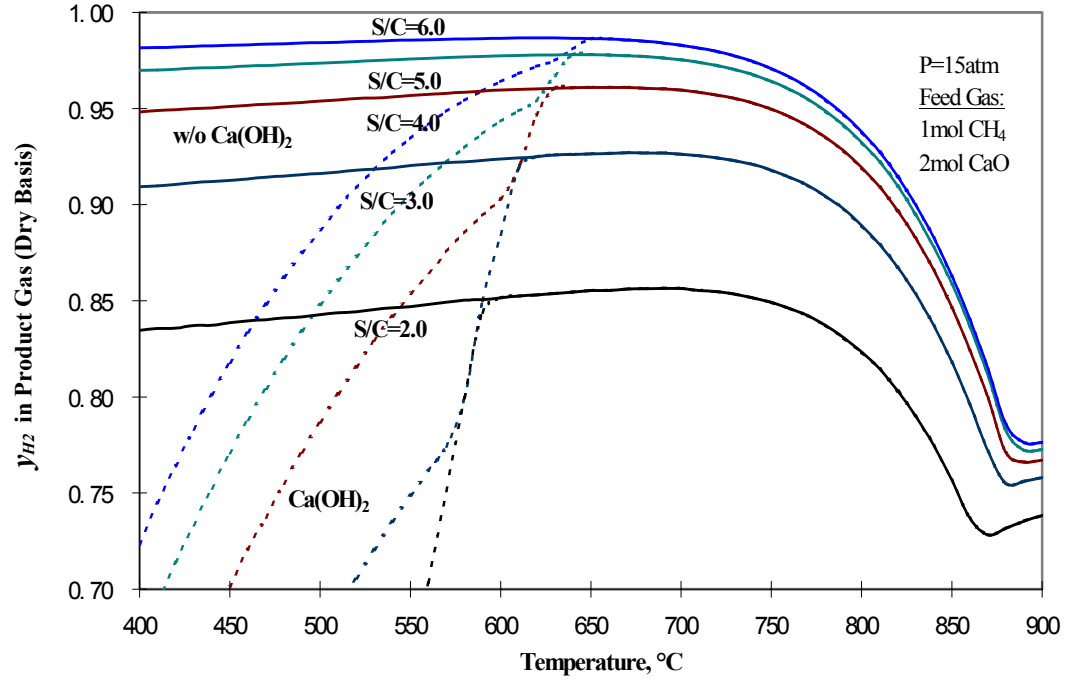

Figure 3-6 Effect of S/C Ratio on Equilibrium Mol Fraction of H_2 for the Sorption-Enhanced SMR at 15atm

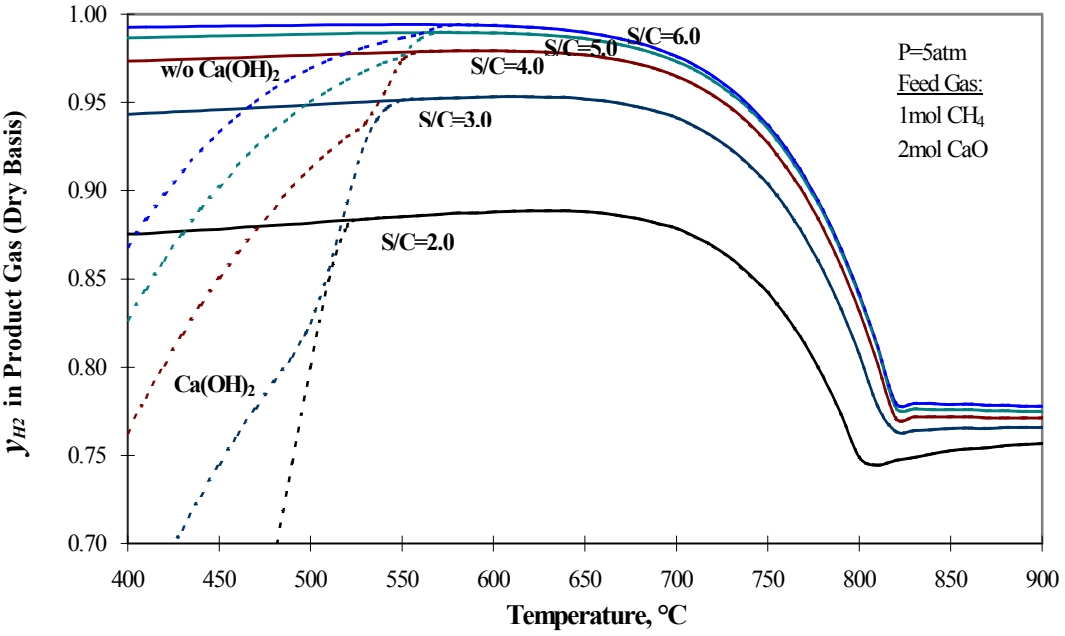

Figure 3-7 Effect of S/C Ratio on Equilibrium Mol Fraction of H_2 for the Sorption-Enhanced SMR at 5atm

range of 400°C to 900°C at 15 atm and 5 atm, respectively.

At 15 atm (Fig 3-6), the H_2 concentration increases with an increase of S/C ratio, and a maximum y_{H_2} of about 0.99 is thermodynamically possible at a S/C ratio of 6.0 at 650°C. When $Ca(OH)_2$ is considered as a possible product, 95+% H_2 is possible between around 575°C and 785°C at a S/C ratio of 6.0, between around 610°C and 775°C at a S/C ratio of 5.0, and between around 625°C and 750°C at a S/C ratio of 4.0. At a S/C ratio of less than 3.0, 95+% H_2 cannot be obtained. At 5 atm (Fig 3-7), even higher H_2 concentration may be achieved at the same S/C ratio. For example, 98% H_2 is obtainable at 650°C and S/C ratio of 4.0, compared to 96% H_2 product at 15 atm at the same temperature and S/C ratio.

The increased H_2 content with increasing S/C ratio can be easily understood from the role H_2O plays in the reforming and shift reactions. Increased S/C will enhance both, resulting in higher conversion of both CH_4 and CO. In the dry basis product gas, more H_2 will be produced. However, because of the energy cost of generating high pressure steam, the optimum S/C ratio is determined by the process economics.

$Ca(OH)_2$ in the product is thermodynamically possible at certain conditions, but is not necessarily formed. For example, at a S/C ratio of 4.0 and 5 atm, when the temperature is below 540°C, $Ca(OH)_2$ may be present in the product. The formation of $Ca(OH)_2$ also depends on the kinetics of this reversible reaction. When the decomposition rate of $Ca(OH)_2$ is faster than the combination rate of CaO and H_2O, $Ca(OH)_2$ does not actually exist. Whether or not $Ca(OH)_2$ is formed during the reactions can only be answered from the experimental data.

Formation of $Ca(OH)_2$ consumes steam from the feed, and thereby reduces the actual S/C ratio. As a result, the equilibrium mole fraction of H_2 in the product gas is lower than the equilibrium value when $Ca(OH)_2$ is not considered. This is also shown from Figures 3-6 and 3-7, where lower S/C ratio leads to lower H_2 production.

Figures 3-8 and 3-9 show the effect of the S/C ratio on the equilibrium CO content in the product gas at different temperatures and pressures of 15 atm and 5 atm, respectively. y_{CO} increases consistently with increasing temperature at all S/C ratios. In addition, higher S/C ratio results in lower CO levels, which are desirable in the production of H_2. For example, at 15 atm, the temperature must be below 530°C to insure that the CO content is below 20 ppm at a S/C ratio of 2.0, and below 545°C at a S/C ratio of 6.0. At 5 atm, the upper temperature limits are lowered to 495°C and 515°C, respectively.

3.4 Range of Process Parameters for Further Study

In the experimental study, two kinds of materials have been examined – TDA samples and reforming nickel catalyst mixed with CaO sorbent. For the TDA samples, our interest was mainly in their activities in the steam reforming reaction. These materials were tested at fixed conditions normally used in conventional reforming by varying the composition of the catalyst. For the nickel catalyst/CaO mixture used in the sorption-enhanced process, our primary interest was the feasibility of the production of high purity H_2 with low CO content. Based on the thermodynamic analysis above, the following ranges of process parameters were chosen for further investigation: S/C ratio from 1 to 4, temperature range from 450°C to 550°C and a fixed pressure of 5 atm.

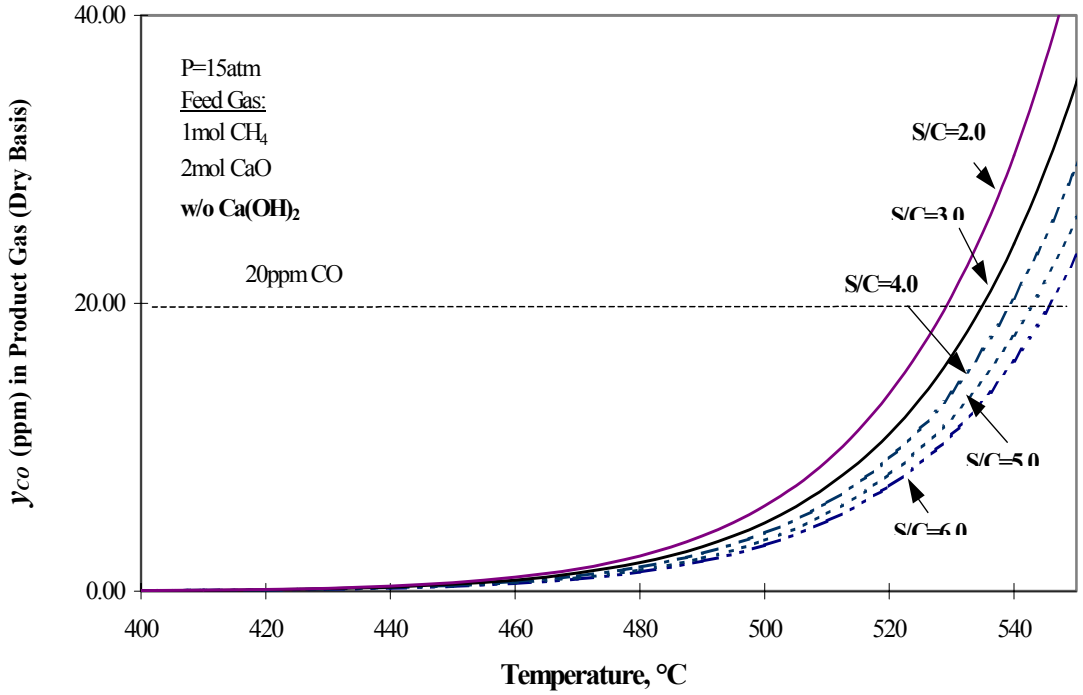

Figure 3-8 Effect of S/C Ratio on Equilibrium ppm Content of CO for the Sorption-Enhanced SMR at 15atm (without $Ca(OH)_2$)

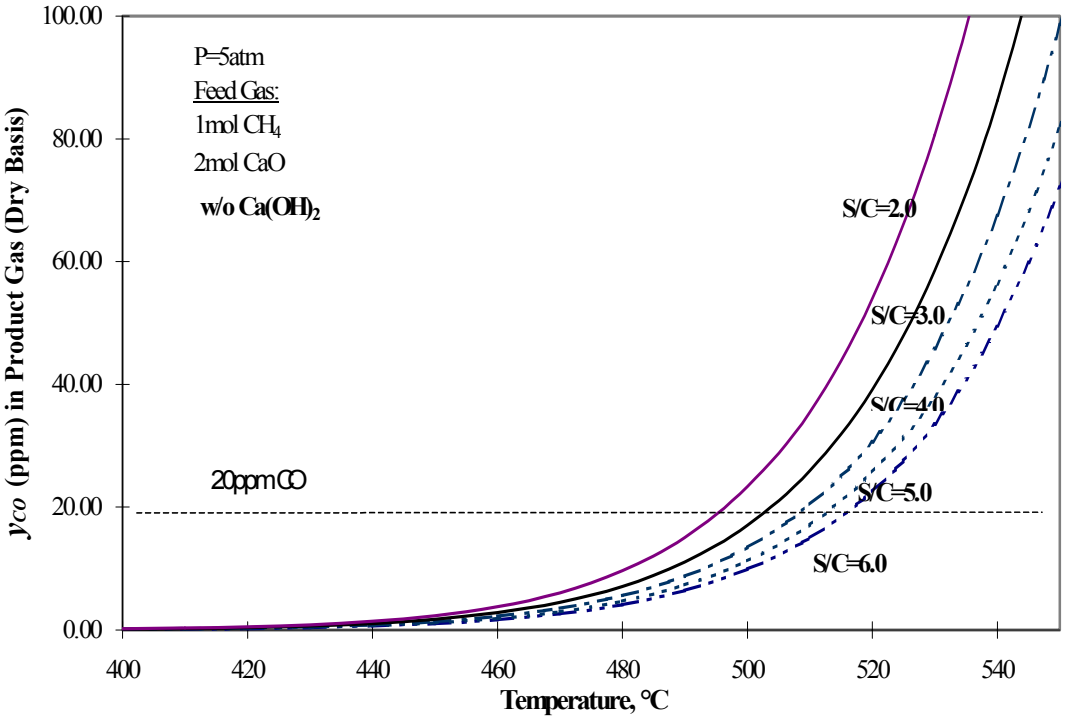

Figure 3-9 Effect of S/C Ratio on Equilibrium ppm Content of CO for the Sorption-Enhanced SMR at 5atm (without $Ca(OH)_2$)

CHAPTER 4

EXPERIMENTAL APPARATUS AND PROCEDURE

In this chapter, the experimental apparatus and procedures, as well as the materials used for the current research, are described.

4.1 The Fixed-Bed Reactor System

A schematic diagram of the reactor system employed in the experiments is presented in Figure 4-1. The gas feed components including nitrogen, methane and carbon dioxide are obtained from high purity gas cylinders regulated by high pressure regulators. Flow rates are controlled using Porter Instruments Model 201 mass flow controllers (MFC) which were pre-calibrated by the manufacturer over the specified flow rate range and re-calibrated by the user before the experiment. Upstream of the MFC a dryer packed with silica gel is placed to adsorb any traces of moisture from the feed gas, and a Matheson Model 6183 filter is placed after the dryer to prevent entry of any solid contaminants. Parker check valves are placed right after the MFCs to prevent any back flow due to possible pressure fluctuations during the course of the experiment. Liquid water is fed using a Harvard Apparatus Model 909 high pressure syringe pump. The feed lines are heat traced to insure vaporization of water as it mixes with the other feed gases. All feed lines are well insulated to prevent condensation of water vapor, particularly around the reactor coupling area. A Parker pressure relief valve is installed in a side stream near the fixed-bed reactor inlet to protect the system against excessive pressure.

The combined feed gas containing methane, steam and nitrogen enters near the bottom of the reactor and is preheated by the furnace as it flows upward in the annular

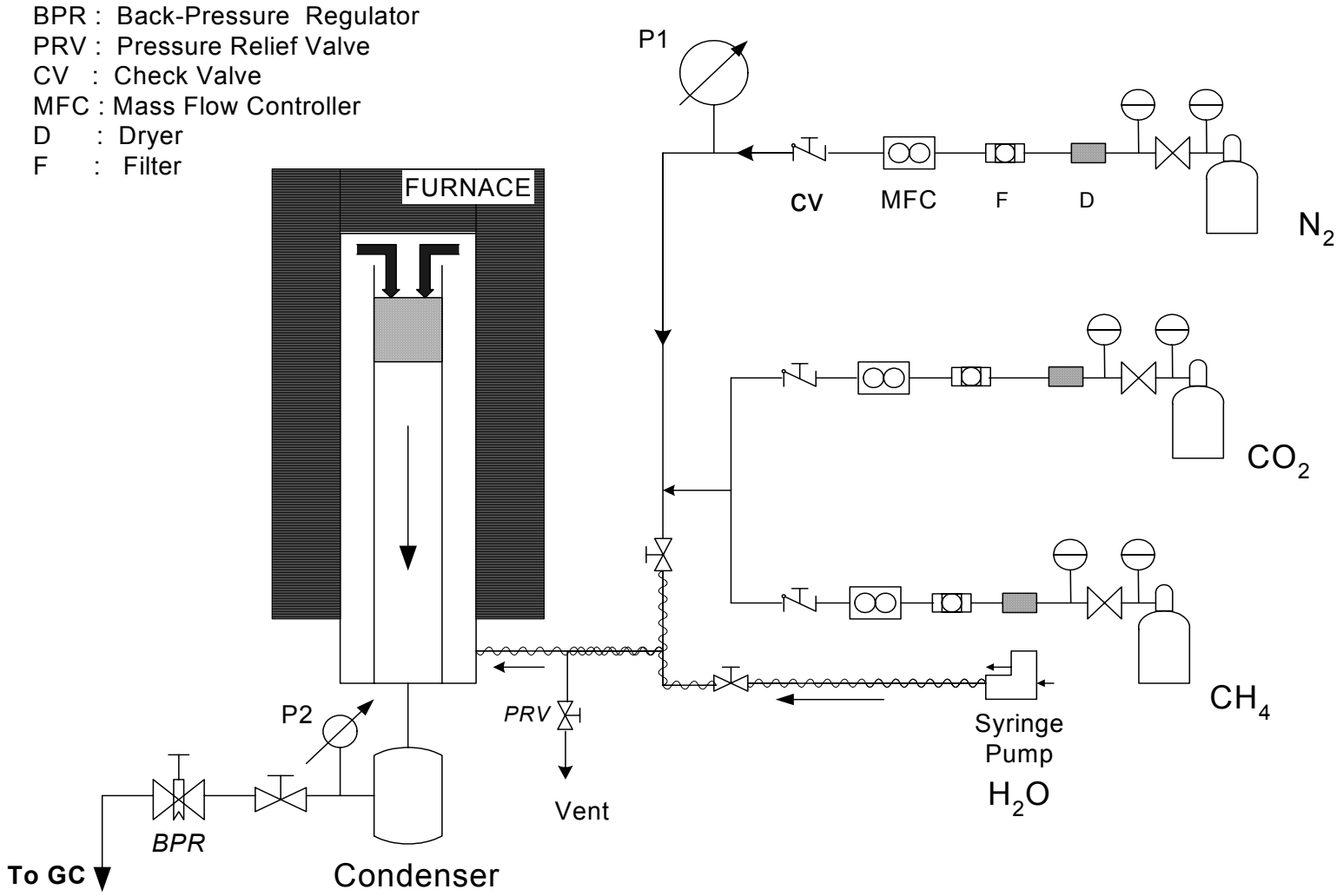

Figure 4-1 Schematic Diagram of the Laboratory-Scale Fixed-Bed Reactor System

area between the reactor insert and the pressure vessel. The preheated feed then flows downward through the solid consisting of a mixture of reforming catalyst and CO_2 sorbent, and exits from the bottom of the reactor. The product gases flow through a condenser immersed in an ice bath to remove unreacted steam. The pressure of the product gases is reduced to 1 atm by a Tescom Series 26-2300 back pressure regulator, and then sent to a gas chromatograph (GC) for analysis. Matheson Model 2242 pressure indicators are installed both upstream and downstream of the reactor to monitor the system pressure.

The reactor was designed by Han (1995) for his research on the simultaneous water-gas shift reaction and carbon dioxide separation for hydrogen production from synthesis gas. Figure 4-2 shows the reactor in greater detail. The reactor is composed of two main parts: the pressure vessel and the reactor insert, both made of 316 stainless steel. Two silicone O-rings capable of withstanding temperatures up to 260°C are placed near the bottom to maintain the pressure in the reactor. The reactor has a capacity of about 20g solid and a maximum temperature limit of 1000°C and pressure limit of 21atm (not simultaneously).

The reactor temperature is controlled and maintained by an Applied Test Systems Series 3210 single zone split-tube furnace which includes a Model 2010 temperature controller and CFE Model 2040 limit controller. The limit controller shuts down the furnace in the event the temperature exceeds 1000°C.

4.2 The Gas Chromatography System

Product gas composition is determined using a Shimadzu Model GC-14A gas chromatograph equipped with an automatic ten-port sampling valve, dual columns,

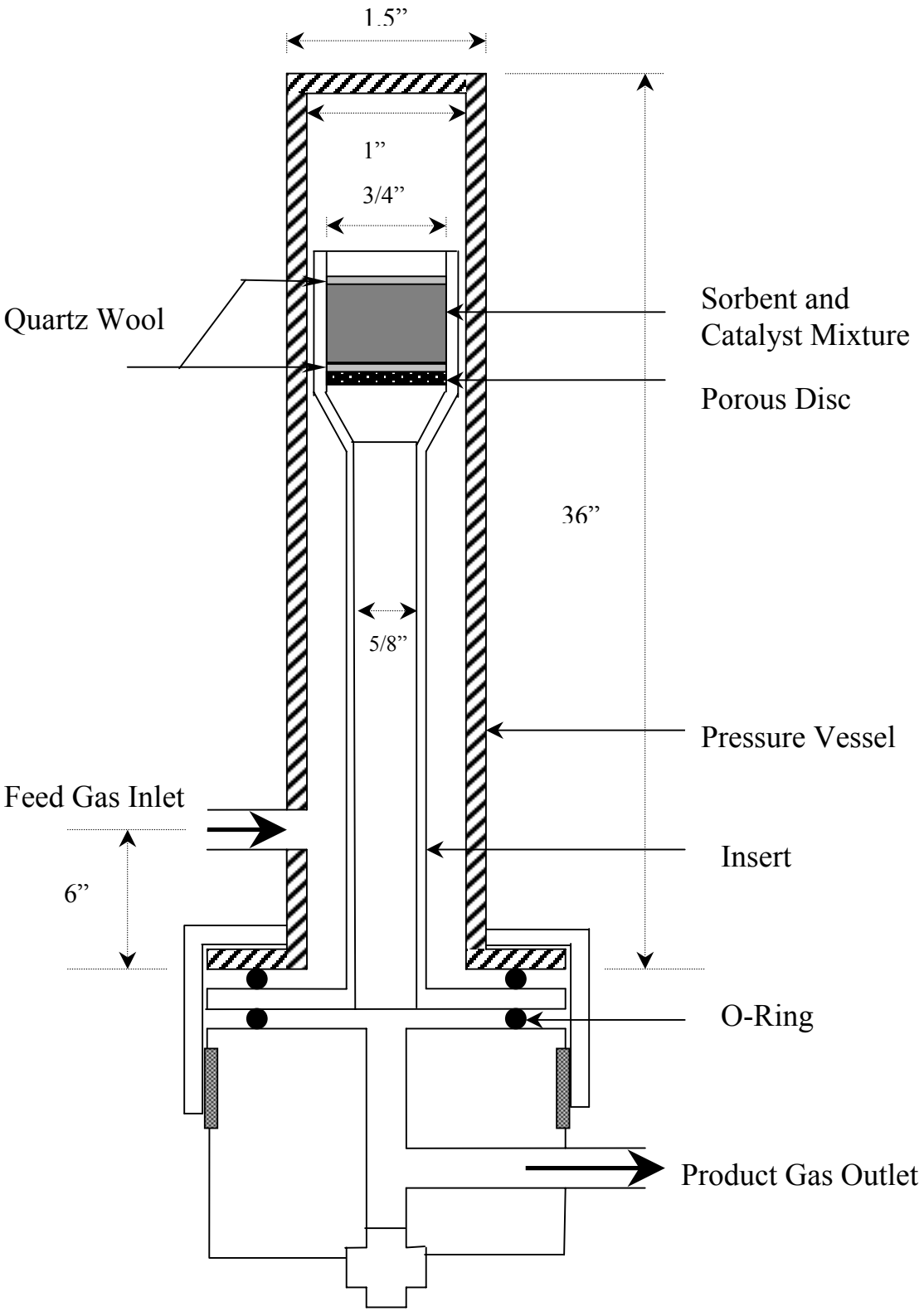

Figure 4-2 The Fixed-Bed Reactor

methanizer, and both a thermal conductivity detector (TCD) and a flame ionization detector (FID). Ultra-high purity (UHP) nitrogen is used as the carrier gas. Separation of the five gas products – H_2, CH_4, N_2, CO, CO_2 – is performed using a Carboxen 1000 column. A HayeSepN column retains moisture which might escape the condenser, and allows the dry gases to flow to the Carboxen 1000 column.

The operation of the sampling system is shown in Figure 4-3. A Valco Instruments automatic ten-port pneumatic valve samples gas product every twelve minutes. The valve is switched between two positions, A, known as LOAD, and B, known as INJECTION. In position A, product gas from the reactor flows into the sampling valve, through the sample loop, which consists of a 1/8" Teflon tubing with an internal volume of approximately 0.5 cm^3, back to the valve and to the vent. Carrier gas CG1 flows into the sampling valve, through the HayeSepN column, back to the valve and to the vent. Carrier gas CG2 is directed into the valve to the Carboxen 1000 column, where component separation occurs, and then through the TCD, methanizer and FID to the vent. In position B, the product gas to be analyzed is displaced from the sample loop by CG1 and directed to the HayeSepN column where trace quantities of moisture were captured. The dry product gas is then fed to the Carboxen 1000 column for component separation.

The separated components are sent first to the TCD and then the FID to determine the composition of the product gas. The TCD is used to detect H_2 and the more sensitive FID is used for analysis of CH_4, CO and CO_2. The TCD effluent gas flows to a Ni-catalyzed methanizer where CO and CO_2 are converted to CH_4, which can be identified by the FID. Excess quantities of UHP H_2 are fed to the methanizer to ensure sufficient H_2 to react with CO and CO_2 and to maintain a stable flame in the FID, which follows the

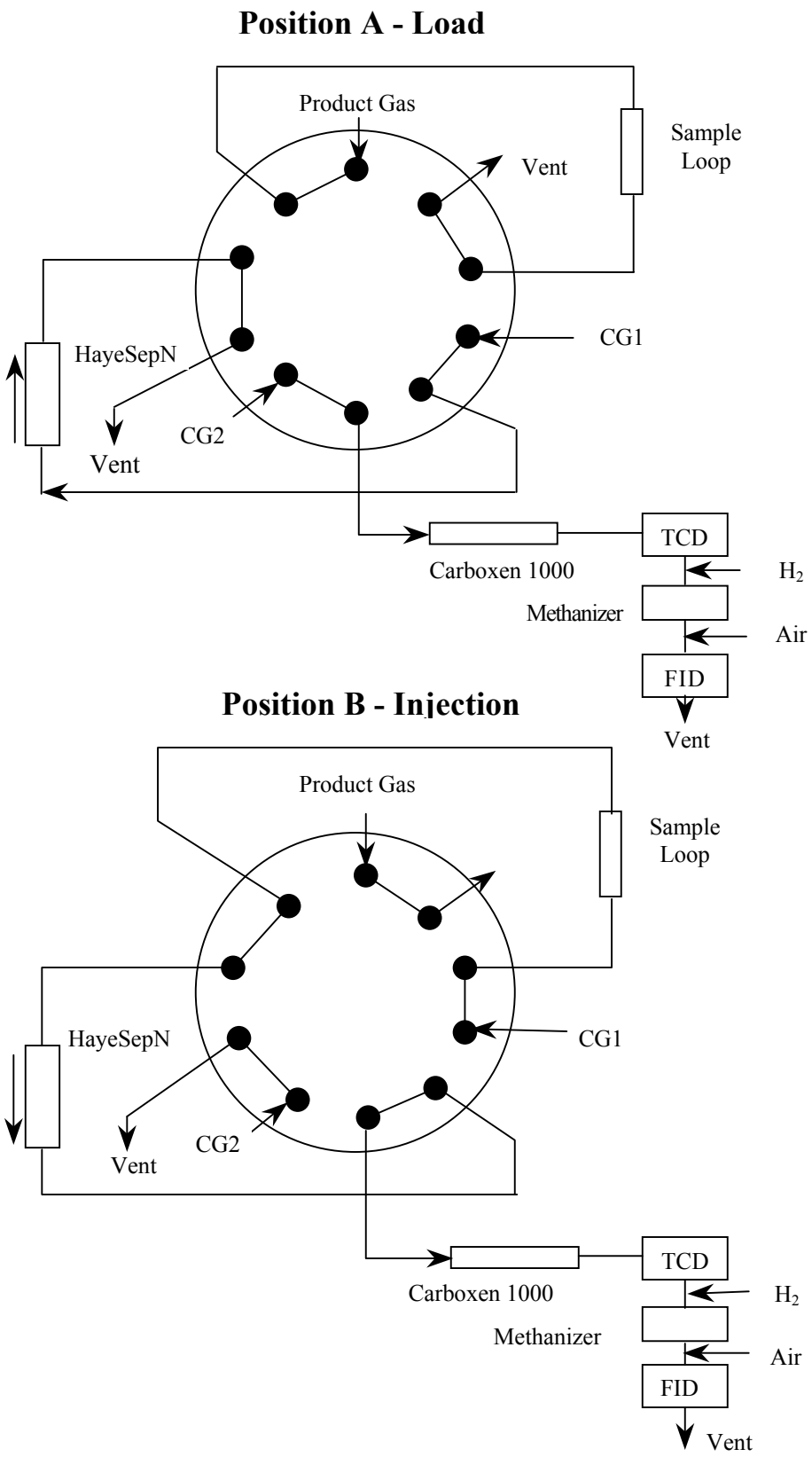

Figure 4-3 Operation of GC Sampling Valve

methanizer. Air and hydrogen at a ratio of at least 10:1 are needed for the FID.

Shimadzu Class-VP Version 4.2 software is used for data acquisition. Operating conditions and valve timing were obtained by trial-and-error. The product gas is sampled every twelve minutes since six minutes are needed for complete separation of all the components in the product gas and six more minutes to back-flush the HayeSepN column.

The GC is operated under conditions shown in Table 4-1. Before the power is switched on, compressed air, UHP H_2 and nitrogen are fed to the GC with their flow rates regulated by flow controllers. Then the heater and both detectors are actuated. The temperatures, heating procedures and operational scheme of the sampling valve are all programmed and saved in a specified file through the Keyboard Panel. The temperatures can also be monitored from the keyboard during heating and running to ensure that detectors and column are operated under their proper conditions.

Table 4-1 GC Operating Conditions

Carrier Gas		Nitrogen
Sample Loop Volume		0.5ml (Approx.)
Columns	HayeSepN	4ft x 1/8 inches
	Carboxen 1000	8ft x 1/8 inches
Column temperature		160°C
TCD temperature		63°C
FID temperature		250°C
Methanizer Temperature		380°C
Carrier Gas Flow Rate (CG1 and CG2)		37.9cm^3/min

The GC was calibrated using standard gases whose compositions are presented in Table 4-2.

Table 4-2 Composition of GC Calibration Gases, mol%

Standard#	CO	CH_4	CO_2	H_2	N_2
1	-	-	1.518	-	Balance
2	1.516	2.003	3.152	20.605	Balance
3	3.108	7.774	7.894	32.133	Balance
4	-	-	-	99.997	-
5	-	99.997	-	-	-
6	-	-	99.997	-	-

Three standard gas mixtures from Quality Gas Inc., along with UHP hydrogen, methane and CO_2 from BOC were used. Additional calibration points were obtained by diluting the calibration gases with a controlled mass flow of N_2. A typical chromatogram for the calibration gas mixture consisting of 1.516% CO, 3.152% CO_2, 2.003% CH_4, 20.605% H_2 and balance N_2 is shown in Figure 4-4. CO is only detected on the FID since its thermal conductivity is very close to that of the carrier gas, nitrogen. H_2 is only detected on the TCD. CO_2 and CH_4 appear on both TCD and FID, but the FID is used because of its higher sensitivity. The calibration formulas relating the mole percent composition and the detector response (area counts) are shown in Table 4-3. The final calibration curves used in data analysis are presented in Figure 4-5.

4.3 Materials

In the steam reforming reaction, the metals of group VIII in the periodic table are usually chosen as the candidates for catalysts. Ni is most frequently used in industrial applications. Some noble metals, such as Pt and Pd, also have high reforming activity, but

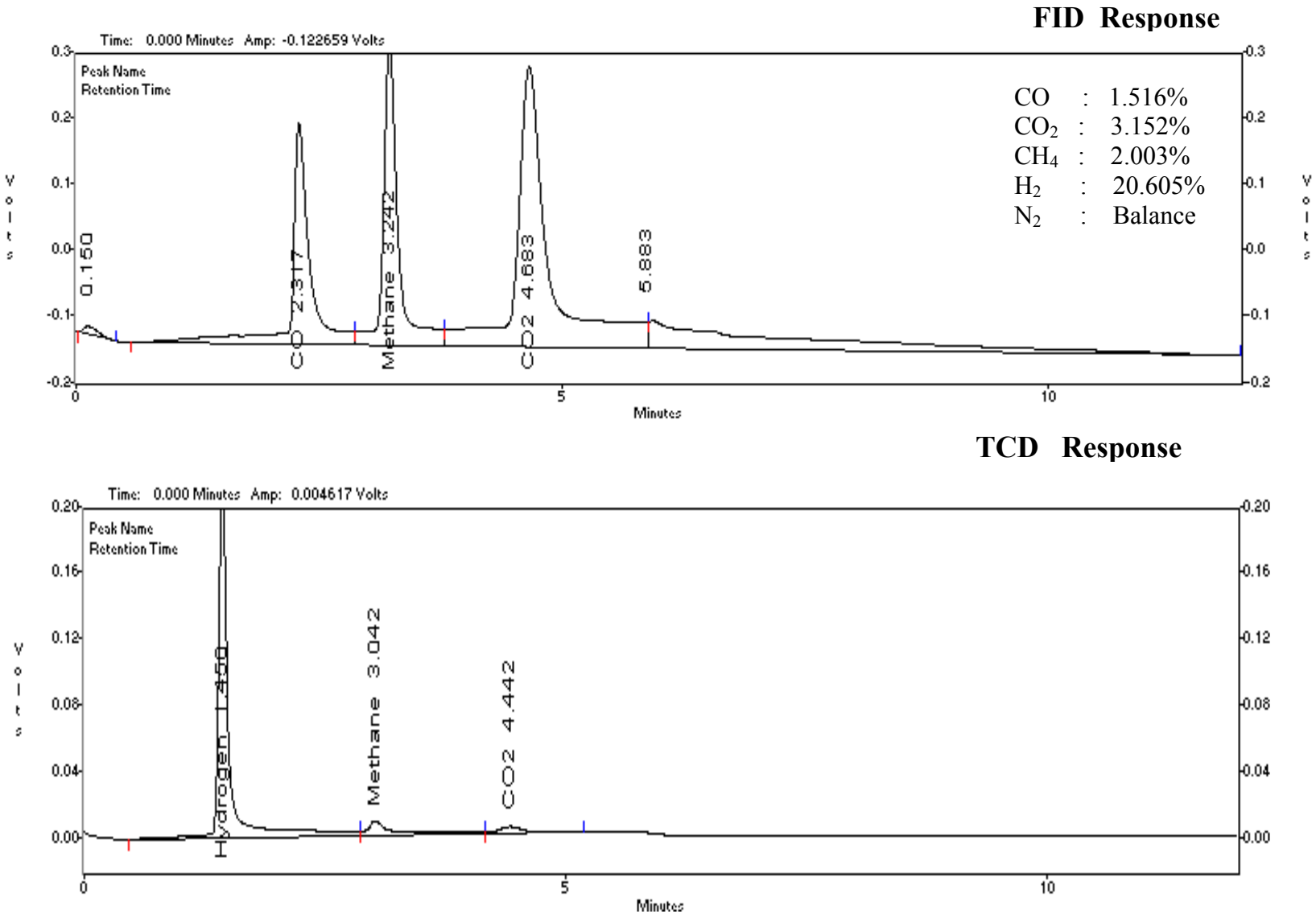

Figure 4-4 FID and TCD Response Curves to a Calibration Gas Mixture

Table 4-3 GC Calibration Formula

$$C=aA+bA^2$$

Component	Detector	Fit Type	*a*	*b*	R^2
H_2	TCD	Quadratic	1.061E-05	2.790E-13	0.9979
CH_4	FID	Quadratic	3.201E-08	4.177E-14	0.9927
CO	FID	Linear	4.931E-07	0	0.9997
CO_2	FID	Quadratic	1.947E-07	1.312E-14	0.9968

A = Area Count
C = mole percent
a, b = calibration formula coefficients
R^2 = correlation coefficient

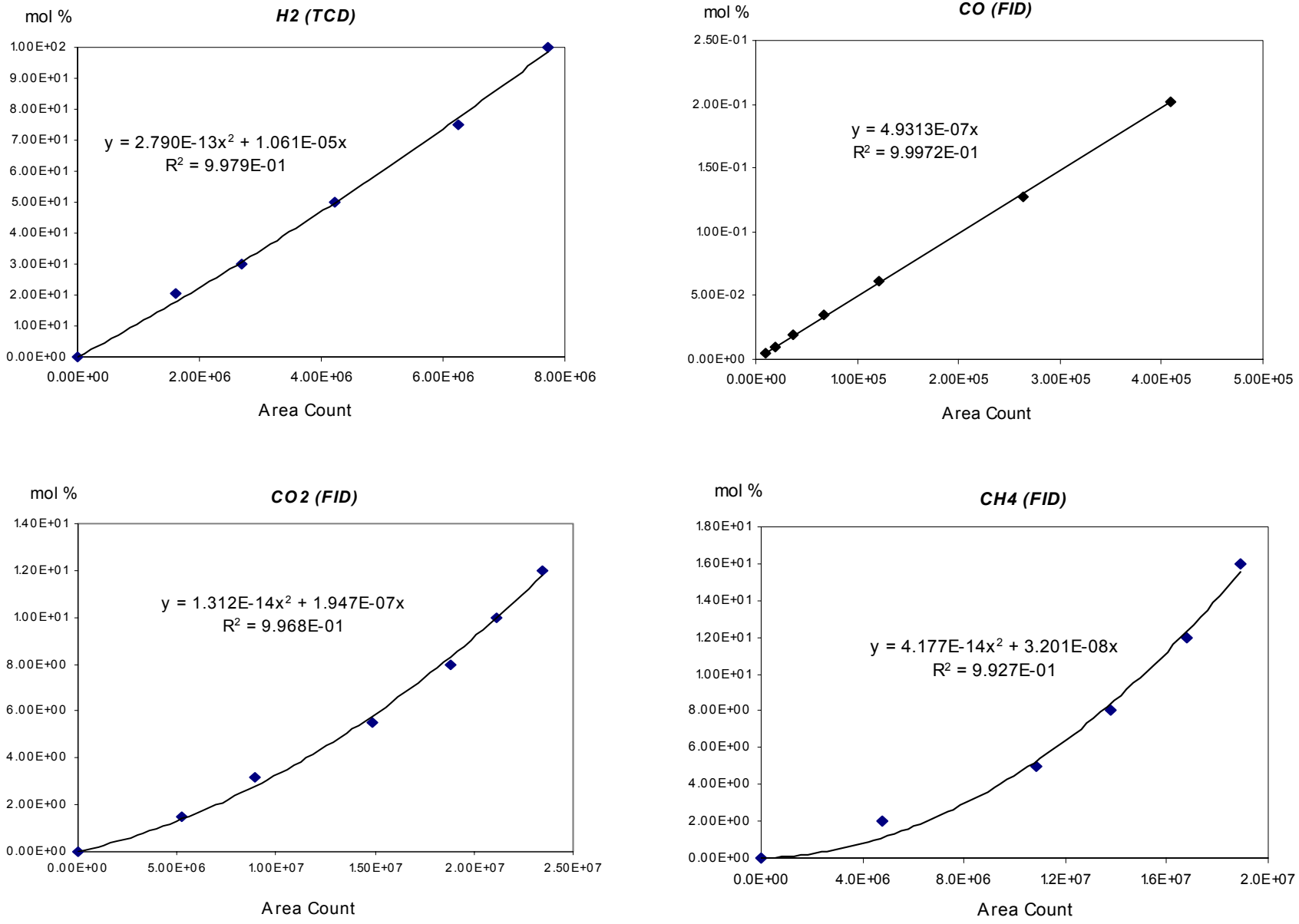

Figure 4-5 GC Calibration Curves

they are too expensive for general commercial use, except in some catalysts they are mixed with Ni in small amount as additives. Most industrial catalysts are supported on ceramic oxides, such as α-alumina or magnesia, to ensure that they have satisfactory mechanical strength. They are often made in the shape of rings, pellets or even more complicated shapes to obtain high surface area and to cause low pressure drop in the reactor.

In the sorption enhanced steam reforming process, the sorbent is utilized to selectively remove CO_2 from the product gas under a large partial pressure of steam. The requirement for the sorbent is that it should have a large adsorption capacity as well as fast kinetics for both adsorption (removal of CO_2 from the reaction zone) and desorption (sorbent regeneration) of CO_2. The material also needs to retain mechanical integrity in thermal cycling operation.

In the experimental study, two types of materials were used. The first material consisted of a commercial reforming catalyst mixed with calcined $CaCO_3$, which is common and relatively cheap. The performance of the catalyst and sorbent in the low temperature range suitable for producing H_2 containing low CO concentrations was studied thoroughly. The second type of material consisted of special catalyst/sorbent combinations developed by TDA. Their activity in the steam reforming reaction at high temperature was evaluated and the impact of the composition of the catalysts on the activity were compared in detail.

4.3.1 Nickel Catalyst and Calcined $CaCO_3$

In one phase of the research, the reactor insert was packed with a mixture of commercial reforming catalyst and calcined $CaCO_3$. The reforming catalyst from United

Catalysts (C11-9-02), originally in the shape of wagon-wheel pellets, was crushed into small particles and then sieved to get a particle size range of 75<dp<150 microns. The catalyst consisted of NiO supported on α-alumina. The mass content of NiO was about 22%.

The sorbent CaO was maded by calcining 99.97% $CaCO_3$ from Fisher Scientific in pure N_2 flowing at 300 cm^3/min (STP) at 850°C and 1 atm. The particle size of $CaCO_3$ precursor ranged from 75 to 150 microns.

4.3.2 Sample Materials from TDA

The other phase of the research used materials developed by TDA. These materials were in the form of small cylindrical pellets of diameter from 3mm to 5mm and consisted of a mixture of reforming catalyst and CO_2 acceptor. The samples were prepared at TDA by mixing the active catalyst and CO_2 sorbent with additives to improve the mechanical strength. The support contained TiO_2 or $CaCO_3$. The catalytic component, primarily Pt, was then impregnated into the support. Platinum was the primary catalyst in most of the samples, with nickel or nickel oxide used alone or mixed with platinum in some samples. A small amount of Rh was introduced into selected samples via impregnation to improve the stability of Pt by minimizing sintering. Cerium dioxide was also used in some samples to provide better oxygen management between the reducing and oxidizing environments, an important factor in the cyclic process. The content of Pt varied from 0.1% to 0.8% while the Ni varied from 0 to 4% (all by weight). The sample support materials were fired by TDA at a temperature near 1000°C for varying periods of time with methocel solution as a binder. Dolomite or $CaCO_3$ acted as the CO_2 sorbent precursor. Most of these materials contained about 20% free CaO which, based on TDA's studies, yields the best CO_2 adsorption capacity. K_2CO_3 was introduced into the sorbent as a promoter in some samples to help to remove small quantities of carbon that may be

deposited over the pellets during the reaction. In some formulations, NaF was added as an enhancer to the binder to improve its crush strength, which is critical to provide long life and mechanical stability.

4.4 Experimental Procedures Using Commercial Reforming Catalyst and $CaCO_3$

4.4.1 Preliminary Steps

Approximately 7g of catalyst powder and 13g of $CaCO_3$ powder were mixed and loaded into the reactor insert and supported by a stainless steel porous disc. A layer of quartz wool covered the porous disc to prevent solid particles from filling the pores of the disc and blocking its path for gases. Another layer of quartz wool was placed on the top of the sorbent to prevent the solid powder from spilling out of the insert due to possible back-flow caused by pressure fluctuations during the experiment. The reactor insert was then coupled to the pressure vessel, with silicone O-ring seals used to maintain the reactor pressure. After all the lines were connected properly, N_2 was fed at 300 cm^3/min (STP) to purge the system.

4.4.2 Calcination

The furnace was switched on and the reactor was heated at a rate of approximately 8°C/min to 800°C where the $CaCO_3$ was calcined to CaO. When the temperature approached 800°C, the GC was switched on to monitor the CO_2 content of the gases eluted from the reactor. Calcination was complete when no CO_2 was observed in the product gas. This step required roughly 2 hours.

4.4.3 Reaction

The back pressure regulator was used to pressurize the system to the desired pressure. Snoop leak detector was used to check for leakage at all connections, especially near the

bottom of the reactor. When no leakage was detected, all feed lines were heated to a temperature above the saturation temperature of H_2O at that pressure. The reactor temperature was then adjusted to the desired isothermal reaction temperature using the furnace controller. After the furnace and the feed line temperatures became steady, CH_4 and steam were fed to the reactor and their flow rates adjusted to the desired values. The GC data acquisition system was started the instant the reactive gases were fed to the reactor. The composition of the product gases as a function of time was then determined using the GC.

At the end of the run, the CH_4 flow was stopped first. The water feed was maintained for additional time to ensure that residual CH_4 would not decompose to carbon over the catalyst. The water was then cut-off and the reactor was purged with N_2. The pressure was then slowly reduced to 1 atm. The power supply for the furnace and the heating tapes were then turned off.

Liquid water from the condenser was drained and the mass was measured for a rough material balance check.

4.5 Experimental Procedures Using TDA Samples

The TDA samples are different from commercial Ni based catalysts in that they need to be activated before use.

4.5.1 Preliminary Steps

Approximately 2g of TDA samples in their original pellet shape were loaded into the reactor insert and supported by a stainless steel porous disc. A layer of quartz wool covered the porous disc to prevent any possible fine solid particles from filling the pores of the disc. The reactor insert was then coupled to the pressure vessel, with silicone

O-ring seals used to maintain the reactor pressure. After all the lines were connected properly, N_2 was fed at 300 cm^3/min (STP) to purge the system.

4.5.2 Activation

98% mol percent of CO_2 and 2% mol percent of H_2 were fed at a total flow rate of 500 cm^3/min (STP) and 1 atm to the reactor insert to clean the surface and form the active catalyst. The furnace was switched on and the reactor was heated at a rate of approximately 8°C/min to 850°C and maintained at 850°C for 4 hours in this step. The presence of CO_2 prevented the decomposition of $CaCO_3$ to CaO at activation conditions.

4.5.3 Calcination

CO_2 and H_2 flows were stopped and N_2 was fed at 300cm^3/min (STP) at 1 atm. The reactor was maintained at 850°C for an additional 2 hours for calcination of the sorbent precursor. The GC was switched on to monitor the composition of the exit gas from the reactor. The calcination was complete when no CO_2 was observed in the product gas.

4.5.4 Reaction

This step followed the same procedures used when testing the commercial reforming catalyst and CaO except that the total flow rate of the feed gas was set at different levels while keeping the composition unchanged to observe the decrease of the reaction rate at a high space velocity. The flow rate was initially set at 360 sccm and kept at that level for sufficient time until the H_2 concentration reached a steady state. Then the flow rate was increased to higher levels, such as 720 sccm and 1080 sccm, to observe the reduced H_2 concentration due to the decreased residence time. Finally the flow rate was returned to 360 sccm to examine the activity maintenance of the catalyst. Sufficient time was allowed at each flow rate for the H_2 concentration to reach a steady state.

The conditions of a standard test using the TDA samples are illustrated in Table 4-4.

4.6 Thermogravimetric Analyzer System (TGA)

A Cahn Instruments Inc. Model 2000 TGA system was used for characterization tests of the reforming catalyst and the sorbent. A diagram of the system is shown in Figure 4-6. The TGA system is composed of a gas flow system, a Cahn 2000 electrobalance, a MicRICON temperature programmer, and a PC for data acquisition. The TGA monitors the weight change of a reacting solid, with a precision of 0.01mg. The temperature is controlled through a temperature programmer which allows either isothermal operation or a linearly increasingly temperature profile. The data center simultaneously records the temperature and weight as a function of time.

All gases were obtained from high purity cylinders and flow rates were regulated by needle valves using calibrated rotameters. Helium was chosen as the inert gas to minimize aerodynamic noise. He was fed through the upper flow path to blanket the balance mechanism and protect it against corrosive gases. Additional He together with reactive gases were premixed and entered the reactor through the sidearm of the hangdown tube. The combined gases flowed downward over the solid held in the sample boat and exited from the bottom of the reactor tube to the laboratory hood. The hangdown wire is made of platinum while the sample boat is made of quartz, both of which can withstand a temperature as high as 1000°C. Reaction temperature was monitored using a chromel-alumel thermocouple positioned approximately 1/4” below the sample boat. The thermocouple signal was transmitted to the MicRIcon temperature controller and to the data center.

Table 4-4 Test Conditions Using TDA Samples

Step	Temperature (°C)	Pressure (atm)	Total Flow Rate (sccm)	Composition of Feed Gas (mol%)				
				CO_2	H_2	CH_4	H_2O	N_2
Reduction	850	1	500	98%	2%			
Calcination	850	1	300					100%
Reaction	800	5	360			11.1%	33.3%	55.5%
			720			〃	〃	〃
			1080			〃	〃	〃
			360			〃	〃	〃

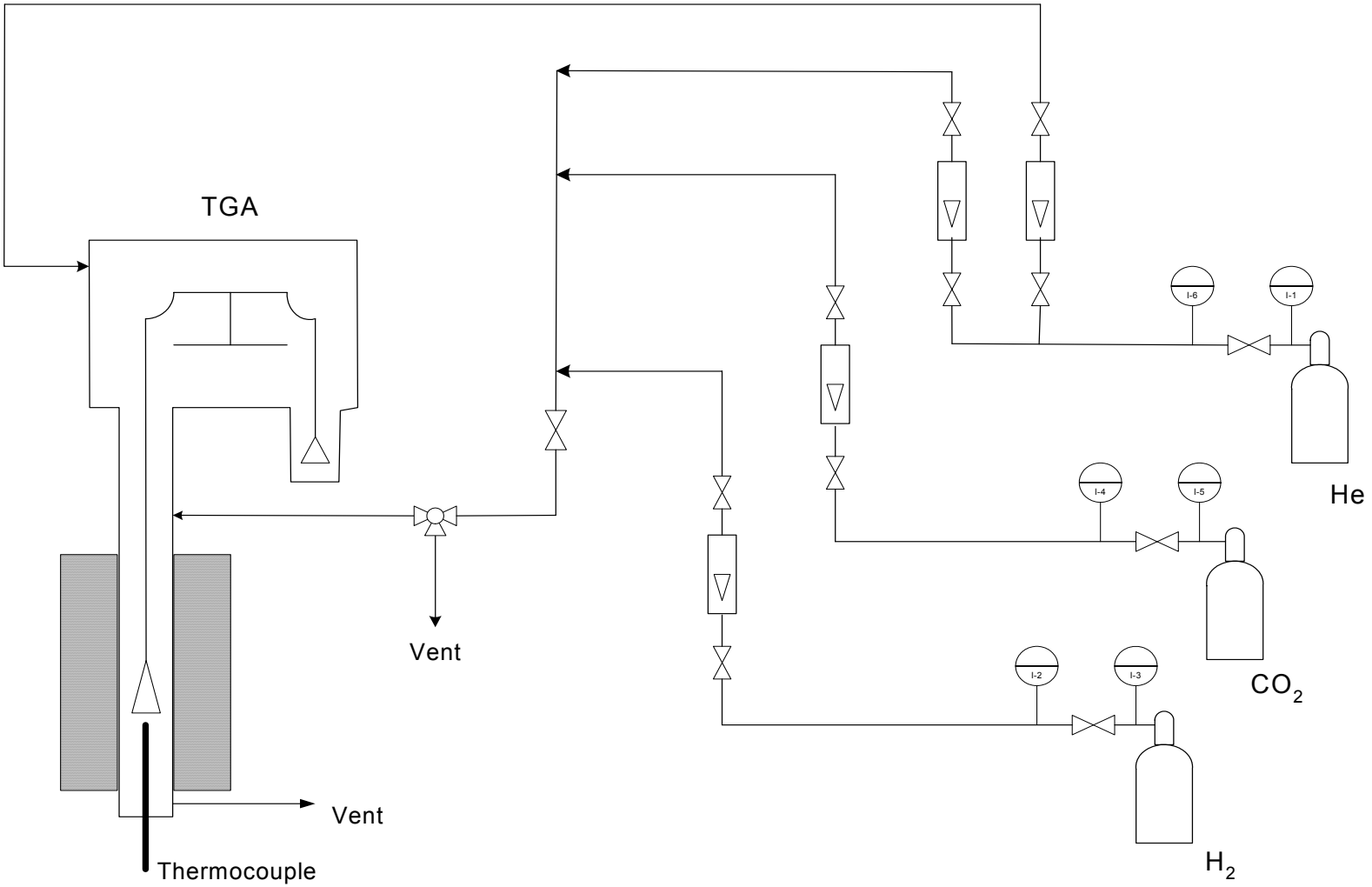

Figure 4-6 Schematic of the TGA System

CHAPTER 5

EVALUATION OF TDA CATALYST-SORBENT SAMPLES

In this chapter, results of tests using the catalyst-sorbent samples from TDA in the fixed-bed reactor and TGA are presented. Their performance was experimentally studied and evaluated with respect to parameters such as temperature, steam-to-carbon (S/C) ratio, flow rate, etc. The catalyst was successively subjected to activation, calcination and reaction steps that were described in Chapter 4. When the run was ended, the temperature and the pressure of the reactor were reduced to 400°C and 1 atm, respectively. Compressed air was fed to burn off any possible coke formed on the surface of the catalyst so it can be regenerated for multicycle runs. The standard test conditions for a catalyst sample are shown in Table 5-1.

Table 5-1 Standard Test Conditions for a Catalyst Sample from TDA

	Activation	Calcination	Reaction	Regeneration
Temperature, °C	850	850	800	400
Pressure, atm	1	1	5	1
Gas Composition	95% CO_2 2% H_2	100% N_2	11.1% CH_4 33.3% H_2O 55.6% N_2	Air
Flow Rate, sccm	500	300	360, 720, 1080, 360	100

During the reaction phase of the test, the total feed rate was incrementally increased from 360sccm to 720sccm, 1080sccm and back to 360sccm. The flow rate was maintained at each level for sufficient time to confirm steady-state conditions. The amount of sample used in the test was determined through trial-and-error. Two grams of sample was found to be suitable to observe an appreciable difference of steady-state H_2

concentration with increased flow rates. A typical experimental result using sample 447-66B under standard testing conditions is presented in Figure 5-1.

The solid horizontal line represents the equilibrium value of H_2 concentration at the test conditions. From this figure, it is seen that the steady-state H_2 concentration decreased with increased flow rate. At the lowest flow rate of 360sccm, the steady-state H_2 concentration was 35.7%, which closely approached the equilibrium value of 35.5%. At a higher flow rate of 720sccm, the steady-state H_2 concentration was 33.5%, which was 1.94% less than the equilibrium value. At the highest flow rate of 1080sccm, the steady-state H_2 concentration further decreased to 27.8%, 8.03% less than the equilibrium value. The decrease of steady-state H_2 concentration with increased flow rate indicated that 2 grams of catalyst was not sufficient to drive the reactions to equilibrium when the residence time of reacting gases was reduced. When the flow rate was set back to 360sccm, the steady-state H_2 concentration returned to 35.4%, which also closely approached the equilibrium value of 35.5% and was just slightly lower than the first steady-state value of 35.7%. This indicated that the activity of this catalyst was well maintained during tests under different flow rates.

In the catalyst/sorbent sample there is only small amount of free CaO (about 20wt% or 0.4 g), while the sampling frequency of the GC was 12 minutes. For a feed gas at 360 sccm that contains 11.1% CH_4, the free CaO is consumed in 4 min assuming 100% CH_4 conversion and 100% CO_2 removal. This is the reason why the first steady-state of the combined reforming-shift-carbonation reactions, or the so-called prebreakthrough period, was not observed during the test. The emphasis of the experimental studies of the TDA catalyst/sorbent materials therefore focused on evaluating the factors influencing the catalyst

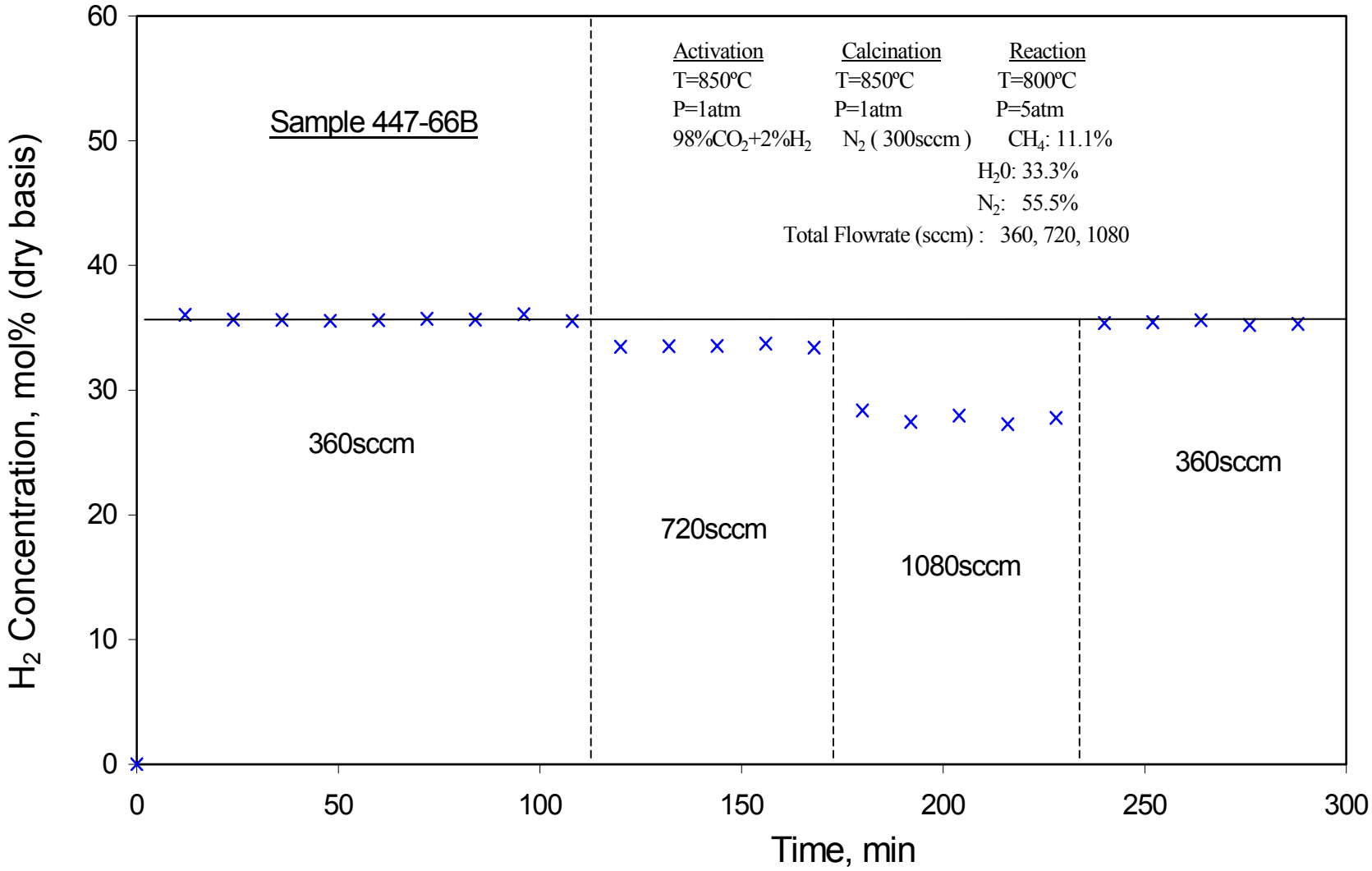

Figure 5-1 H_2 Concentration as a Function of Time and Volumetric Feed Rate

activity under conditions where only the reforming, shift and calcination reactions could occur.

A total of 7 groups of catalyst/sorbent samples were supplied by TDA with their compositions summarized in Table 5-2. Among these samples, the catalysts from group 3 were thoroughly investigated. Volumetric flow rate (or space velocity), reforming temperature and steam-to-carbon ratio were considered to be the main factors that influence the activity of the catalyst. During the experiments, the reforming temperature was varied in the range of 600°C to 800°C and the S/C ratio was varied in the range of 3.0 to 0.8. The volumetric flow rate was changed between 360sccm, 720sccm, and 1080sccm, which correspond to the space velocities of 9750 hr^{-1}, 19500 hr^{-1}, and 29250 hr^{-1}, respectively. Catalysts from the remaining groups were tested only at standard conditions.

5.1 Factors Influencing the Activity of Catalyst

5.1.1 Effect of Temperature and Volumetric Flow Rate

Figure 5-2 shows the H_2 concentration with time as a function of reaction temperature and feed rate for group 3 catalyst 447-66B (0.8wt% Pt). This catalyst was tested at reaction temperatures of 800°C, 700°C, and 650°C. The feed gas contained 11.1% CH_4 with a S/C ratio of 3.0.

To facilitate comparison of the experimental results at the different test conditions, the original gas composition plot has been simplified by using the concept of normalized H_2 content. The average H_2 content at each steady-state was first determined. The normalized H_2 content is defined as the ratio of the H_2 content at a certain reaction temperature, feed rate and S/C ratio to the H_2 content at 800°C, 360sccm and a S/C ratio of 3.0.

$$\text{Normalized } H_2 \text{ Content} = \frac{\%H_2(T,Q,S/C)}{\%H_2(800^\circ C,360sccm,3)}$$

Table 5-2 Summary of Composition of TDA Samples

Sample ID	**Sample Support Composition**	Active Component Composition
Group 1		
413-85-1	20% $CaO/CaTiO_3$	0.05 wt% Pt
413-85-2		0.1 wt% Pt
413-85-3		0.2 wt% Pt
413-85-5		2.0 wt% Ni
413-85-6		4.0 wt% Ni
Group 2		
359-97A	20wt% dolomite (E-2) 28wt% $TiO_2/CaCO_3$	0.1 wt% Pt
359-97A (remake)		
359-97B		0.4 wt% Pt
359-97B (remake)		
Group 3		
415-73	20wt% dolomite (E-2) 28 wt% $TiO_2/CaCO_3$	0.764 wt% NiO
415-73Pt (large batch)		0.764 wt%NiO / 0.4 wt% Pt
447-66B		0.8 wt% Pt
447-66H		0.1 wt% Pt
Group 4		
447-93	63wt% CaO / 24wt% TiO_2 / 8wt% K_2CO_3 / 5wt% $Ni(NO_3)_2$	0.8 wt% Pt
447-93A		0.8 wt% Pt / 1wt% Ni
447-88B		0.4 wt% Pt
Group 5		
413-89		0.8wt%Pt-TiONa-CO2
475-43	20wt% dolomite 28wt% $TiO_2/CaCO_3$	none
475-45		0.8 wt% Pt
475-46		0.8 wt% Pt / 0.1 wt% Rh
475-46A	$MgAl_2O_4$	2.0 wt% Ni
Group 6		
475-47A	20wt% dolomite 28wt% $TiO_2/CaCO_3$	0.8 wt% Pt
475-47B		0.8 wt% Pt / 0.1 wt% Rh
475-47C		0.8 wt% Pt / 2.5 wt% CeO_2
475-47D		0.8 wt% Pt / 0.1 wt% Rh / 2.5 wt% CeO_2
475-48A		0.8 wt% Pt / 2.5 wt% CeO_2
475-48C		0.8 wt% Pt / 0.1 wt% Rh / 2.5 wt% CeO_2
Group 7		
475-49	N/A	N/A
475-50A		
475-50B		
475-50C		
475-50D		

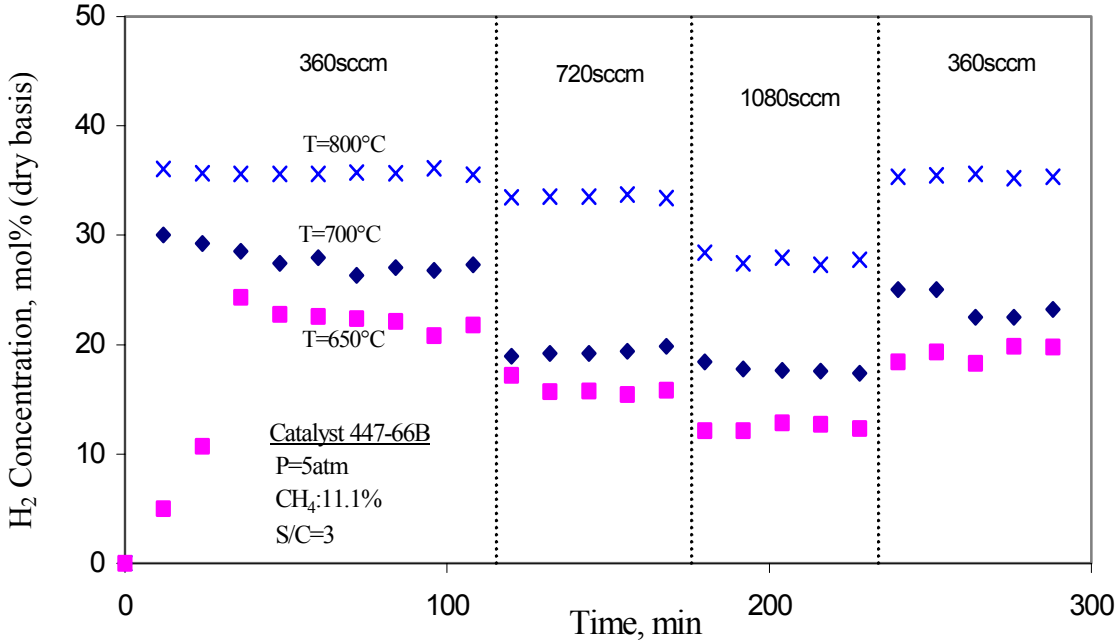

Figure 5-2 H_2 Concentration with Time as a Function of Reaction Temperature: Catalyst 447-66B

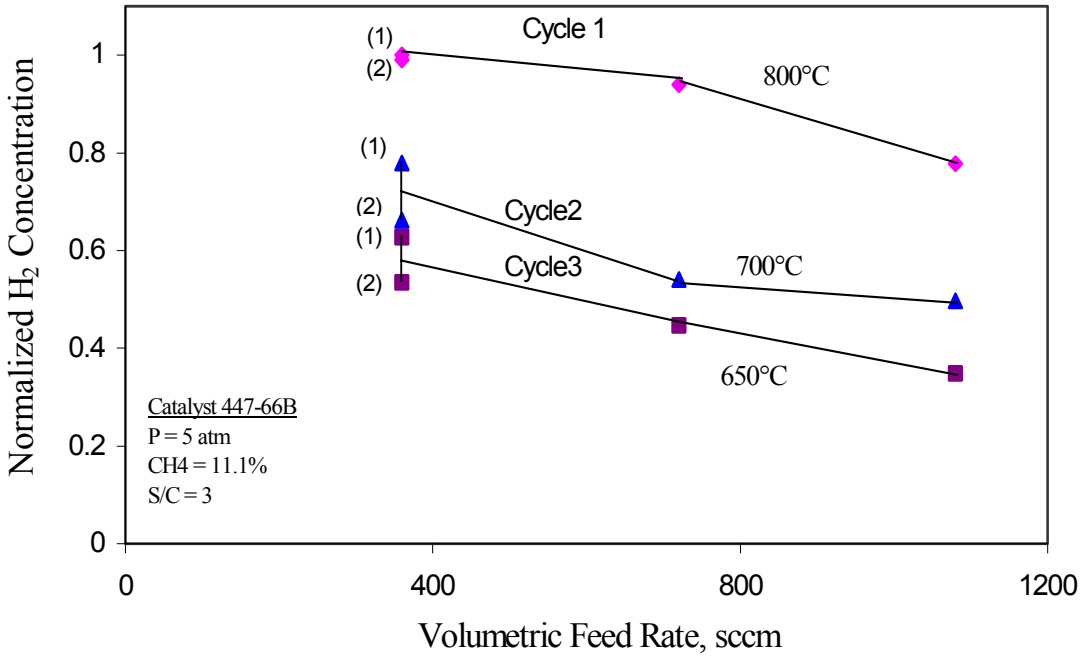

Figure 5-3 Normalized H_2 Concentration as a Function of Reaction Temperature and Volumetric Feed Rate: Catalyst 447-66B

The H_2 content during the first 360sccm steady-state period was used in this definition because usually the H_2 content at the second 360sccm steady-state was lower.

The simplified representation of Figure 5-2 is presented in Figure 5-3. The normalized H_2 content is plotted against volumetric feed rate instead of time. This sample was first tested at 800°C, therefore the results at 800°C are labeled as cycle 1 in the plot. The results at 700°C and 650°C are labeled as cycle 2 and cycle 3, respectively. In the plot, the H_2 content during the first and the second 360sccm periods are distinguished by labels (1) and (2).

From Figures 5-2 and 5-3, it is clear that the H_2 content decreases with increased volumetric feed rate at all temperatures. This can be explained from the point of heterogeneous reactions. The molecules in the gas phase are first absorbed on the surface of the catalyst, then the absorbed molecules react with the aid of the catalyst. Finally the product molecules are desorbed from the surface of the catalyst and returned to the gas phase. When the flow rate, or the space velocity, increased over some threshold, not all of the molecules had the chance to be absorbed and reacted on the catalyst. The reaction cannot reach thermodynamic equilibrium and this results in a decrease in the H_2 content in the product gas.

Figures 5-2 and 5-3 also show that the activity of catalyst 447-66B decreased with decreasing temperature. The normalized H_2 content decreased from 1.0 at 800°C and 360sccm to 0.78 at 700°C and 360sccm, and to 0.63 at 650°C and 360sccm. At 800°C, the difference in H_2 content between the first period of 360sccm and the second period of 360sccm was only 1%, suggesting that there was effectively no decrease in catalyst

activity. At 700°C and 650°C, the difference in H_2 content between the first period of 360sccm and the second period of 360sccm was more significant.

Similar results for catalyst 447-66H (0.1wt% Pt), also from group 3, are presented in Figures 5-4 and 5-5. In Figure 5-4, the catalyst was tested at 800°C, 700°C and 600°C, consecutively. The lowest temperature was 600°C rather than 650°C used for catalyst 447-66B. The gas feed also contained 11.1% CH_4 with a S/C ratio of 3. In Figure 5-5, the catalyst was tested under similar conditions except a S/C ratio of 2 instead of 3 was used, and the temperature sequence was reversed with cycle 1 at 600°C. At all temperatures and S/C ratios, the H_2 content decreased with increased feed rate. At 800°C and a S/C ratio of 3 (Figure 5-4), the normalized H_2 content returned to 0.89 when the flow rate was set back to 360sccm from the highest value of 1080sccm, indicating a moderate loss in activity. At 600°C, the catalyst was nearly inactive, with the normalized H_2 content below 0.2. The results were similar for a S/C ratio of 2 and 800°C as shown in Figure 5-5.

Another point worthy of note is that the loss of activity of the catalyst with decreased temperature cannot be attributed to the test sequence. The lowest catalyst activity occurred at 600°C regardless of the temperature sequence.

5.1.2 Effect of Steam-to-Carbon Ratio

According to thermodynamic calculations presented in Chapter 3, reducing the S/C ratio should result in a decrease in the H_2 content in product gas. Experimental results, which are presented in Figure 5-6 for catalyst 447-66H (0.1wt% Pt) and Figure 5-7 for catalyst 415-73Pt (0.4wt% Pt+0.764wt% NiO), agree with thermodynamic calculations. Both of these two catalysts are from group 3. The feed gas contained 11.1% CH_4 in all

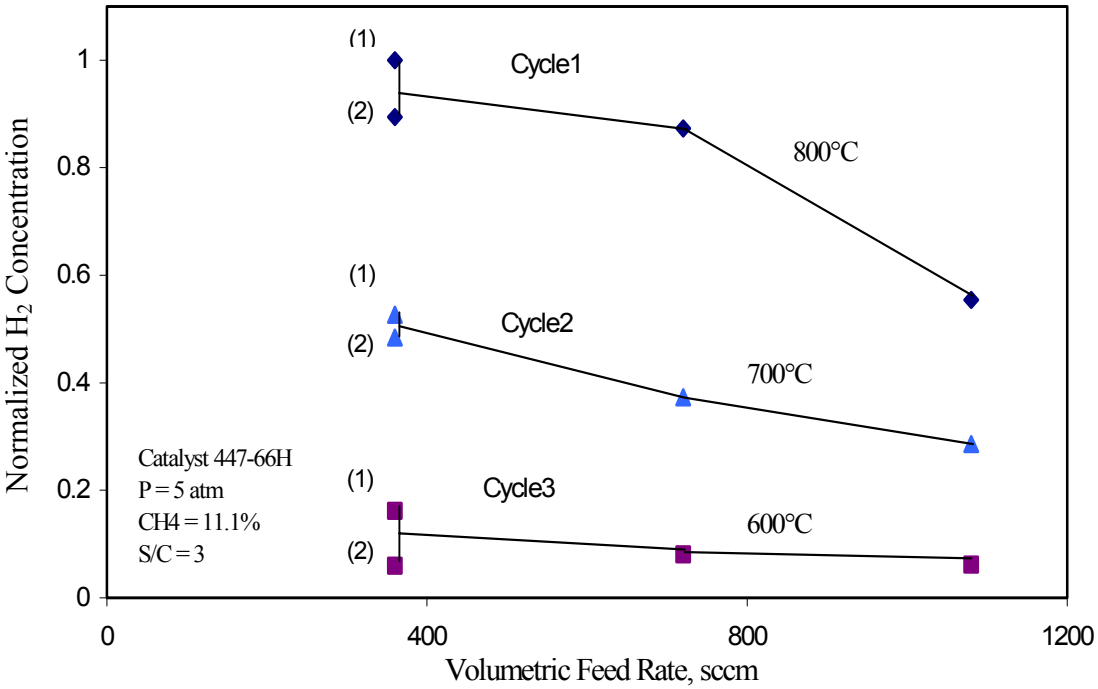

Figure 5-4 H_2 Concentration as a Function of Reaction Temperature and Volumetric Feed Rate at a S/C Ratio of 3.0: Catalyst 447-66H

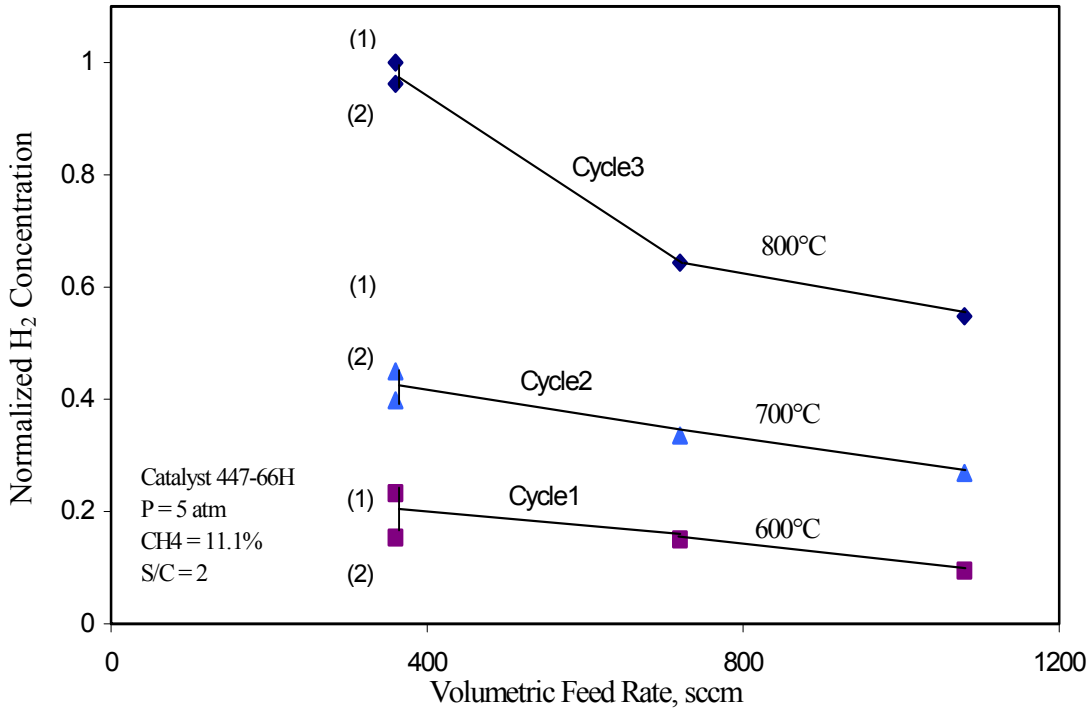

Figure 5-5 H_2 Concentration as a Function of Reaction Temperature and Volumetric Feed Rate at a S/C Ratio of 2.0: Catalyst 447-66H

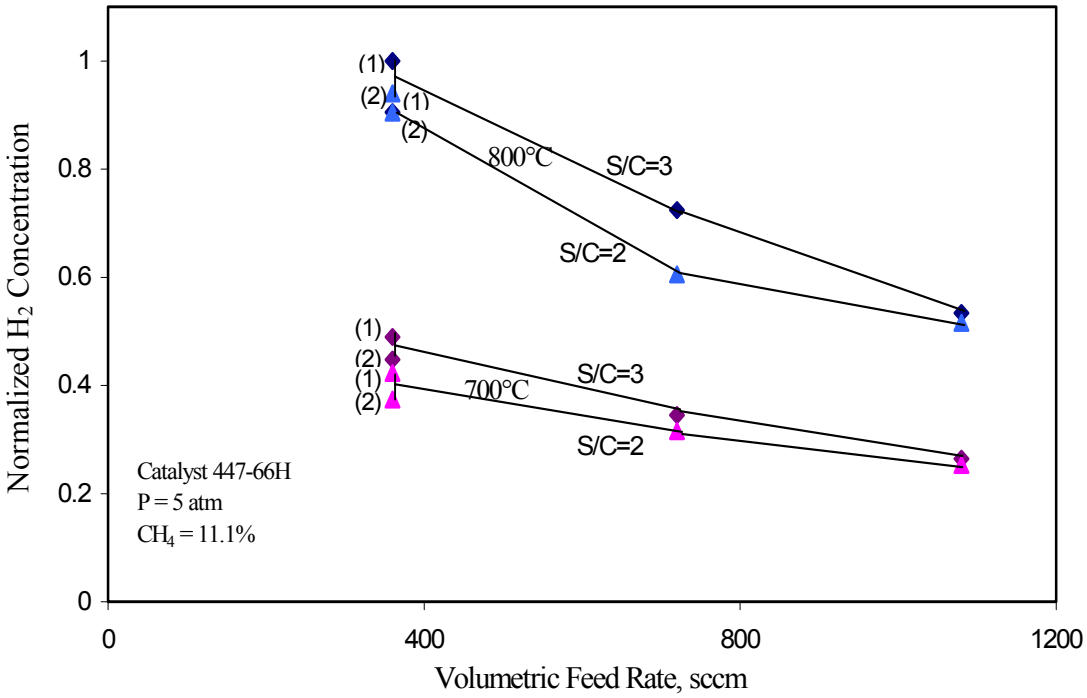

Figure 5-6 H_2 Concentration as a Function of Reaction Temperature and S/C Ratio: Catalyst 447-66H

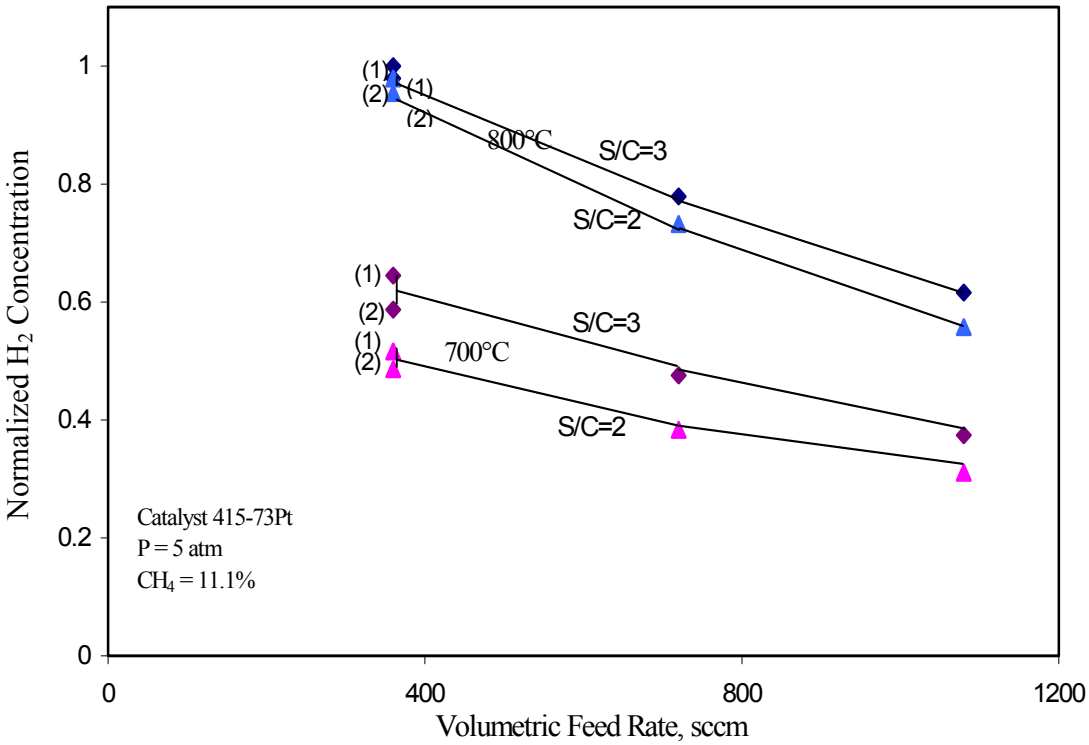

Figure 5-7 H_2 Concentration as a Function of Reaction Temperature and S/C Ratio: Catalyst 415-73Pt

tests. The S/C ratio was reduced by decreasing the H_2O feed rate while increasing the N_2 to keep the total feed rate constant.

From Figures 5-6 and 5-7, we see that reducing the S/C ratio resulted in a decrease in H_2 content at all temperatures and feed rates for both catalysts. In Figure 5-6, where catalyst 447-66H was used, the normalized H_2 content decreased from 1 to 0.94 at 800°C and 360sccm when the S/C ratio was reduced from 3 to 2. At 700°C, the reduction in the S/C ratio produced a similar effect on the H_2 content except that the extent of the decrease varied. In Figure 5-7, where catalyst 415-73Pt was used, the most significant decrease of H_2 content, from 0.64 to 0.51, occurred at 700°C and 360sccm when the S/C ratio was reduced from 3 to 2. Thus a 33% reduction in H_2O feed resulted in a much smaller reduction in H_2 content.

Further experimental studies of the effect of S/C ratio on the H_2 concentration of theproduct gas were carried out using catalyst 447-66B. The temperature was kept at 800°C and the total feed rate was maintained at 720sccm in all experiments. The S/C ratio was decreased stepwise from 3 to 1.5 or even lower and restored to 3 at the end of run.

The results are presented in Figures 5-8 and 5-9 for catalyst 447-66B. In Figure 5-8, the S/C ratio was incrementally reduced from 3 to 2.5, 2.0, 1.5, and back to 3.0 at the end of the run. Steady-state H_2 content was achieved for all the S/C ratios. The H_2 content was 34.1% during the first steady-state period at S/C=3.0, and decreased to 31.9%, 30.4%, 28%, respectively, when the S/C ratio was decreased to 2.5, 2.0, 1.5. When the S/C ratio was set back to 3.0, the H_2 content was restored to 33%. The H_2 contents at S/C=3.0 and S/C=2.5 are slightly lower than the corresponding equilibrium values of

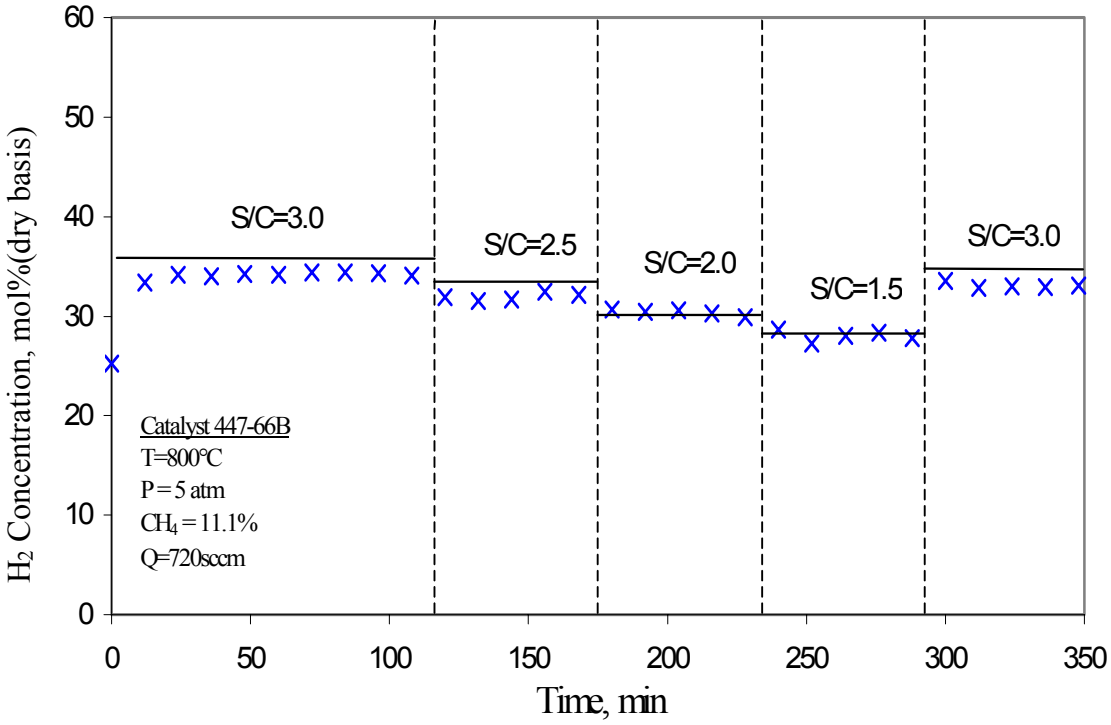

Figure 5-8 H_2 Contentration with Time as a Function of S/C Ratio (1.5 - 3)

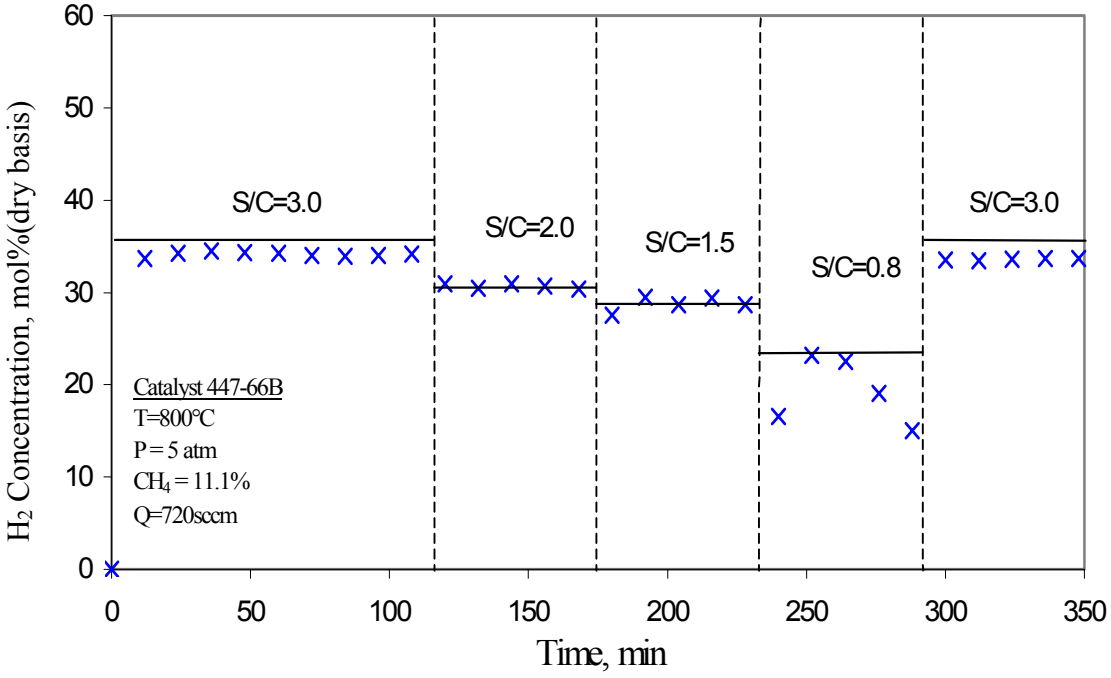

Figure 5-9 H_2 Contentration with Time as a Function of S/C Ratio (0.8 - 3)

35.5% and 33.0%, while at S/C=2.0 and S/C=1.5, the H_2 contents closely approached the equilibrium values. These results suggested there was no significant carbon deposition during the test, which was consistent with equilibrium calculations at the S/C ratios tested.

In Figure 5-9, the S/C ratio was incrementally reduced from 3 to 2.0, 1.5, 0.8, and back to 3.0 at the end of the run. The lowest S/C ratio of 0.8 was tested because it is the ratio at which carbon deposition becomes favored in equilibrium calculations. In the test, steady-state H_2 content was achieved at all S/C ratios except at S/C=0.8. The H_2 content approached the equilibrium values at S/C ratios of 2.0, and 1.5 and was slightly lower than the equilibrium value at S/C ratio of 3.0, similar to the results in Figure 5-8. However at S/C=0.8 the H_2 content decreased continually with time, and was well below the equilibrium value of 23%. But when the S/C ratio was returned to 3.0, the H_2 content was quickly restored to near equilibrium steady-state. No significant carbon deposition was found by a visual check after the test. Therefore we conclude that if the decrease in H_2 content at S/C=0.8 was caused by formation of coke, it was immediately oxidized by steam when the S/C ratio was returned to 3.0.

5.1.3 Comparison of Pt-based Catalysts

Among the catalysts in group 3, two catalysts contained only Pt, one catalyst contained only Ni, and the other contained a mixture of Pt and Ni. The Pt content in these catalysts ranged from 0.1% to 0.8wt%. The performance of these catalysts was evaluated and compared based on their Pt content. The concept of Turnover Ratio (TR), which is defined as the mols of H_2 produced per second per mol of Pt, was introduced to facilitate

this evaluation. Although NiO was also present in the catalyst containing 0.4% Pt, it was ignored in this analysis because the content of NiO was only 0.764wt%, while in commercial reforming catalysts the NiO content is usually as high as 20%.

In Figure 5-10, turnover ratio is plotted versus volumetric flow rate for reaction conditions of 800°C, 5atm, 11.1% CH_4 and a S/C ratio of 3.0. From this figure, it is seen that the turnover ratio increased slightly with increased volumetric flow rate for all three catalysts. The increase was significant between feed rates of 360 sccm and 720 sccm, while the further increase to 1080sccm produced only a minor increase in turnover ratio, suggesting that the Pt was efficiently utilized at 720sccm. The turnover ratio was the lowest at 360 sccm for all the three catalysts because, at this flow rate, the H_2 content closely approached its equilibrium value and the full potential activity of the catalysts was not achieved. It is also seen that the order of turnover ratio of the catalysts was opposite to the order of the Pt content. Catalyst 447-66H with the lowest Pt content of 0.1wt% had the highest turnover ratio while catalyst 447-66B with highest Pt content of 0.8wt% had the lowest turnover ratio. Thus catalyst 447-66H made the most efficient use of the Pt. The lower turnover ratio of catalysts 415-73Pt and 447-66B containing higher levels of Pt may be attributed to agglomeration of the Pt molecules, making a portion of the Pt inaccessible to the reacting gases.

Higher turnover ratio does not mean higher H_2 content in the product gas. In Figure 5-11, the experimental results of H_2 concentration at 700°C using catalysts containing different levels of Pt are presented as a function of feed rate. From this figure, it is clearly seen that catalysts 447-66B and 447-66H, containing the highest and lowest level of Pt (0.8wt% and 0.1wt%), also produced the highest and lowest H_2 concentration.

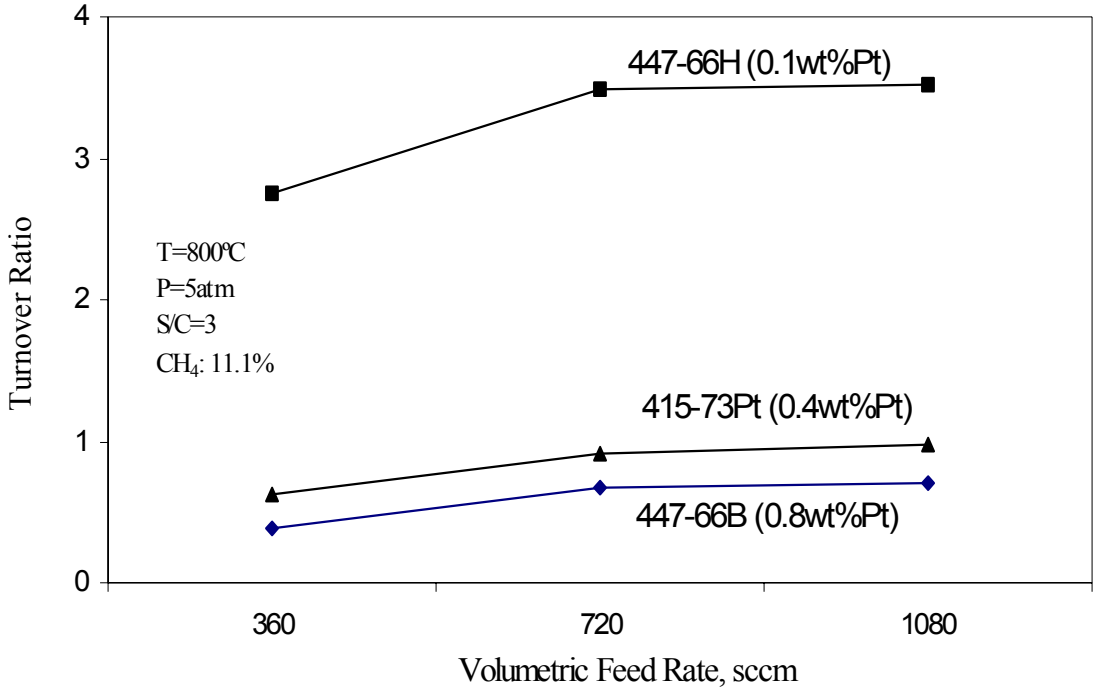

Figure 5-10 Turnover Ratio as a Function of Volumetric Feed Rate for Catalysts Containing Pt

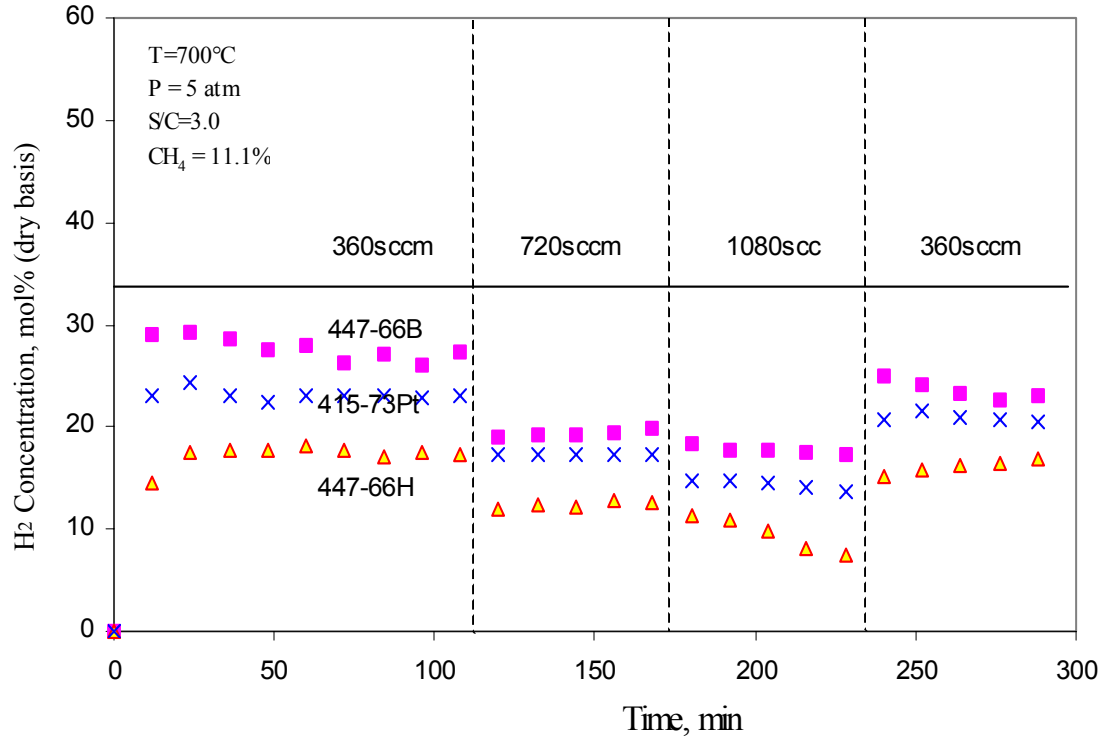

Figure 5-11 H_2 Concentration as a Function of Time for Catalysts from Group 3

In Figure 5-12, turnover ratio is plotted as a function of temperature at reaction conditions of 5atm, 11.1% CH_4, a S/C ratio of 3.0 and a constant feed rate of 720sccm. From this figure, it is seen that the turnover ratio increased with increasing temperature. The turnover ratio of catalyst 447-66H (0.1wt% Pt), which contained the least amount of Pt, was the most sensitive to the change of temperature and increased by a factor of 14, from 0.25 to 3.5, when the temperature increased from 600°C to 800°C. The turnover ratio of the other two catalysts containing more Pt showed a smaller increase with increasing temperatures. At 800°C, all these three Pt-based catalysts displayed their largest turnover ratio. As a result, 800°C was chosen as the standard test temperature for most of the remaining catalyst evaluation experiments.

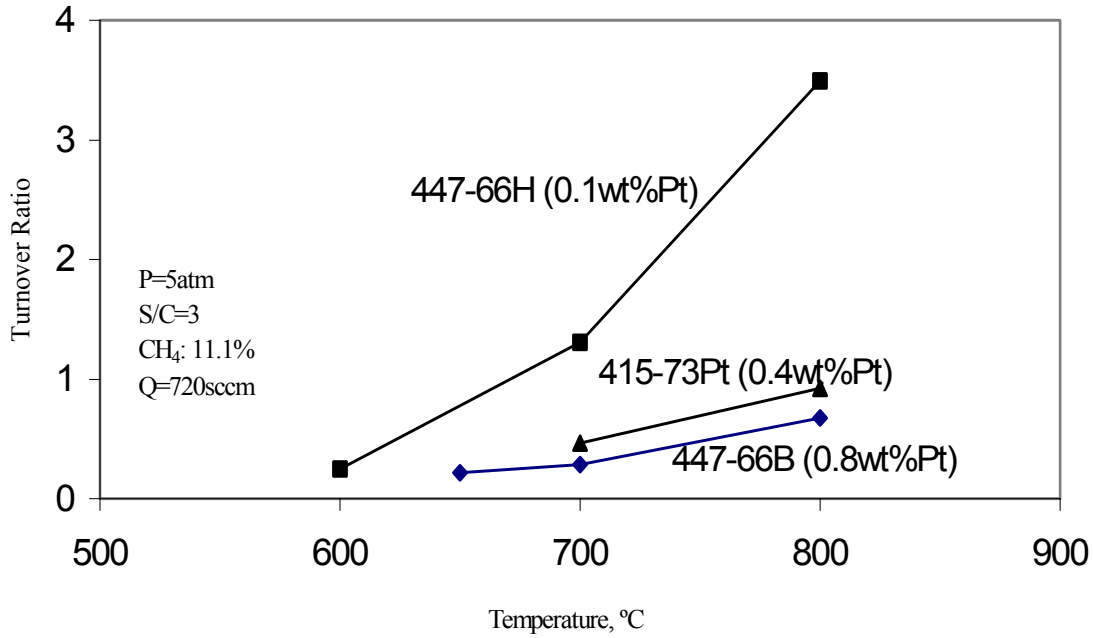

Figure 5-12 Turnover Ratio as a Function of Temperature for Catalysts Containing Pt

5.2 Screening of Catalysts Based on Their Reforming Activities

In the tests of the remaining catalysts, the feed rate was varied between 360sccm and 1080sccm. The feed rate of 720sccm was sufficiently large that none of the catalysts

drove the reforming reaction to equilibrium. Thus changes in the average H_2 concentration at 720sccm provided a direct comparison of catalyst activity.

Catalysts from groups 1 and 2 were not considered in this evaluation. Initial tests showed that all of group 1 catalysts possessed very low activity. Group 2 catalysts had been produced by TDA as part of an earlier program; these materials were tested only to the extent of proving their activity and verifying the reliability of the reactor system. Catalysts from group 3 to group 7 were rated based on the average H_2 they produced at standard reaction conditions shown in Table 5-1. They were assigned into one of three categories: Active, Moderately Active, and Less active. Active catalysts were defined as those producing greater than 30% H_2, moderately active catalysts were those producing between 25% and 30% H_2, and less active catalysts were those producing less than 25% H_2. The results are presented in Table 5-3.

In the active category, there was only a slight difference in H_2 content between the three catalysts. The H_2 produced by the active catalysts at a higher feed rate of 1080sccm was also higher than produced by the other two groups of catalysts, although the order was somewhat different. The catalysts in the moderately active category generally produced higher H_2 than the less active catalysts at a higher feed rate of 1080, although there were some exceptions such as catalysts 415-73Pt and 447-66H.

Both Catalysts 447-66B and 475-45 containing 0.8% Pt without additives are in the active category. Other catalysts containing different levels of Pt without additives fall into either the moderately active or less active categories. Catalysts 475-46 and 475-47B, containing 0.8% Pt and 0.1% Rh additive, fall at the top of the moderately active and less active catalyst groups, respectively. Several catalysts from group 6 contain 0.8% Pt, 2.5%

Table 5-3 Comparison of Catalyst Activity Based on Mol Percent H_2

Designation	Group	Active Component Composition (Weight%)	%H_2 at 720sccm Feed Rate	%H_2 at 1080sccm Feed Rate
Active Catalysts				
447-66B	3	0.8%Pt	33.5	27.8
475-45	5	0.8%Pt	33.1	25.0
475-50C	7	N/A	33.0	28.7
Moderately Active Catalysts				
475-46	5	0.8%Pt/0.1%Rh	29.2	26.3
475-50D	7	N/A	28.9	24.5
415-73Pt	3	0.4%Pt/0.764%NiO	27.7	21.9
475-46A	5	2.0%Ni	27.6	23.9
475-49	7	N/A	27.6	23.2
475-48C	6	0.8%Pt/0.1%Rh/2.5%CeO_2	26.2	22.3
447-66H	3	0.1%Pt	26.0	19.2
475-47D	6	0.8%Pt/0.1%Rh/2.5%CeO_2	25.1	22.0
Less Active Catalysts				
475-47B	6	0.8%Pt/0.1%Rh	24.4	22.7
475-50B	7	N/A	23.4	20.6
475-47C	6	0.8%Pt/2.5%CeO_2	22.4	20.4
475-48A	6	0.8%Pt/2.5%CeO_2	21.2	17.8
475-50A	7	N/A	20.3	18.0
475-47A	6	0.8%Pt	20.2	16.3
413-89	5	0.8%Pt-TiONa-CO_2	18.4	16.1
415-73	3	0.764%NiO	11.9	9.2
447-88B	4	0.4%Pt	7.9	6.5
447-93	4	0.8%Pt	5.9	4.9
447-93A	4	0.8%Pt/1%Ni	3.9	2.9

CeO_2, and sometimes 0.1% Rh. Two of these catalysts fall near the bottom of the moderately active group while the other two are in the less active group. No information about the composition of the catalysts in group 7 was available from TDA. In addition, we have no information on the composition and preparation conditions for most of the catalysts, which makes it impossible to carry out a complete evaluation.

5.3 Durability Testing of Catalyst

Durability is an important parameter of the performance of catalysts. The durability was examined by conducting multicycle runs at the same reaction conditions. In a standard fixed-bed reactor test the duration of the reforming reaction was about 5 hours, and is limited by the capacity of the syringe pump. By refilling the syringe pump as quickly as possible, it was possible to make an extended duration test lasting about 25 hours. Catalyst 415-73Pt (0.764wt% NiO+0.8wt% Pt) was selected as the sample for this durability test. Two grams of this catalyst were first activated and calcined at the standard test conditions. The feed gas contained 11.1% CH_4 with a S/C ratio of 2.5. 720sccm was used as the feed rate because at this condition the H_2 concentration does not reach equilibrium and a decrease in the H_2 content in the product gas with time will directly reflect the loss of catalyst activity. The reaction temperature was raised to 900°C, 100°C higher than the normal temperature to make the durability test more sensitive to time.

The H_2 concentration in the product gas as a function of time is shown in Figure 5-13. Each cycle in this figure represented a refilling of the syringe pump. The long horizontal line across the plot represents the equilibrium H_2 content at the test conditions. The short solid lines represent the average steady-state H_2 content in that cycle. During the first cycle the H_2 content was more scattered than usual due to uncertainties in the flow rate of

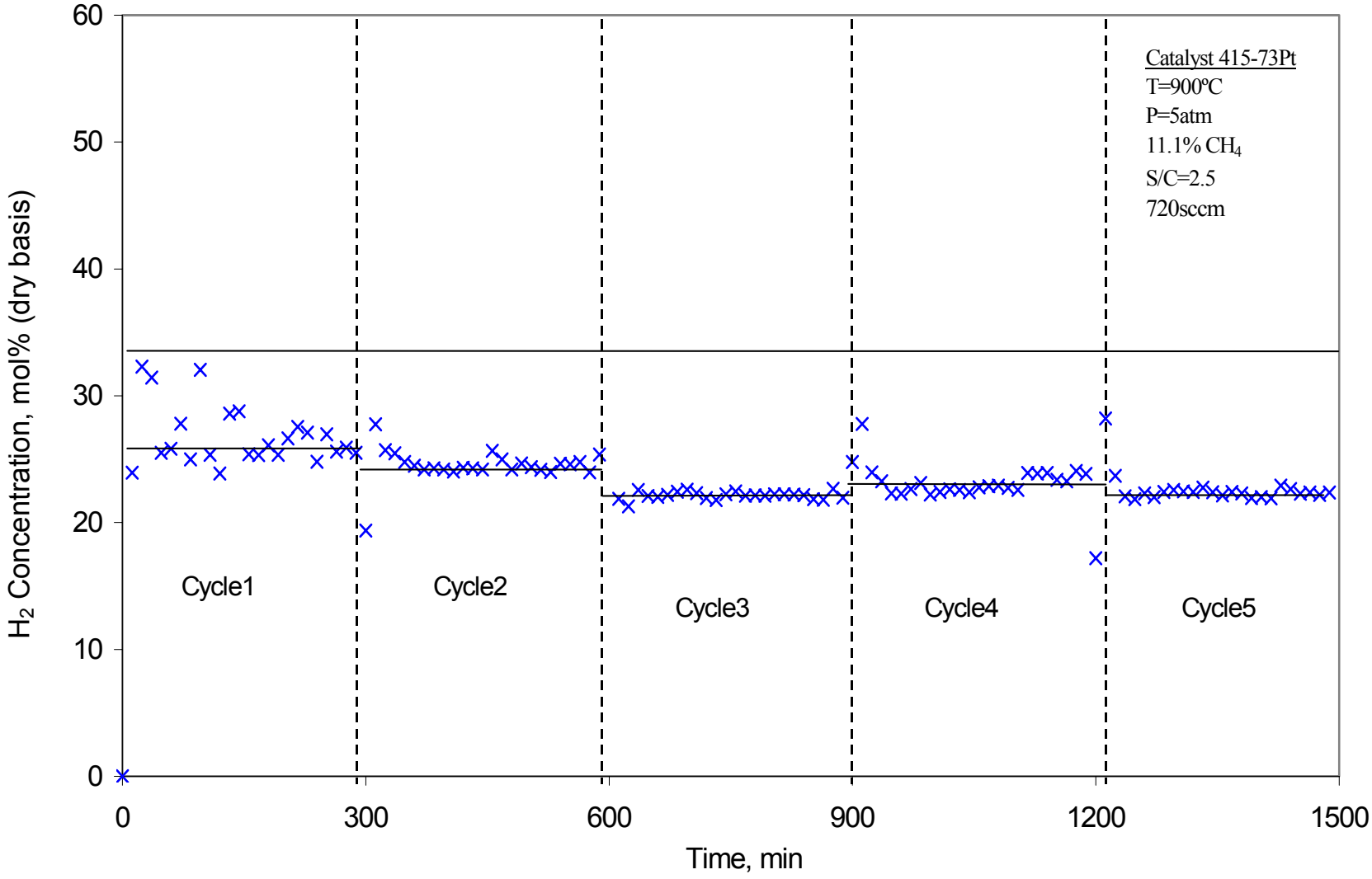

Figure 5-13 H_2 Concentration with Time in Extended Duration Test: Catalyst 415-73Pt

H_2O and/or CH_4. The average H_2 content in this cycle was about 26.5%, well below the equilibrium value of 33.2%. In the subsequent cycles, the first two or three samples usually displayed considerable scatter, which was attributed to the refilling of the syringe pump, but the remaining samples were quite consistent. The average H_2 contents in the second and the third cycles were 24.5% and 22.2%, respectively, 2% and 4.3% lower than that in the first cycle. There was no further decrease of H_2 content in the following cycles. In addition, all decreases occurred between cycles, and the H_2 content within a cycle was quite stable. From this result, we conclude that the catalyst was quite durable in the 25 hours test period, even at the abnormally high reaction temperature.

5.4 TGA Test on the CO_2 Adsorption Capacity of the Catalyst

The TDA samples were a combination of reforming catalyst and CO_2 sorbent. All the samples contained a certain amount of dolomite, $CaCO_3$, or free CaO that enabled them to remove CO_2 from the reaction gas. However, as stated earlier, the amount of sorbent was too small to detect CO_2 removal in the fixed-bed tests. The CO_2 sorption tests were carried out using the electrobalance reactor (TGA). The catalysts from groups 3 and 4 were employed in these tests.

5.4.1 Two-Cycle Runs

The test results of a two-cycle run using catalyst 415-73 (0.764wt% NiO) are presented in Figure 5-14 with weight and temperature plotted versus time. The feed gas contained 10% CO_2 and 90% He at a flow rate of 200 sccm. The test lasted for about 14 hours. From Figure 5-14, it is seen that the sample gradually lost weight as the temperature approached about 200°C, suggesting that the sample was losing H_2O. Calcination cannot occur at that low temperature. The catalyst was heated to 700°C and

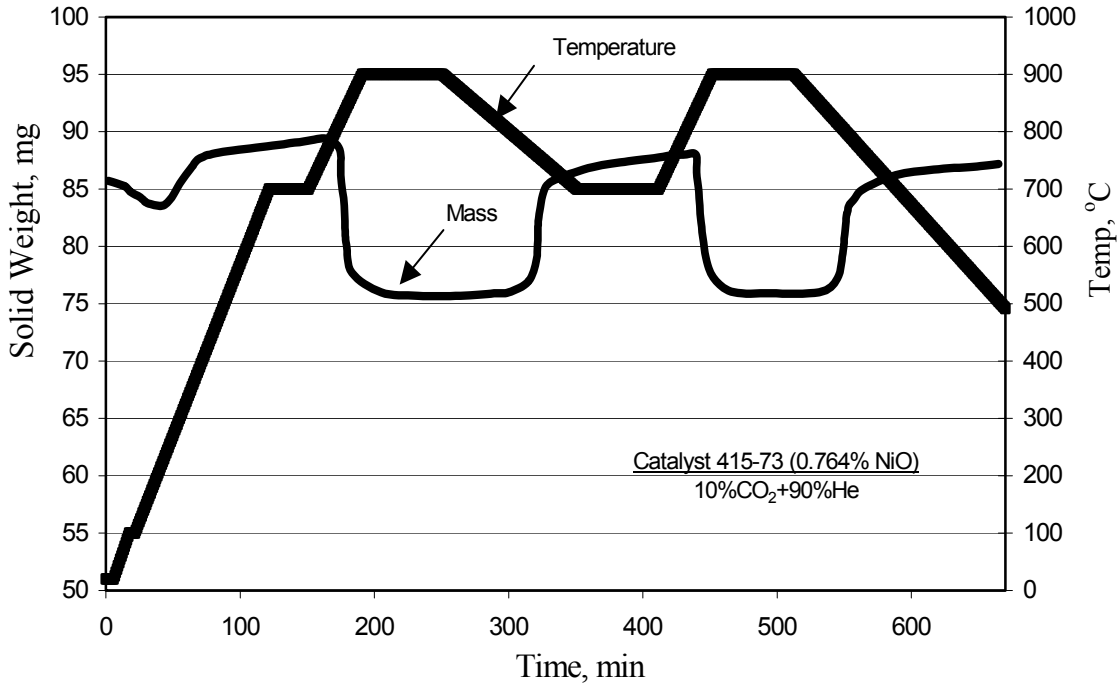

Figure 5-14 Weight as a Function of Temperature: Catalyst 415-73 (0.764% NiO)

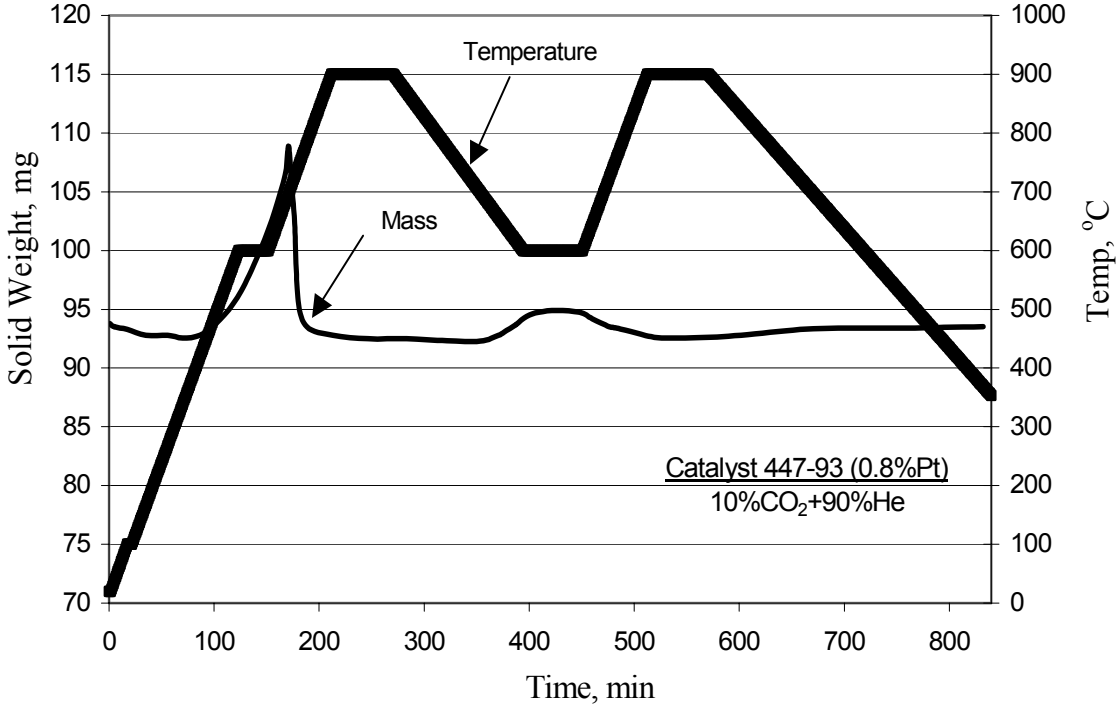

Figure 5-15 Weight as a Function of Temperature: Catalyst 447-93 (0.8% Pt)

held at that temperature for 30 min. Calcium present in the catalyst was a mixture of CaO, $CaCO_3$ and calcium titanate. A small weight increase occurred beginning at about 400°C, which is attributed to carbonation of the free CaO in the catalyst. The temperature was then increased to 900°C and held for 1 hour. A significant weight loss occurred beginning at about 800°C until a steady weight of 75.7 mg was reached. The equilibrium CO_2 pressure at 800°C is 0.2 atm, while the CO_2 pressure of the experimental gas was 0.1atm. Therefore this weight loss was associated with the calcination of all free $CaCO_3$ to CaO. The temperature was then decreased to 700°C and held for 1 hour. The free CaO was carbonated at these conditions and a final weight of 88 mg was reached, about 98.4% of the weight after the initial carbonation. The temperature was then increased to 900°C and decreased to 700°C by the same scheme, so that the catalyst was calcined and carbonated again. The final weights after the first and second calcinations were basically equal, suggesting that the calcinations were complete. During the test all temperature increases and decreases were linear to ensure uniform heating and cooling within the sample. The results in this test proved the CO_2 sorption capability of catalyst 415-73.

Figure 5-15 shows the results of a similar test using catalyst 447-93 (0.8wt% Pt). The temperature cycle was the same except that the temperature was reduced to 600°C for carbonation. During the first 600°C isothermal period, the weight of the catalyst increased significantly, suggesting that carbonation occurred. When the temperature was further increased, the weight dropped to its initial value, indicating that all of the free calcium was initially present as CaO. When the temperature was decreased to 600°C, the weight gain was slight, indicating little carbonation activity. Then when the temperature was increased to 900°C, the weight decreased to its initial value. We conclude that the

initial carbonation ability of catalyst 447-93 during the first 600°C period was destroyed in heating to 900°C. From Table 5-1, catalyst 447-93 contains 63wt% free CaO, or 58.6 mg for this sample. Calculation from the weight gain in Figure 5-15 suggested that only a small portion of CaO was involved in CO_2 removal during the first carbonation-calcination cycle. The low carbonation activity of this catalyst maybe caused by sintering of the CaO at high temperature due to improper preparation methods.

5.4.2 Multicycle Runs

Catalysts 447-66H and 415-73Pt were examined in multicycle runs for their CO_2 sorption durability. The feed gas to the electrobalance reactor contained 10% CO_2 and 90% He and the temperature was programmed as follows. The sample was first heated from room temperature to 100°C at 8°C/min and held for 5 min to drive off moisture. Then the temperature was increased to 650°C at 10°C/min and held for 5 min, during which time carbonation occurred. The temperature was then increased to 900°C at 10°C/min, and the carbonate was calcined to CaO and CO_2. The temperature remained at 900°C for 15 min, after which time the temperature was decreased to 650°C at 3°C/min and held for 15 min for recarbonation. The temperature was then repeatedly cycled between 650°C for carbonation and 900°C for calcination with 15 min isothermal periods.

The results for a 29-cycle test using catalyst 447-66H are shown in Figure 5-16. The weight was normalized by dividing the actual weight at the end of each carbonation and calcination cycle by the initial weight of the sample. The upper data represents the normalized weight of the sample after carbonation at 650°C while the lower data represents the normalized weight after calcination at 900°C. The lower data were quite

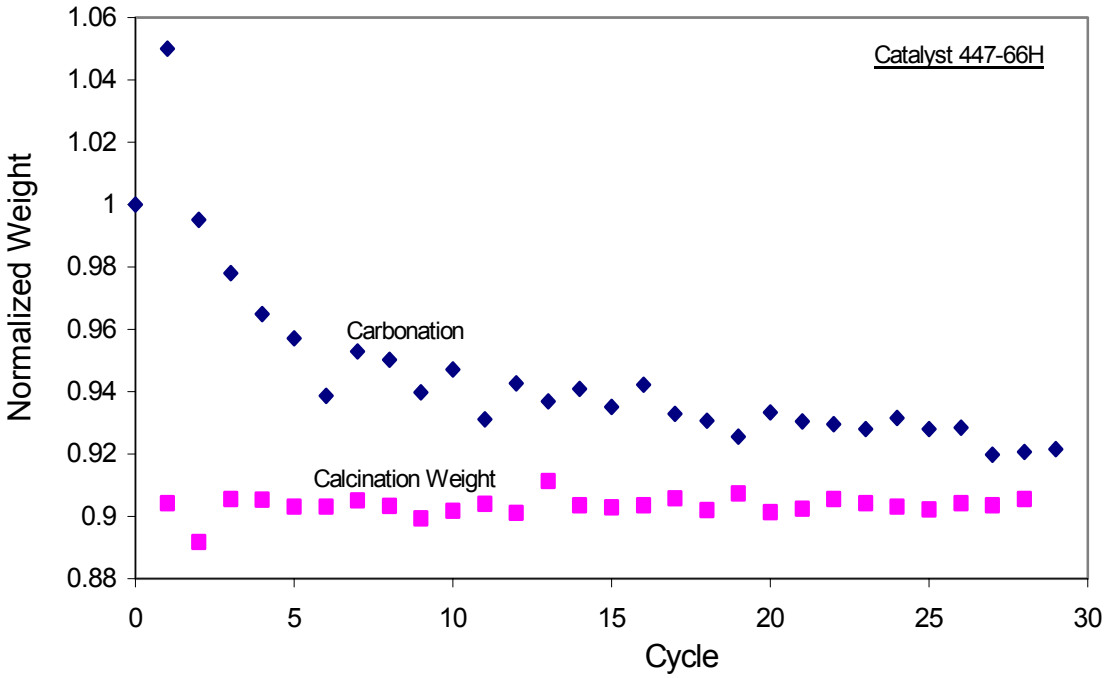

Figure 5-16 Results of Multiple Carbonation-Calcination Cycles: Catalyst 447-66H

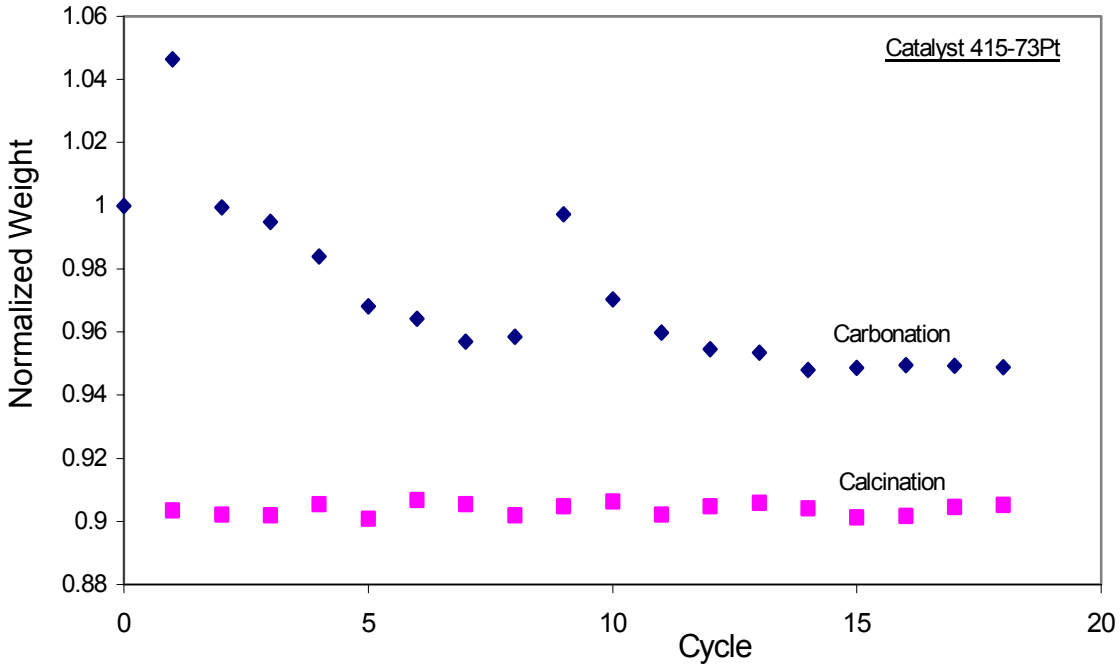

Figure 5-17 Results of Multiple Carbonation-Calcination Cycles: Catalyst 415-73Pt

constant, suggesting that calcination was complete in each cycle. The weight gain to 1.05 at the end of the first carbonation cycle suggested the initial presence of free CaO. The carbonation weight decreased with cycle number until after 20 cycles it tended to stabilize. Actually the carbonation reaction was still occurring at the end of the 15 min, 650°C isothermal period. Therefore the loss of carbonation weight does not represent loss of overall carbonation capacity, but represents a loss of carbonation rate, or carbonation activity.

The results of another 18-cycle test using catalyst 415-73Pt at the same reaction conditions are shown in Figure 5-17. The results are similar except there was a large increase in normalized weight at the end of carbonation cycle 8. This occurred because in this cycle the 650°C isothermal period was extended for several hours to prove that the carbonation was not complete at the end of each carbonation cycle. Again, calcination was complete in each cycle, and the carbonation activity of this catalyst, initially decreased with cycle number and tended to stabilize after 14 cycles.

CHAPTER 6

LOW CARBON MONOXIDE HYDROGEN BY SORPTION-ENHANCED REACTION

When CO and H_2 contact a catalyst surface, the CO molecule usually has a much stronger binding force with the catalyst than the H_2 molecule. The CO molecules will preemptively occupy the active sites on the surface of catalyst and prevent the H_2 molecules being adsorbed and subsequently reacted on the catalyst. Therefore a very small concentration of CO will "poison" the catalyst and greatly reduce the reaction rate of H_2. Several current and potential uses of H_2, for example a proton exchange membrane (PEM) fuel cell, require that the CO content in the H_2 feed gas be reduced to low ppmv levels to avoid catalyst poisoning.

In the conventional steam-methane reforming process, the CO may be reduced to the desired levels through methanation during the H_2 gas purification step. In applications of PEM fuel cells, the CO content in H_2 gas can also be reduced through PROX (preferential oxidation). Each of these methods requires an additional process step and also consumes H_2, thus adding extra cost to the production of H_2.

Previous research in this laboratory by Balasubramanian (1998) on the sorption-enhanced H_2 production process proved that 95%+ H_2 can be produced over a range of temperatures using the combination of a commercial Ni-based reforming catalyst and a Ca-based CO_2 acceptor. However, CO concentrations were not examined seriously in that study. In this study, the previous work was extended so that CO concentration was also emphasized. The CO content was limited by carefully controlling the process parameters, so that no extra CO reduction step was needed.

In the tests, 6g of a standard Ni-based reforming catalyst and 14g of high purity $CaCO_3$ were mixed homogeneously and loaded into the reactor insert. The reforming catalyst from United Catalysts (C11-9-02), was crushed into small particles and then sieved to get a particle size range of 75<dp<150 microns. The catalyst consisted of about 22wt% NiO supported on α-alumina. The $CaCO_3$ was from Fisher Scientific with a 99.97% purity. The particle size of $CaCO_3$ precursor ranged from 75 to 150 microns. The mixture was calcined at 800°C in pure N_2 in the reactor to produce about 7.8 g of CaO sorbent. In each test, the reactor was recharged with fresh materials. The spent CO_2 sorbent was not regenerated for cyclic use in this study.

In the experimental study, the effects of temperature, volumetric feed rate, and feed gas composition on the production of H_2 and the content of CO were investigated. The temperature was varied between 400°C and 650°C with 480°C as the most common test temperature. The steam-to-carbon (S/C) ratio was maintained at 4.0 in all tests. The CH_4 concentration in the feed gas was varied from 10% to 20% with the corresponding N_2 diluent concentration decreased from 50% to 0%. The total volumetric feed rate was varied from 100 sccm to 600 sccm, with most tests at 200 sccm. The pressure was maintained at 5 atm based on the thermodynamic analysis in Chapter 3.

Figure 6-1 shows the concentration of H_2 and CO as a function of time for a typical test. Reaction conditions are shown on the figure. The plot uses logarithmic scale for concentration so that both H_2 and CO concentrations are clearly visible. In this figure, both the first steady-state, or prebreakthrough, and the second steady-state, or postbreakthrough, periods are clearly shown. During the prebreakthrough period, the average H_2 concentration was 42.8%, closely approaching the equilibrium value

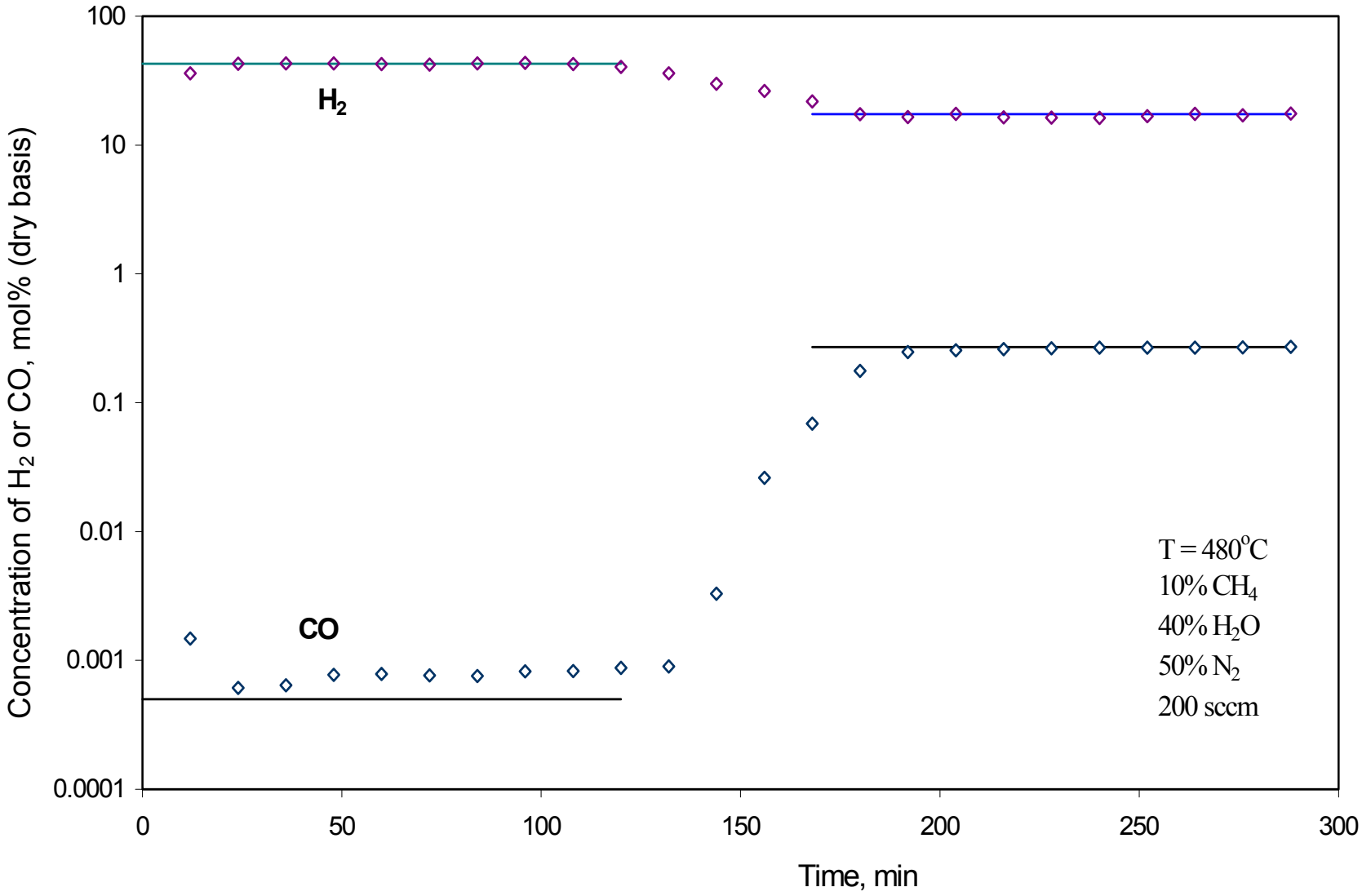

Figure 6-1 H_2 and CO Concentrations as a Function of Time

of 42.7%. The average CO concentration was 8 ppmv, compared to the equilibrium value of 5 ppmv. During the postbreakthrough period, the measured H_2 and CO concentrations were 16.9% and 0.27%, compared to the equilibrium values of 17.4% and 0.27%, respectively. The decrease in H_2 concentration and increase of CO concentration began at about 130 min, which corresponded to the leading edge of the carbonation reaction front reaching the exit of the packed bed. The second steady-state period, corresponding to post-breakthrough, began at about 190 min. During this period, the rate of the carbonation reaction approached zero and only reforming and shift reactions were active. From material balance calculations, the conversion of CaO to $CaCO_3$ was about 89% at the beginning of postbreakthrough.

The results in this test confirmed that equilibrium could be closely approached at 480°C, 5 atm and a S/C ratio of 4.0 with a feed gas containing 10% CH_4.

6.1 Thermodynamic Analysis

The process parameters applied in the experimental study were first determined through thermodynamic analysis using HSC. Detailed thermodynamic calculations and comparisons were presented in Chapter 3. Results of an additional thermodynamic calculation are presented in Figure 6-2, which shows the effects of temperature and pressure on the concentration of both H_2 and CO in a single plot. The solid lines represent equilibrium concentration of H_2 and the dashed lines represent the concentration of CO. The feed gas containing 20% CH_4, 80% H_2O and no N_2 diluent, was "contacted" with excess CaO. From this figure, it is seen that the equilibrium concentration of H_2 is nearly constant in the temperature range of 400°C to 550°C. For example, at 3 atm, the

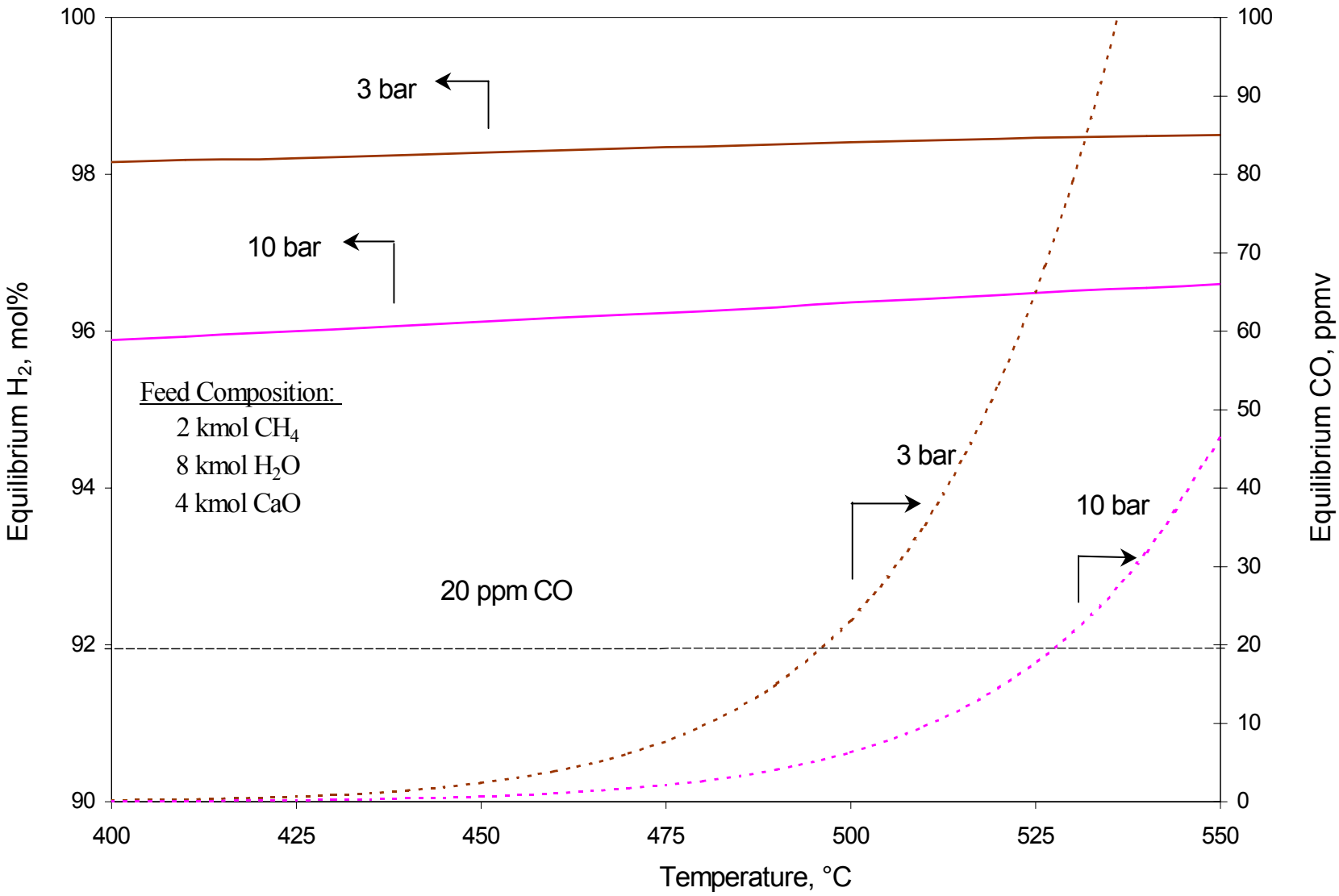

Figure 6-2 Equilibrium CO and H_2 concentrations as a Function of Temperature and Pressure

concentration of H_2 only increased from 98.2% to 98.5%. However, the equilibrium concentration of CO increased greatly over the same temperature range, especially when the temperature was higher than 475°C. An increase in pressure results in a decrease of the concentration of H_2, but reduces the CO content as well. 5 atm was selected as the experimental reaction pressure to study the possibility of producing high purity H_2 and at the same time satisfying the requirement for low CO content. At 5 atm, the equilibrium concentration of H_2 was about 97.5% in the temperature range between 450°C and 500°C while the CO content ranged from 1 to 13 ppmv, which is within the 20 ppmv CO needed for PEM fuel cell applications.

6.2 The Effect of Temperature

The experimental study concentrated on the temperature range between 450°C and 500°C. Figure 6-3 shows the effect of temperature on the concentration of H_2 and CO during the pre-breakthrough period of the combined sorption-enhanced steam reforming reactions. The equilibrium values of the concentrations of H_2 and CO are represented by the solid lines while the experimental concentrations of H_2 and CO are represented by the discrete points. The feed gas contained 10% CH_4, 40% H_2O and balance N_2 diluent. The total feed rate was maintained at 200 sccm. At temperatures between 450°C and 500°C, the equilibrium H_2 concentration was nearly constant at 42.7%, while the equilibrium CO concentration increased from 1 to 11 ppmv. The experimental values of H_2 concentration at 450°C and 460°C were 37.8% and 38.9%, respectively, significantly lower than the equilibrium value of 42.7%. The deviation of H_2 concentration from equilibrium may be caused by formation of $Ca(OH)_2$, which is favored by lower temperature. However, at temperatures between 470°C and 500°C, the experimental values of H_2 concentration

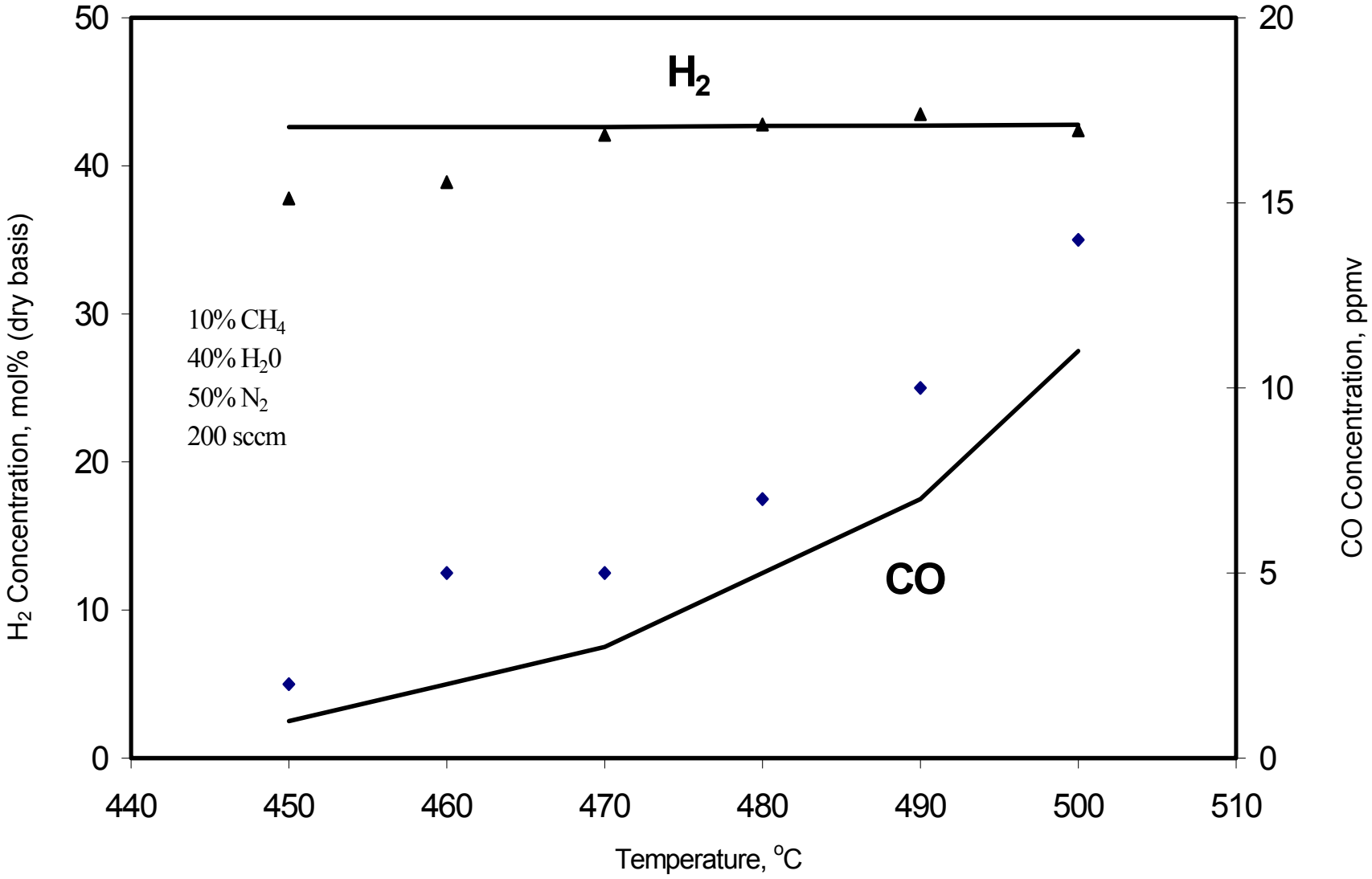

Figure 6-3 H_2 and CO Concentrations as a Function of Temperature

ranged from 42.1% to 43.5%, effectively equal to the equilibrium value of 42.7%. The CO content ranged from 2 to 14 ppmv, only 1 to 3 ppmv higher than the corresponding equilibrium value.

6.3 The Effect of Volumetric Feed Rate

Figure 6-4 shows the concentration of H_2 and CO as a function of volumetric feed rate. Three tests were carried out at 480°C and 5 atm, using a feed gas containing 10% CH_4, 40% H_2O and 50% N_2 diluent with different volumetric flow rates.

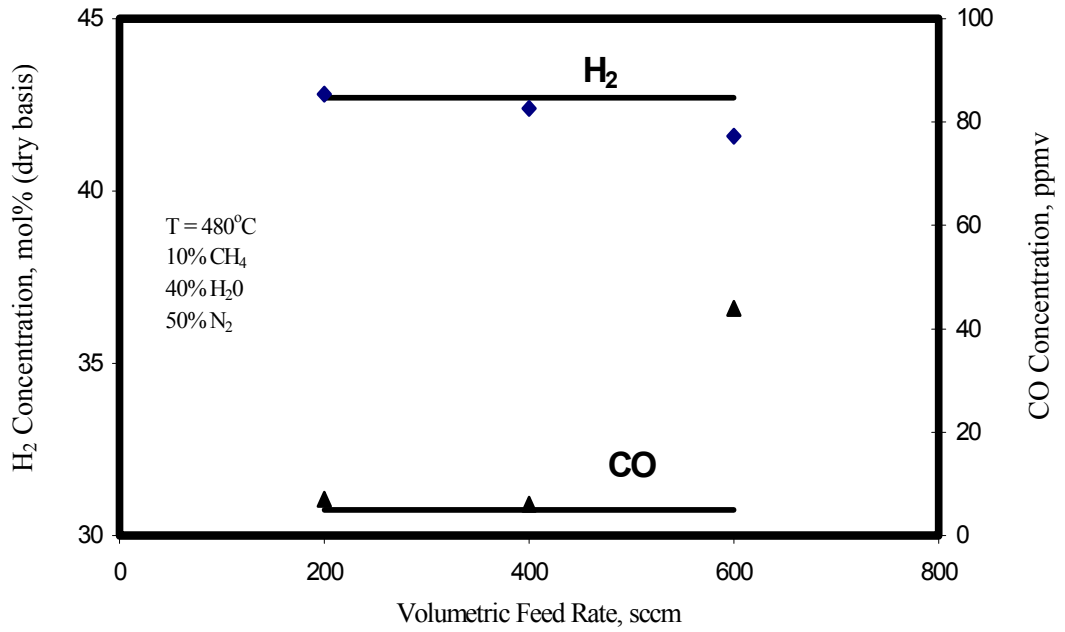

Figure 6-4 H_2 and CO Concentrations as a Function of Volumetric Feed Rate

The equilibrium concentrations of H_2 and CO at these conditions are 42.7% and 5 ppmv, respectively. The volumetric flow rate was varied from 200 sccm to 400 sccm and 600 sccm in the tests. The experimental values of H_2 concentration at 200 sccm and 400 sccm were 42.8% and 42.4%, respectively, closely approaching the equilibrium value of 42.7%. The CO contents at these two feed rates were 7 and 6 ppmv, also effectively equal

to the equilibrium value of 5 ppmv. However, at 600 sccm, the H_2 concentration decreased to 41.6%, while the CO content increased to 44 ppmv, both significantly different than the equilibrium values. Higher flow rate leads to higher space velocity, thus less residence time. The failure to achieve equilibrium at the highest feed rate of 600sccm is regarded as the result of insufficient residence time of the reacting gas in the packed bed.

6.4 The Effect of Gas Composition

In the tests discussed previously, the feed gas contained 10% CH_4, 40% H_2O and balance N_2. The N_2 was added as diluent so that it would be easier to achieve complete vaporization of the H_2O. In the tests described in this section, the concentration of N_2 diluent was reduced, and the CH_4 concentration was increased from 10% to 20% while maintaining the S/C ratio at 4.0. These tests were carried out at 480°C with a total feed rate of 200 sccm.

Figure 6-5 shows the effect of gas composition on the prebreakthrough concentration of H_2 and CO. At 10% CH_4, both the H_2 and CO concentrations closely approached the equilibrium values. When the CH_4 concentration was increased, the H_2 concentration was significantly lower and the CO content was significantly higher than the equilibrium values. For example, at 20% CH_4, the experimental H_2 and CO concentrations were 87.9% and 25 ppmv, compared to the equilibrium values of 97.6% and 6 ppmv. Clearly the residence time was not sufficient to allow the reactions to approach equilibrium with the increased CH_4 feed rate.

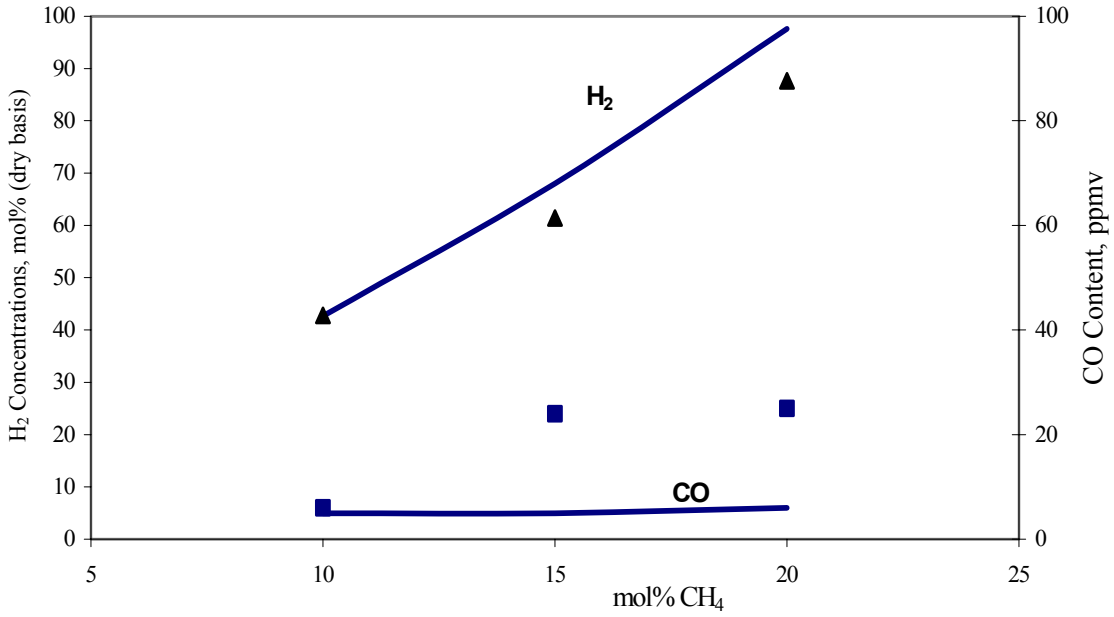

Figure 6-5 H_2 and CO Concentrations as a Function of mol% CH_4

6.5 The Result of a Successful Run without N_2 Diluent

Although increasing the CH_4 concentration in the feed gas imposed a heavier burden to both the catalyst and the sorbent, equilibrium can still be approached by lowering the total volumetric feed rate. In the test shown in Figure 6-6, the feed rate was decreased to 100 sccm. The feed gas contained 20% CH_4 and 80% H_2O without N_2 diluent. The steady-state H_2 concentrations for both prebreakthrough and postbreakthrough periods closely approached the equilibrium values represented by solid lines in the plot. The CO content during the postbreakthrough period was 0.56%, closely approaching the equilibrium value of 0.59%, and the CO content during the prebreakthrough period was 18 ppmv. While significantly above the equilibrium value of 6 ppmv, the product could be used in downstream catalytic processes without the need of further purification.

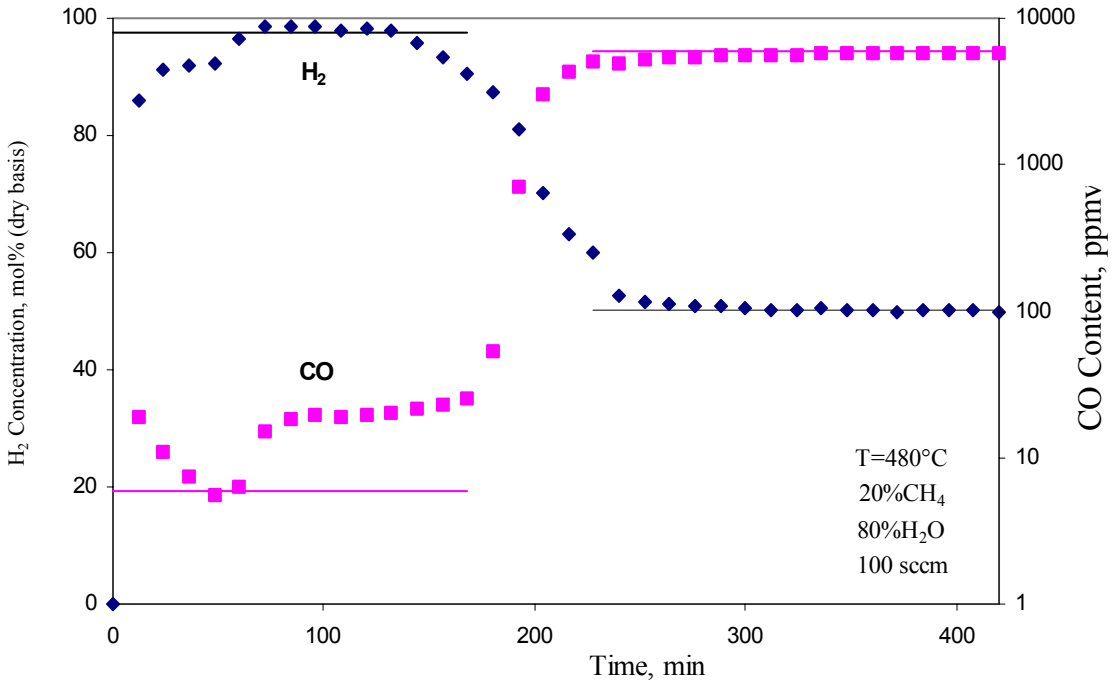

Figure 6-6 H_2 and CO Concentrations as a Function of Time

This test experimentally demonstrated the feasibility of producing 95%+ H_2 while limiting the CO content to less than 20 ppmv through the sorption-enhanced steam reforming process using the standard Ni-based reforming catalyst and the calcium-based CO_2 sorbent by carefully controlling the reaction parameters.

CHAPTER 7

PROCESS SIMULATION AND EVALUATION OF THE HYDROGEN AND OXYGEN CO-PRODUCTION PROCESS

Both hydrogen and oxygen are very important industrial gases. Except for the significance for production of hydrogen described in Chapter 1, oxygen is also extensively used in the steel industry, chemical industry, etc. In addition, low cost high purity liquid hydrogen and oxygen are also in great demand in NASA's aerospace program, where both of them serve as rocket propellant. Hydrogen is primarily produced through the steam reforming process, where methane is converted into hydrogen by reacting with steam at high temperature and pressure. The endothermic reforming reaction and generation of steam, which require a huge amount of energy to vaporize water at high pressure, are highly heat-intensive. Oxygen is primarily produced by the liquefaction and rectification of air through a cryogenic air distillation process. To cool down the gaseous air into partially liquid air at an extremely low temperature, the air feed has to be first compressed to a high pressure by a centrifugal compressor, which consumes a great amount of power. Both the hydrogen and oxygen production processes are energy intensive, which adds to the operating costs. By combining these two processes together through careful energy integration with addition of another gas turbine and heat recovery steam regeneration (HRSG), the energy can be provided internally from the overall system and efficiently used. A schematic diagram of the hydrogen and oxygen co-production process is presented in Figure 7.1.

The hydrogen and oxygen co-production process consists of four subsystems: (1) the sorption-enhanced steam methane reforming (SMR) process for hydrogen production,

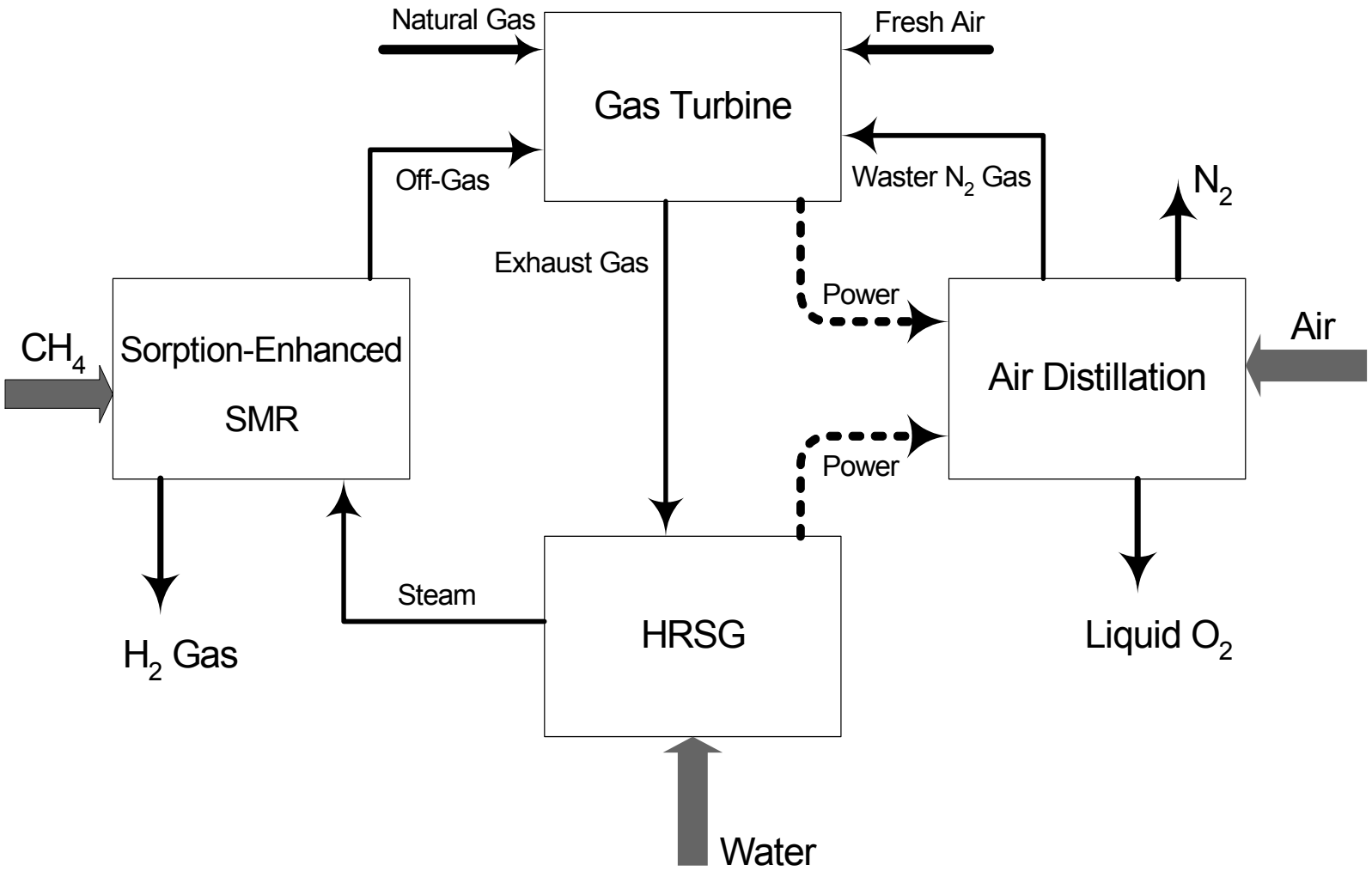

Figure 7-1 Schematic Diagram of the Hydrogen and Oxygen Co-production Process

(2) the cryogenic air distillation process for oxygen production, (3) the gas turbine process for power generation, and (4) the heat recovery steam generation (HRSG) process. To decrease the complexity of the simulation and ensure robust convergence, the overall process is divided into four parts corresponding to the four subsystems described above, which were studied individually. The sorption-enhanced reforming process mainly contains a reformer, a regenerator, as well as other units such as heat exchangers, cyclones and turbines. The core of the cryogenic air distillation process is the double distillation columns coupled through a reboiler/condenser combination. The multistream heat exchanger is another important component that is crucial to the heat integration of this process. The gas turbine generates power that supplies the compressors and all the other equipment that utilizes electricity. The feed to the combustor in this process includes fuel gas and air. Fuel gas comes from the off-gas in the hydrogen purification step in the sorption-enhanced reforming process. Supplemental fuel is added to generate the additional power needed by the overall process. The waste nitrogen stream from the air distillation process, which is rich in oxygen, was mixed with fresh air to supply oxygen to the combustor. The heat recovery steam generation process contains a series of heat exchangers, pumps and turbines. Liquid water was heated to produce steam by the high temperature exhaust gas from the gas turbine through the heat exchanger train. Part of the steam generated drove the gas turbines to produce power and the remaining steam was fed to the steam reforming process.

7.1 The Aspen Plus Simulator

The process simulation and evaluation were carried out using Aspen Plus® (Aspen Tech, 2001) process simulator for a detailed study of the overall process. Aspen Plus is a

widely used software package in process design, steady-state simulation, optimization and parameter sensitivity analysis. The simulation is created by first selecting the unit operation and stream modules provided by the simulator and arranging them in the worksheet through the graphic user interface. The simulator contains a complete collection of unit operations such as reactors, columns, heat exchangers, pumps, turbines, etc. that are employed in the process industry. These units are then connected by streams to form an integrated process system that is capable of converting raw materials to the desired products by chemical or physical processes with consumption of energy. The software package has a comprehensive species databank that enables it to handle a variety of components from simple ones like pure substances to complex ones like petroleum fractions. Its thermodynamic system contains various models for thermodynamic property calculation.

After the flow sheet of the simulation is set up, the detailed specifications of the streams and unit operations such as temperature, pressure, flow rate, composition and reactions, if required, are input to the datasheet. The appropriate thermodynamic model is selected as well. The simulation applies the sequential modular or equation-oriented method to ensure fast convergence of the overall process. During the execution of the simulation, possible error messages are displayed on the control panel, which enables the user to diagnose the problems in the simulation. The results of the simulation can be reviewed conveniently after the simulation.

7.2 Simulation of the Sorption-Enhanced Steam Methane Reforming (SMR) Process

The complete flow sheet of the sorption-enhanced SMR process is described in Figure 7-2. This process involves a reformer for the combined reforming-shift-

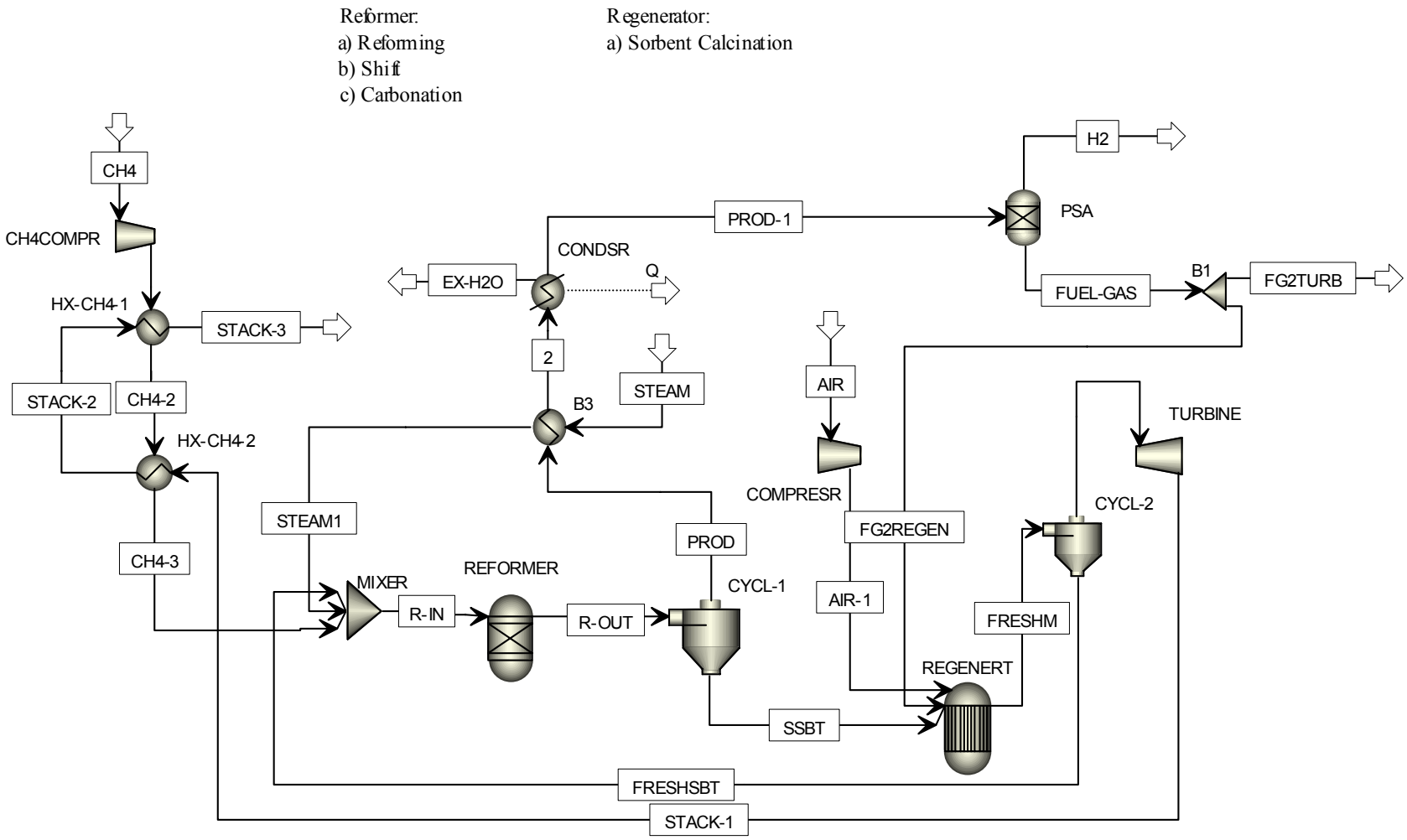

Figure 7-2 Flow Sheet of the Sorption-Enhanced Steam Methane Reforming Process

carbonation reactions, and a regenerator for the regeneration of the CO_2 sorbent. A mixture of CH_4, H_2O and fresh CaO sorbent were fed to the reformer operating at 480°C and 5 atm. The reaction mixture exiting the reformer was then fed to a cyclone to separate solids from gases. The product gases were sent to a pressure swing adsorption (PSA) unit for purification of the H_2 product. The solids containing the spent sorbent and make-up catalyst exited from the bottom of the cyclone and were sent to the regenerator for regeneration of the CaO sorbent. The regenerator was operated at 900°C and 5 atm. Additional fuel was supplied from the PSA off-gases to provide enough heat for regenerating the CaO sorbent. The effluent mixture from the regenerator was fed to another cyclone, with fresh solid sorbent sent back to the reformer, and high temperature stack gas fed to a gas turbine to generate extra power.

The simulation was based on 100 kmol/hr of process methane and 400 kmol/hr of steam, at a S/C ratio of 4.0. The product composition for the reformer and the regenerator were based on thermodynamic equilibrium calculations using the Gibbs free energy minimization approach. The complete simulation results are shown in Appendix 1. A total of 16.2 ton/day of H_2 product gas with a purity above 99% is produced in this process. 55% of the off-gas containing CH_4 and H_2 and other impurities from the pressure swing adsorption (PSA) is fed to the regenerator to supply additional heat and the remaining part of the off-gas is fed to the gas turbine process to generate power.

Table 7-1 summarizes the simulation results of the reformer, and makes a comparison between the simulation results and the experimental results from the fixed-bed reactor system. The H_2 concentration in the reformer product gas in the simulation is 97.61%,

compared to the experimental result of 97.74%. The concentrations of CO, CO_2 and CH_4 impurities in the reformer product gas from simulation are 6ppmv, 22ppmv, and 2.39%, respectively, compared to 18ppmv, 85ppmv, 2.25% from the fixed-bed reactor test. The simulation results agree well with the experimental results using the fixed-bed reactor, except the concentrations of CO and CO_2 in the simulation significantly deviate from the experimental results, which is due to the fact that the shift and carbonation reactions didn't reach equilibrium.

Table 7-1 Comparison between Simulation Results and Experimental Results of the Sorption-Enhanced Reforming Process

	Aspen Simulation				Fixed-Bed Reactor Test		
Gas Components	Reformer Feed		Reformer Product		Reactor Feed		Reactor Product
	kmol/hr	mol% (dry)	kmol/hr	mol% (dry)	sccm	mol% (dry)	mol% (dry)
H_2	0	0	358.9	97.61	0	0	97.74
CO	0	0	0.002	0.0006	0	0	0.0018
CO_2	0	0	0.008	0.0022	0	0	0.0085
CH_4	100	0.2	8.777	2.39	20	0.2	2.25
H_2O	400	0.8	223.6	-	80	0.8	-

7.3 Simulation of the Cryogenic Air Distillation Unit for Oxygen Production

The flowsheet of the production of oxygen through cryogenic air distillation is illustrated in Figure 7-3.

Separation of air is achieved by first expanding part of the compressed air to a low pressure so that it cools to a low enough temperature to condense the balance of the air. The low temperature, or cryogenic, air is subsequently separated in distillation units into

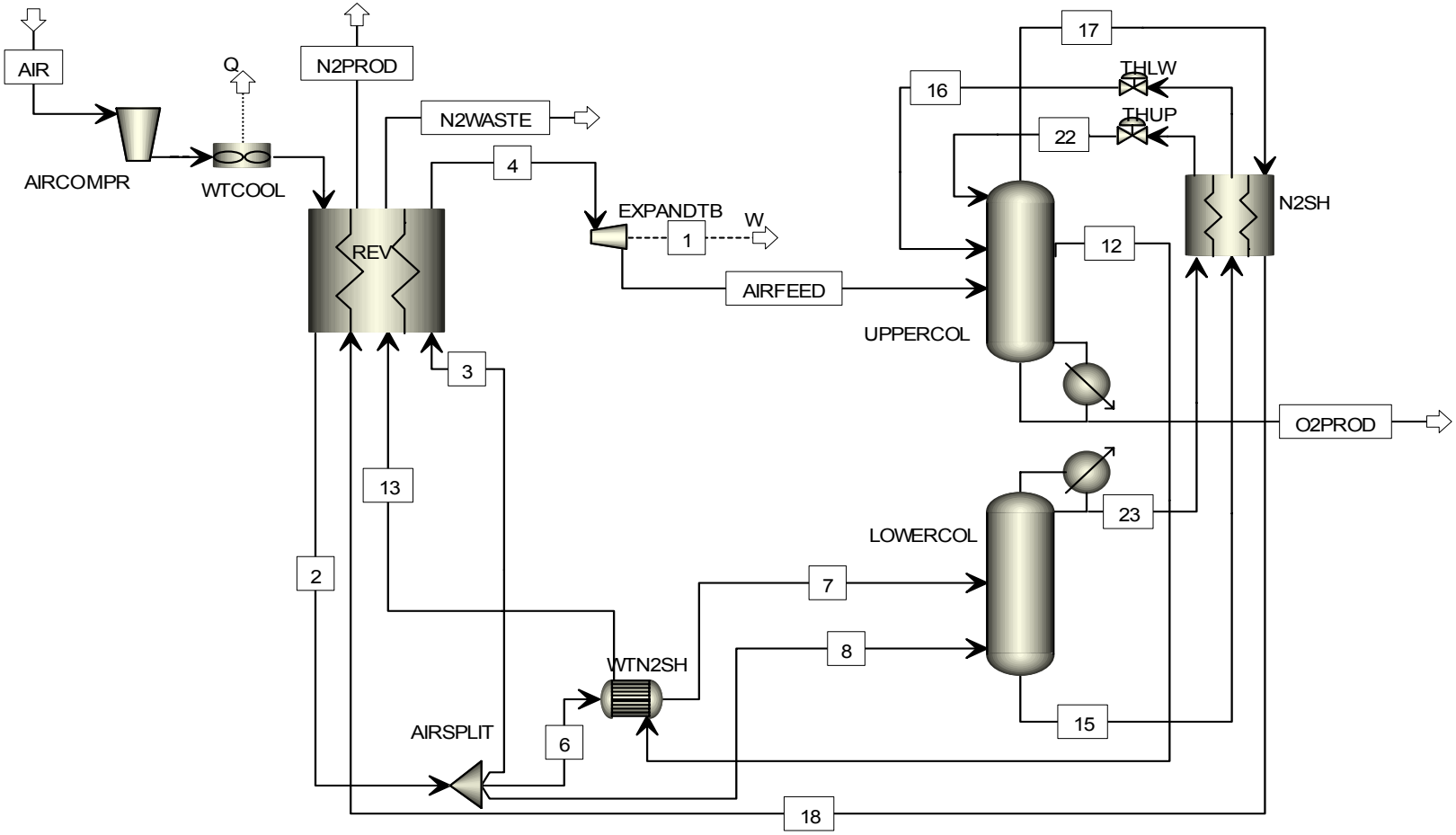

Figure 7-3 Flow Sheet of the Cryogenic Air Distillation Process

its components of N_2 and O_2. The core of this process is a set of two columns, which are thermally connected at the center through a dual-function heat exchanger. This heat exchanger serves as a reboiler for the upper column and as a condenser for the lower column. The upper column operates at low pressure of about 0.6 atm while the lower column operates at middle pressure of about 5 atm.

Filtered air is first compressed to 30 atm and cooled to ambient temperature in a water-cooled exchanger. The compressed air then enters a reversing heat exchanger and is further cooled by countercurrent heat exchange with the cold nitrogen streams from the columns. The passages of the air and the waste nitrogen stream are periodically reversed every few minutes so that condensed water from the air can be purged from the exchanger to make it in a clean and operable condition. The air is split into three streams to be fed to the columns at different positions. A small portion (~5%) of the air directly enters the lower column at a position near the bottom of the lower column. A portion (~27%) of the air is fed at a position in the middle of the lower column after being subcooled by waste nitrogen stream in an exchanger. The majority (~68%) of the air is fed to the upper column after being subcooled by an expansion turbine to cryogenic level.

In the columns, because the normal boiling point of O_2 is 12.8°C higher than that of N_2, therefore the more volatile N_2 ascends each tray while the less volatile O_2 descends. In the upper column, high purity N_2 product is obtained from the top of the column. This stream serves as a cooling stream in the N_2 superheater. A high-purity O_2 stream is extracted from the bottom of the upper column directly as liquid O_2 product. The remaining gas is removed as a low purity waste N_2 stream in the middle of the upper column. This stream also serves as a cooling stream in another N_2 superheater to subcool

the air fed to the lower column. Both the product N_2 and waste N_2 streams cross-exchange with the warm incoming air in the reversing heat exchanger to further retrieve their sensible heat. In the lower column, the condensed N_2 exiting from the condenser is split into two streams with one stream diverted to the upper column as a secondary feed and the other stream back to the lower column as reflux. The O_2-enriched stream from the bottom of the lower column returns to the upper column as another feed. Both of these returning streams from the lower column are subcooled in a N_2 superheater and throttled to the lower pressure of the upper column. For simplicity, the units for separation of trace amounts of hydrocarbons, carbon dioxide, and water, are omitted.

The simulation is based on 2000 ton/day of air processing capacity. The complete simulation results are listed in Appendix 2. In this simulation, a total of 259 ton/day of liquid O_2 product with greater than 99% purity is produced. This equals to a yield of 55%. Gaseous N_2 product with a purity of 93% is also produced at a flow rate of 1581 ton/day. This stream can be further separated to obtain high purity N_2 product if desired. Another N_2 stream with a purity of 58.8% N_2 is discharged from the side of the upper column at a flow rate of 160 ton/day as waste N_2. Heat duties of the reboiler of the upper column and the condenser of the lower column are matched through carefully adjusting the split ratio of the air splitter. 12.3 MW of power is consumed in the air compressor, which is partially compensated by the power of 1.1 MW generated in the expansion gas turbine. The remaining power needed for the air compressor will be primarily supplied from the gas turbine process, and also the steam generation process, which are subsequently described.

7.4 Simulation of the Gas Turbine for Power Generation

Combustion of fuel gas, such as CH_4, produces a large amount of heat. This high temperature and high pressure hot gas mixture, when fed to an expander, will drive the blades installed on the shaft thus the heat energy of the hot gas is converted to mechanical energy. When the shaft is attached to a generator, it will output electricity.

The gas turbine process consists of an expansion gas turbine, a combustor, and two compressors. Figure 7-4 shows the flowsheet of the overall gas turbine process. Fuel gas from the off-gas in H_2 purification step in the sorption-enhanced SMR process, together with supplemental natural gas, were pressurized to 15 atm through a compressor before they are fed to the combustor. The waste N_2 stream from the air distillation process, which consisted of 41% O_2, was fed to the combustor after being compressed to 15 atm. Extra air was provided to the combustor to ensure complete combustion of the fuel gas. The waste N_2 and the additional air streams were preheated by the hot exhaust gas from the gas turbine before they enter the combustor. The combustor operating at 1289°C and 15 atm is simulated as a RGibbs reactor which is based on thermodynamic equilibrium calculations. The compressors and the expander are assumed to be isentropic model with an efficiency index of 0.85.

The complete simulation results are presented in Appendix 3. From these results it is seen that the gas turbine produces a power of 19.7 MW. The compressors for the air feed and the fuel gas feed consume 11 MW and 0.4 MW, respectively. Thus the process produces a net power output of 8.3 MW. The exhaust gas at 602°C is further used in the steam generation process to recover its enthalpy and generate extra power.

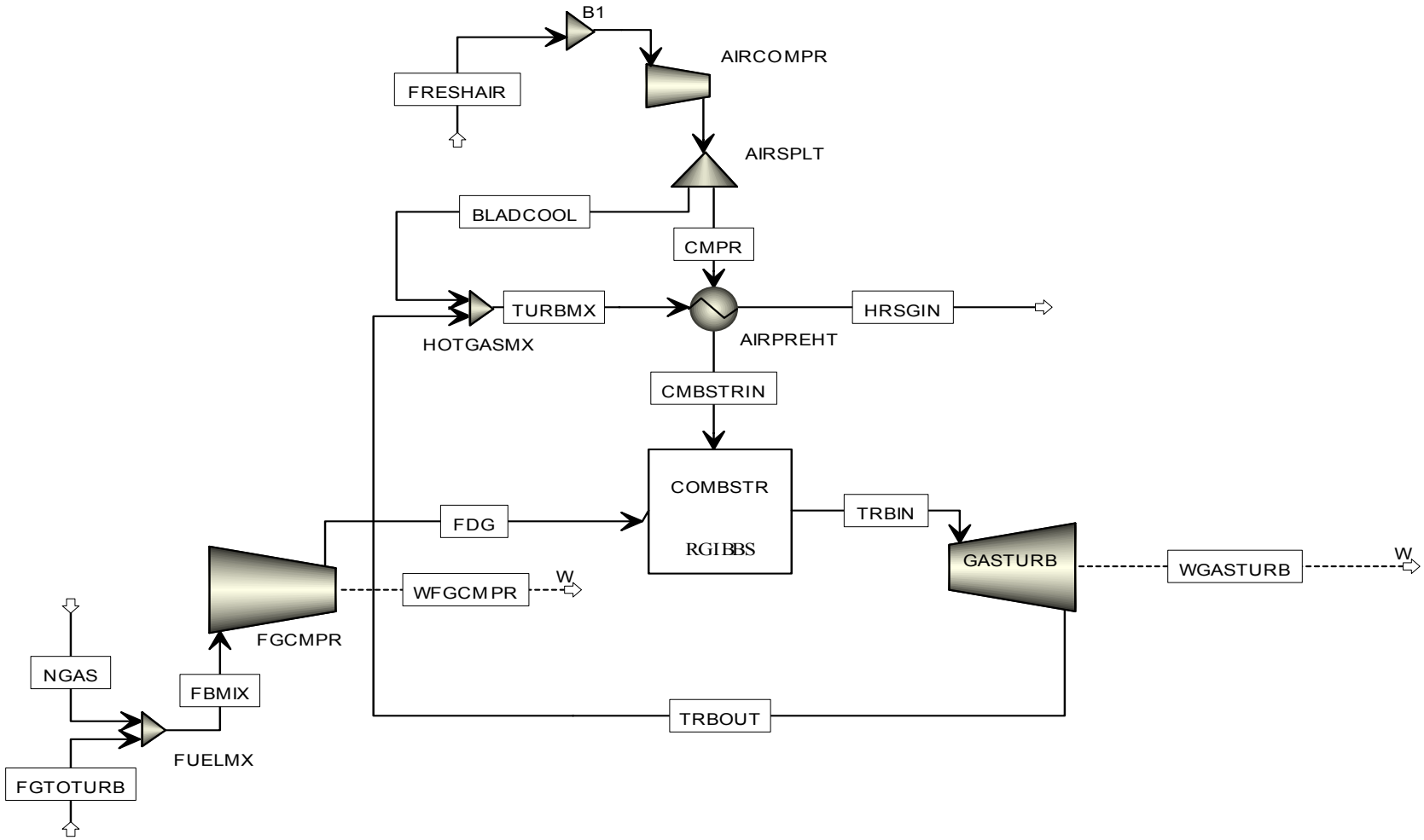

Figure 7-4 Flow Sheet of the Gas Turbine Process

7.5 Heat Recovery Steam Generation Process

The heat recovery steam generation (HRSG) process includes a chain of heat exchangers, three pumps, and three gas turbines. The flow sheet of the HRSG process is shown in Figure 7-5. The exhaust gas from the gas turbine process at high temperature cross exchanges heat with water or steam sequentially in each heat exchanger. The enthalpy recovered in the HRSG process is used primarily to generate steam for H_2 production in the sorption-enhanced SMR process, and secondly to drive the gas turbines to generate extra power for the overall process.

This simulation is based on a water feed of 1000 kmol/hr. The whole process is divided into three stages: low pressure stage at 7.1 atm, intermediate pressure stage at 41.6 atm, and high pressure stage at 104.6 atm. The heat exchangers operating at each pressure level can be further classified into an economizer, a boiler, and a superheater according to its function. An economizer heats up the liquid water feed. A boiler vaporizes the liquid water into steam. A superheater further increases the temperature of the steam. Water or steam cross exchanges heat with hot exhaust gas in each heat exchanger in sequence and their pressure is also increased by pumps to the level of the corresponding steam. The liquid water is first pressurized to 7.1 atm, then enters the low pressure economizer. The exiting liquid water from the low pressure economizer is split into two streams. One stream is completely vaporized in the boiler with part of the steam directly extracted as product, and the remaining steam sent to the low pressure steam turbine after further heating in the low pressure superheater. The other stream of liquid water is further pressurized to 41.6 atm and sent to the intermediate pressure economizer.

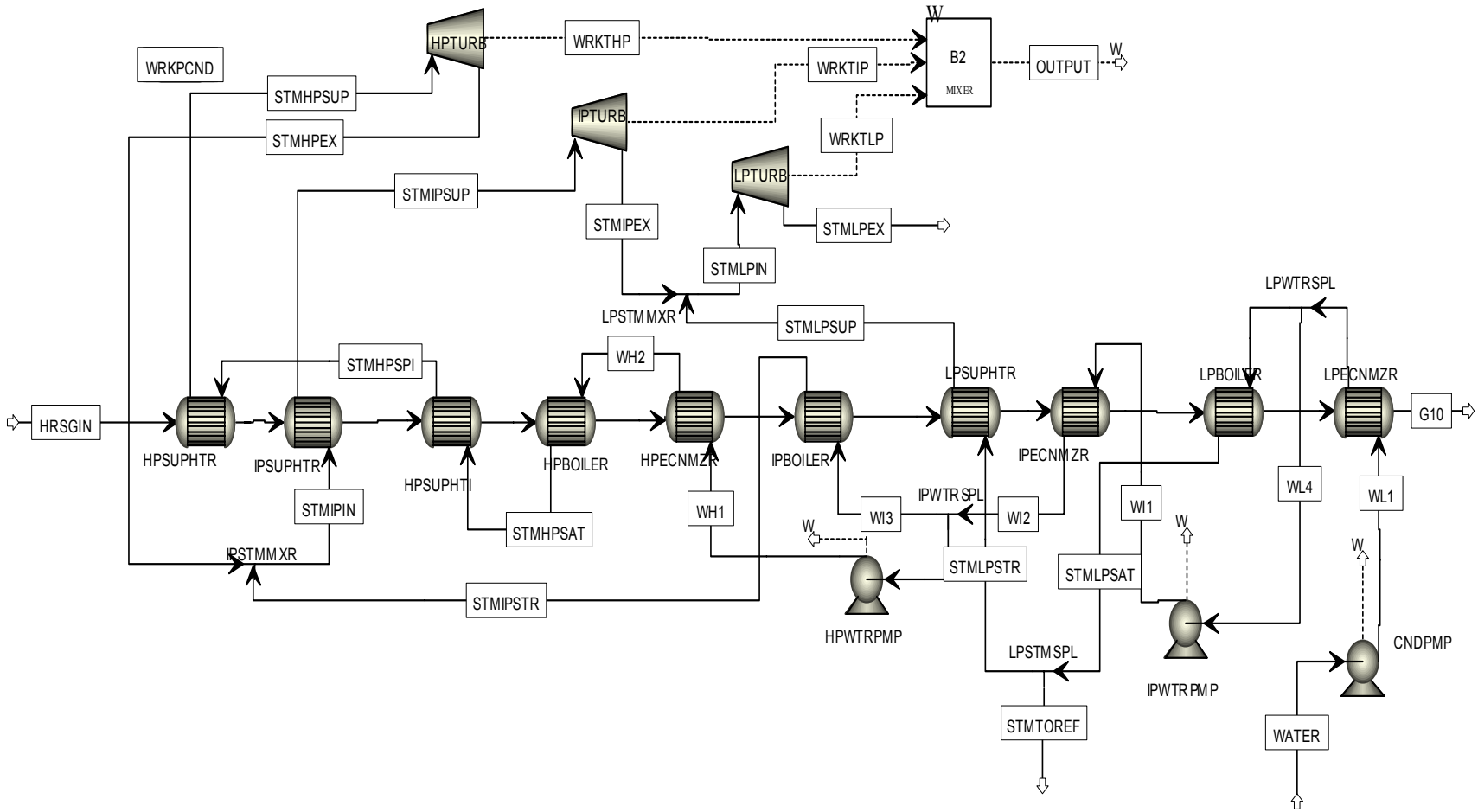

Figure 7-5 Flow Sheet of the Heat Recovery Steam Generation (HRSG) Process

The exiting liquid water at intermediate pressure is split into two streams. One stream is sent to the intermediate pressure steam turbine after being heated in a boiler and a superheater. The other stream is first pressurized to 104.6 atm, then sent to the high pressure steam turbine after being heated in a boiler and two superheaters. The enthalpy in the exhaust steam from the high pressure steam turbine is further recovered by mixing it with the intermediate pressure steam as feed to the intermediate pressure steam turbine. The enthalpy in the exhaust steam from the intermediate pressure steam turbine is recovered in the same way by mixing it with the low pressure steam to be fed to the low pressure steam turbine.

The complete simulation results are presented in Appendix 4. In this simulation, the temperature of the exhaust gas from gas turbine is lowered from 602°C to 100°C with a total of 15.698 MW of enthalpy recovered. Among the recovered enthalpy, 0.376 MW is converted into power by the three steam turbines operating at different pressure levels, and the remaining enthalpy is used to generate steam for H_2 production. 400 kmol/hr of steam at 162.5°C and 6.5 atm is produced which meets the needs of the sorption-enhanced SMR process. The remaining water exits from the low pressure steam turbine at ambient temperature.

7.6 Evaluation of the Overall Process

The detailed simulation of the four parts in the hydrogen and oxygen co-production process is described and discussed above separately.

16.2 ton/day 99+% H_2 and 259 ton/day 99+% O_2 are produced in the overall process. No extra fuel or electricity are directly needed for the generation of steam, which is fed to the steam reforming process for H_2 production.

Table 7-2 gives a complete list of the power balance in the overall process. From this table it is found that a total of 26.1 MW power was generated by all the turbines used in the process, which exceeds the total power consumption of 24.7 MW by the compressors in the process. The whole process is almost balanced on power consumption and generation and no extra power is hence needed for this process.

Table 7-2 Power Balance List of the H_2 and O_2 Co-Production Process

	Power, MW	New Power, MW
H_2 Production		
CH_4 Compressor	-0.158	
Air Compressor	-0.675	
Gas Turbine	+1.535	+0.702
O_2 Production		
Air Compressor	-12.582	
Gas Turbine	+1.082	-11.5
Gas Turbine Process		
Air Compressor	-10.961	
Gas Turbine	+19.727	
Fuel Gas Compressor	-0.371	+8.395
HRSG Process		
Steam Turbines Total	+3.762	
Pumps Total	-0.028	+3.734
Overall Net Power, MW		+1.359

Note: "+" means generation of power, and "-" means consumption of power.

CHAPTER 8

SUMMARY, CONCLUSIONS AND RECOMMENDATIONS

8.1 Summary

The demand for hydrogen has been growing rapidly in recent years. More hydrogen is needed in today's refineries to improve the quality of petroleum products by further processing of heavy hydrocarbons and desulfurization as environmental regulations become more stringent. In the chemical industry, large amounts of hydrogen are consumed in ammonia synthesis. Hydrogen is the basic feedstock of fuel cells, which are a promising future energy source. As fuel cell technologies mature and reach commercial development, hydrogen will be consumed in transportation and power generation sectors. NASA's aerospace program also requires an efficient method for production of liquid hydrogen and oxygen as rocket fuel.

On a commercial scale, steam methane reforming (SMR) is currently the major process for production of hydrogen, and is predicted to maintain its superiority for the next few decades. The conventional SMR process involves multiple steps of steam reforming, water gas shift, and H_2 purification. Among these steps, the reforming reaction occurs at severe conditions of about 800°C~850°C and 20 atm. Large quantities of supplemental fuel must be supplied to the reformer to maintain temperature because the reforming reaction is highly endothermic. A direct fired furnace and expensive alloy tubes are needed for the reformer, which increases the capital and operating costs.

The concept of combining reaction with product separation could provide significant improvement to the conventional SMR process. By adding a CO_2 sorbent to the reforming catalyst, CO_2 can be removed in situ from the reaction gas mixture as it is

formed. The normal thermodynamic equilibrium of the reforming and water gas shift reactions are changed and it is possible to produce high purity hydrogen in a single process step without needing the shift reaction and product purification steps. Sorption-enhanced SMR simplifies the overall SMR process into two steps -reaction and sorbent regeneration-, which has the potential to reduce costs for production of hydrogen. The sorption-enhanced SMR process is almost thermally neutral and does not need supplemental fuel and expensive heat exchangers to provide energy for the reforming reaction. Supplemental energy is needed to regenerate the spent CO_2 sorbent, but a reduction of 20-25% energy consumption has been estimated (Lopez, 2000). Balasubramanian (1998) experimentally proved the feasibility of producing 95+% hydrogen at 650°C and 15 atm in a single step using a fixed-bed reactor system. However, the CO content in the product gas was not examined seriously in that study.

This research examined three aspects of the sorption-enhanced SMR process including: 1) production of H_2 with low CO content using a standard reforming catalyst and a high purity CaO sorbent precursor, 2) evaluation of catalytic activity of innovative catalyst-sorbent samples provided by TDA Research Inc., and 3) a systematic study of the process for simultaneous production of liquid O_2 and H_2 using Aspen simulation software.

The study on the production of low-CO hydrogen was conducted at a lower temperature range (450°C~500°C) at lower pressure (5 atm) than previously studied. Both the content of CO and H_2 purity were emphasized. The effects of temperature, volumetric feed rate, and feed gas composition on the production of H_2 and the content of CO were investigated. In this thesis, the performance of the catalyst-sorbent samples

received from TDA was also extensively studied and evaluated in the fixed-bed reactor and thermogravimetric analyzer (TGA). The effects of temperature, volumetric flow rate, and steam-to-carbon (S/C) ratio on the activity of the catalyst were carefully examined. The material and energy balances for the overall H_2 and O_2 co-production process were evaluated using the Aspen Plus simulator.

8.2 Conclusions

8.2.1 Evaluation of the Catalyst-Sorbent TDA Samples

From the experimental results using the TDA samples, the following major conclusions were reached:

1) The maximum catalytic activity was reached at 800°C for all the catalyst-sorbent samples. At temperatures below 800°C, the catalysts showed decreased activity. At 800°C, the more active catalyst-sorbent samples were capable of driving the reforming reaction to equilibrium when the catalyst was properly activated. Equilibrium was not reached using the less active catalyst-sorbent samples.
2) Space velocity is an important process parameter in the steam reforming reaction. The decrease in the H_2 concentration with increased space velocity in all test results showed that the equilibrium could only be achieved below a certain space velocity.
3) No carbon was deposited at a steam-to-carbon ratio as low as 0.8 at 800°C and 5 atm with a feed gas containing 11.1% CH_4 and N_2 diluent.
4) Platinum is a more efficient catalyst than nickel. Two grams of catalyst containing 0.1 wt% Pt were sufficiently active to drive the reforming reaction to equilibrium, while the same amount of catalyst containing 0.764 wt% NiO did not produce an equilibrium product.

5) Based on turnover ratio analysis, the efficiency of Pt use decreased with increased Pt content in the catalyst. The catalyst sample with the least amount (0.1wt%) of Pt produced the largest turnover ratio. But at equal reaction conditions, the concentration of H_2 in the product increased with increased Pt content in the catalyst.

6) In a single test, TDA sample 415-73Pt proved to be quite durable even at abnormally high reforming temperature. After 25 hours at 900°C, 100°C above the anticipated maximum reaction temperature, the sample maintained its activity very well and no apparent decrease in the concentration of H_2 in the product gas was observed.

7) The sorption capacity of all TDA samples is small due to the small content of free CaO and the amount of sample used in the tests. Multicycle runs in the TGA system with temperature cycling between 900°C and 650°C showed that the calcination reaction is fast and complete in each cycle, while carbonation, or sorption, is slow and incomplete within an approximately 60 min carbonation period. Sorption rate, or sorption activity, decreased gradually in the first cycles and tended to stabilize as the number of cycles increased.

8.2.2 Production of Low-CO Hydrogen

From the experimental results using the standard Ni-based catalyst and high purity $CaCO_3$ sorbent precursor, the following conclusions were reached:

1) The equilibrium for the combined steam-methane-reforming (SMR), water-gas-shift (WGS), and carbonation reactions was closely approached at 5 atm and a S/C ratio of 4.0 over a range of temperatures, flow rates, and gas compositions.

2) Experimental results showed no evidence of $Ca(OH)_2$ formation, although it is favored thermodynamically.

3) By carefully controlling the operating parameters, it is possible to produce 95%+ H_2 and limit the CO content to below 20 ppmv. No extra CO purification step is needed to reduce the CO content to levels required for PEM fuel cells.

8.2.3 Process for Hydrogen and Oxygen Co-production

The following conclusion was reached from the simulation results for the process of hydrogen and oxygen co-production.

1) It is feasible to co-produce high purity hydrogen and oxygen by careful energy integration. Steam needed for the sorption-enhanced SMR phase is produced from the heat recovery steam generation (HRSG) process. The HRSG retrieves heat from the high temperature exhaust gas of the gas turbine process. Fuel needed for CO_2 sorbent regeneration comes from the off-gas in the H_2 purification step in the sorption-enhanced SMR process. Power consumed by all the compressors and electrical utilities are generated by the gas and steam turbines. The overall process is power balanced and no external power supply is required.

8.3 Recommendations

The following work is recommended:

1) The activity of TDA catalyst-sorbent samples should be improved so that reforming equilibrium can be reached at lower temperatures.
2) The sorbent in the TDA samples needs improvement to increase their sorption rate, or sorption activity.
3) Since the high purity $CaCO_3$ used in the experimental work is too expensive for commercial application, a low-cost CO_2 sorbent like dolomite should be examined in

the sorption-enhanced SMR process at the same operating conditions as defined in this research for production of 95+% H_2 with low ppmv CO.

4) If dolomite is found to be successful as a CO_2 sorbent for production of low-CO hydrogen, a fluidized-bed process containing a reactor and a sorbent regenerator should be applied to study the continuous operation.

REFERENCES

Abrardo, J. M. and Khurana, V., "Hydrogen Technologies to meet refiners' future needs", *Hydrocarbon Processing*, P43, February (1995)

Adris, A. M., Elnashaie, S. S. E. H. and Hughes R., "A Fluidized Bed Membrane Reactor for the Steam Reforming of Methane", *Can. J. Chem. Eng*. V69, 1061 (1991)

Adris, A. M., Pruden, B. B., Lim, C. J. and Grace, J. R., "On the reported Attempts to Radically Improve the Performance of the Steam Methane Reforming Reactor", *Can. J. Chem. Eng*. V74, 177 (1996)

Aitani, A. M., "Processed to Enhance Refinery-Hydrogen Production", *Int. J. Hydrogen Energy*, V21 (4), 267 (1996)

Anand, M., Hufton, J.R., Mayorga, S., Nataraj, S., Sircar, S. and Gaffney T. R., "Sorption-Enhanced Reaction Process for Production of Hydrogen", *Proceedings of the 1996 U.S. DOE Hydrogen Program Review*, 1, 537 (1996)

Armor, John N., "The multiple roles of catalysis in the production of H_2", *Applied Catalysis A: General*, V176, 159 (1999)

Balasubramanian, B., "A Single-step Process for Hydrogen Production from Methane", *M.S. Thesis, , Louisiana State University,* (1998)

Borgwardt, Robert H. "Methanol Production from Biomass and Natural Gas as Transportation Fuel", *Ind. Eng. Chem. Res.* V37, 3760 (1998)

Brun-Tsekhovoi, A. R., Zadorin, A. N., Katsobashvili, Ya. R., and Kourdyumov, S. S, "The Process of Catalytic Steam-Reforming of Hydrocarbons in the Presence of Carbon Dioxide Acceptor", *Hydrogen Energy Process VII, Proc. World Hydrogen Energy Conf.*, V2, New York (1986)

Carvill, B. T., Hufton, J. R., Anand, M. and Sircar, S., "Sorption-Enhanced Reaction Process", *AIChE J*., V42 (10), 2765 (1996)

Cole, Jerald A. and Lyon, Richard K.. "Thermally limited selective oxidation methods and apparatus", *U.S. Patent No. 6,475,454* (2002)

Edmonds, Jae, "Hydrogen and Climate", Hydrogen Vision Meeting, Park Hyatt Washington, Washington DC (2001)

Gaudernack, B. and Lynum, S. "Hydrogen from natural gas without release of CO_2 to the atmosphere." *Int. J. Hydrogen Energy*, V23, 1087 (1998)

Han, C. and Harrison, D.P., "Simultaneous Shift and Carbon Dioxide Separation for the Direct Production of Hydrogen", *Chem. Engng. Sci.*, V49, 5875 (1994)

Hufton, J. R., Mayorga, S., Gaffney, T. R., Nataraj, S., Rao, M. B. and Sircar, S., "Sorption-Enhanced Reaction Process for Production of Hydrogen", *Proceedings of the 1998 U.S. DOE Hydrogen Program Review*, 2, 693 (1998)

Hufton, J. R., Mayorga, S. and Sircar, S., "Sorption-Enhanced Reaction Process for Hydrogen Production", *AIChE J.* V45 (2), 248 (1999)

Itoh, N., "A Membrane Reactor Using Palladium", *AIChE J.*, V33, 1576 (1987)

Jin, Hongguang, Okamoto, Toshihiro and Ishida, Masaru, "Development of a Novel Chemical-Looping Combustion: Synthesis of a Looping Material with a Double Metal Oxide of CoO-NiO", *Energy & Fuels*, V12, 1272 (1998)

Kim, Jun-Hun, Choi, Byung-Seok and Yi, Jongheop, "Modified Simulation of Methane Steam Reforming in Pd-Membrane Packed-Bed Type Reactor", *Journal of Chemical Engineering of Japan*, V32 (6), 760 (1999)

Kirk-Othmer, "Concise Encyclopedia of Chemical Technology", 4th Edition, March 1999, Wiley, New York, V12, 950 (1999)

Kumar, Ravi V., Cole, Jerald A. and Lyon, Richard K., "Unmixed reforming: an advanced steam reforming process" *Preprints of Symposia - American Chemical Society, Division of Fuel Chemistry* V44 (4), 894 (1999)

Lanz, Andre, "Hydrogen Fuel Cell Engines and Related Technologies", Palm Desert, CA, 2001

Lyon, Richard K., Clark, Wyman, Schmidt, Darren D. and Hutton, Phillip N. "The use of unmixed combustion to convert biomass to fuel cell hydrogen", *Chemical and Physical Processes in Combustion*, 53 (2001)

Lyon, Richard. K., Garthier, Phillippe J. and Cole, Jerald A. "Unmixed combustion: an alternative to fire" *Chemical and Physical Processes in Combustion*, 149 (1999)

Lyon, Richard K. and Cole, Jerald A. "Unmixed Combustion: An Alternative to Fire", *Combustion and Flame*, V121, 249 (2000)

Lopez, Ortiz A. "Sorption Enhanced Process for the Production of Hydrogen", *Ph.D Dissertation, Louisiana State University*, (2000)

Madia, Giuseppe S., Barbieri, Giuseppe and Drioli, Enrico, "Theoretical and Experimental Analysis of Methane Steam Reforming in a Membrane Reactor", *Can. J. Chem. Eng*. V77, 698 (1999)

Mayorga, S. G., Hufton, J. R., Sircar, S. and Gaffney, T. R., "Sorption Enhanced Reaction Process for Production of Hydrogen", Air Products and Chemicals, Inc. (1997)

Meyer, Steinberg and Cheng, Hsing C., "Modern and Prospective Technologies for Hydrogen Production from Fossil Fuels", *Int. J. Hydrogen Energy*, V14, 797 (1989)

Nagamoto, H. and Inoue, H., "A Reactor with Catalytic Membrane Permeated by Hydrogen", *Chem. Eng. Commun.*, V34, 315 (1985)

Spath, Pamela L. and Mann, Margaret K., "Life Cycle Assessment of Hydrogen Production via Natural Gas Steam Reforming", National Renewable Energy Laboratory, Golden, CO, NREL/TP-570-27637 (2001)

Roine, A., HSC 4.0 User's Manual (1999)

Roy, S., Cox, B. G., Adris, A. M. and Pruden, B. B., "Economics and Simulation of Fluidized Bed Membrane Reforming", *Int. J. Hydrogen Energy*, V23 (9), 745 (1998)

Scholz, W. H., "Processes for industrial production of hydrogen and associated environmental effects." *Gas Separation & Purification*, V7 (3), 131 (1993)

Shah, Naresh, Panjala, Devadas and Huffman, Gerald P. "Hydrogen Production by Catalytic Decomposition of Methane." *Energy & Fuels*, V15 (6), 1528 (2001),

Sircar, S. and Kratz, W. C., "Simultaneous Production of Hydrogen and Carbon Dioxide from Steam Reformer Off-Gas by Pressure Swing Adsorption", *Sep. Sci. and Tech.*, V23, 2397 (1988)

Sircar, S. and Golden, T.C., "Purification of Hydrogen by Pressure Swing Adsorption", *Sep. Sci. and Tech.*, V35 (5), 667 (2000)

Towler, Gavin P., Doshi, Kishore J., Vanden, Bussche Kurt M. and Senetar, John J., "Process for Providing a Pure Hydrogen Stream for Use with Fuel Cells", *U.S. Patent No. 6,299,994* (2001)

Waldron, W.E., Hufton, J.R. and Sircar, S.; "Production of Hydrogen by Cyclic Sorption Enhanced Reaction Process", *AIChE J.*, V47 (6), 1477 (2001)

US Department of Energy, "A National Vision of America's Transition to a Hydrogen Economy—To 2030 and Beyong", (2002)

APPENDIX: ASPEN SIMULATION RESULTS

	2	3	AIR	AIR-1	CH4	CH4-2	CH4-3	EX-H2O	FG2REGEN	FG2TURB	FRESHM	FRESHSBT	FUEL-GAS
Mole Flow, kmol/hr													
CH4	8.78	100.00	0.00	0.00	100.00	100.00	100.00	0.00	4.82	3.95	0.00	0.00	8.77
H2O	223.56	0.00	0.00	0.00	0.00	0.00	0.00	220.43	1.72	1.41	24.19	0.00	3.12
CO	2.16E-03	0	0	0	0	0	0	0	1.19E-03	9.70E-04	0	0	2.15E-03
CO2	7.95E-03	0	0	0	0	0	0	0	4.37E-03	3.58E-03	96.04	0	7.94E-03
H2	358.89	0.00	0.00	0.00	0.00	0.00	0.00	0.00	12.83	10.50	0.00	0.00	23.33
O2	0.00	0.00	75.51	75.51	0.00	0.00	0.00	0.00	0.00	0.00	56.45	0.00	0.00
N2	0.00	0.00	324.49	324.49	0.00	0.00	0.00	0.00	0.00	0.00	324.49	0.00	0.00
Total Flow, kmol/hr	591.23	100.00	400.00	400.00	100.00	100.00	100.00	220.43	19.38	15.85	501.17	0.00	35.23
Temperature, K	623.15	439.38	298.15	500.29	298.15	521.15	823.15	303.15	303.15	303.15	1173.15		303.15
Pressure, atm	5	5	1	5	1	5	5	5	5	5	5		5
Vapor Frac	1.00	1.00	1.00	1.00	1.00	1.00	1.00	0.00	0.92	0.92	1.00		0.92
Liquid Frac	0.00	0.00	0.00	0.00	0.00	0.00	0.00	1.00	0.08	0.08	0.00		0.08
Solid Frac	0	0	0	0	0	0	0	0	0	0	0		0
Enthalpy, cal/sec	-3228500	-459960	-177	157883	-496860	-435030	-322310	-4174600	-56464	-46198	-1874000		-102660
Substream: $TOTAL													
Total Flow, kg/hr	4892.11	1604.28	11506.34	11506.34	1604.28	1604.28	1604.28	3971.07	134.41	109.98	28092.56	12533.53	244.39
Enthalpy, cal/sec	-3228500	-459960	-177	157883	-496860	-435030	-322310	-4174600	-56464	-46198	-12061000	-10187000	-102660
Substream: CISOLID													
Mole Flow, kmol/hr													
CAO	0	0	0	0	0	0	0	0	0	0	99.99685	99.99685	0
CACO3	0	0	0	0	0	0	0	0	0	0	3.15E-03	3.15E-03	0
MGO	0	0	0	0	0	0	0	0	0	0	100	100	0
NI	0	0	0	0	0	0	0	0	0	0	0	0	0
NIO	0	0	0	0	0	0	0	0	0	0	6	6	0
ALUMI-01	0	0	0	0	0	0	0	0	0	0	24	24	0
Total Flow, kmol/hr	0	0	0	0	0	0	0	0	0	0	230	230	0
Temperature, K											1173.15	1173.15	
Pressure, atm	5	5	1	5	1	5	5		5	5	5	5	5
Vapor Frac											0	0	
Liquid Frac											0	0	
Solid Frac											1	1	
Enthalpy, cal/sec											-1.02E+07	-1.02E+07	

Appendix 1 Simulation Results of the Sorption-Enhanced SMR Process

	H2	PROD	PROD-1	R-IN	R-OUT	SSBT	STACK	STACK-1	STACK-2	STACK-3	STEAM	STEAM1
Mole Flow, kmol/hr												
CH4	0.01	8.78	8.78	100.00	8.78	0.00	0.00	0.00	0.00	0.00	0.00	0.00
H2O	0.00	223.56	3.13	400.00	223.56	0.00	24.19	24.19	24.19	24.19	400.00	400.00
CO	2.16E-06	2.16E-03	2.16E-03	0	2.16E-03	0	0	0	0	0	0	0
CO2	7.95E-06	7.95E-03	7.95E-03	0	7.95E-03	0	96.04	96.04	96.04	96.04	0	0
H2	335.56	358.89	358.89	0.00	358.89	0.00	0.00	0.00	0.00	0.00	0.00	0.00
O2	0.00	0.00	0.00	0.00	0.00	0.00	56.45	56.45	56.45	56.45	0.00	0.00
N2	0.00	0.00	0.00	0.00	0.00	0.00	324.49	324.49	324.49	324.49	0.00	0.00
Total Flow, kmol/hr	335.58	591.23	370.81	500.00	591.23	0.00	501.17	501.17	501.17	501.17	400.00	400.00
Temperature, K	303.15	753.15	303.15	866.53	753.15		1173.15	874.75	780.94	759.89	433.15	607.86
Pressure, atm	5	5	5	5	5		5	1	1	1	5	5
Vapor Frac	1.00	1.00	1.00	1.00	1.00		1.00	1.00	1.00	1.00	1.00	1.00
Liquid Frac	0.00	0.00	0.00	0.00	0.00		0.00	0.00	0.00	0.00	0.00	0.00
Solid Frac	0	0	3.04E-18	0	0		0	0	0	0	0	0
Enthalpy, cal/sec	3248	-3060700	-92911	-6176500	-3060700		-1874000	-2248000	-2360800	-2385700	-6303600	-6135900
Substream: $TOTAL												
Total Flow, kg/hr	676.65	4892.11	921.04	21343.91	21343.91	16451.81	15559.03	15559.03	15559.03	15559.03	7206.11	7206.11
Enthalpy, cal/sec	3248	-3060700	-92911	-16645000	-16848000	-13787000	-1874000	-2248000	-2360800	-2385700	-6303600	-6135900
Substream: CISOLID												
Mole Flow, kmol/hr												
CAO	0	0	0	100.00	8.78	8.78	0	0	0	0	0	0
CACO3	0	0	0	3.15E-03	91.22	91.22	0	0	0	0	0	0
MGO	0	0	0	100	100	100	0	0	0	0	0	0
NI	0	0	0	0	6	6	0	0	0	0	0	0
NIO	0	0	0	6	0	0	0	0	0	0	0	0
ALUMI-01	0	0	0	24	24	24	0	0	0	0	0	0
Total Flow, kmol/hr	0	0	0	230	230	230	0	0	0	0	0	0
Temperature, K				866.53	753.15	753.15						
Pressure, atm	5		5	5	5	5		1	1	1	5	5
Vapor Frac				0	0	0						
Liquid Frac				0	0	0						
Solid Frac				1	1	1						
Enthalpy, cal/sec				-1.05E+07	-1.38E+07	-1.38E+07						

Appendix 1 Simulation Results of the Sorption-Enhanced SMR Process (Continued)

	2	3	4	5	6	7	8	9	11	12	13	14	15	16	17	18	22	23	AIR	AIRFEED	N2PROD	N2WASTE	O2PROD
Substream: MIXED																							
Mole Flow kmol/sec																							
N2	0.58	0.39	0.39	0.58	0.16	0.16	0.03	0.58	0.09	0.03	0.03	0.09	0.09	0.09	0.54	0.54	0.09	0.09	0.58	0.39	0.54	0.03	0.00
O2	0.15	0.10	0.10	0.15	0.04	0.04	0.01	0.15	0.00	0.02	0.02	0.04	0.04	0.04	0.05	0.05	0.00	0.00	0.15	0.10	0.05	0.02	0.08
H2O	0	0	0	0	0	0	0	0	0	0	0	0	0	0	0	0	0	0	0	0	0	0	0
Total Flow, kmol/sec	0.73	0.50	0.50	0.73	0.20	0.20	0.03	0.73	0.09	0.06	0.06	0.14	0.14	0.14	0.59	0.59	0.09	0.09	0.73	0.50	0.59	0.06	0.09
Total Flow, tons/day	2000	1366	1366	2000	540	540	94	2000	247.89	160.00	160.00	386.11	386.11	386.11	1581.04	1581.04	247.89	247.89	2000.00	1366	1581.04	160.00	258.95
Total Flow, cum/sec	0.20	0.14	0.16	1.72	0.05	0.02	0.01	0.60	0.00	0.00	1.08	0.00	0.00	0.03	6.42	7.82	0.03	0.00	18.10	4.39	26.34	2.40	0.00
Temperature,C	-133.15	-133.15	-122.62	583.13	-133.15	-146.19	-133.15	30	-197.15	-197.25	-138.15	-196.15	-176.11	-197.76	-198.72	-183.39	-200.02	-178.84	30	-196.32	25	25	-187.02
Pressure, atm	30	30	30	30	30	30	30	30	4.90	0.58	0.58	4.97	4.97	0.59	0.54	0.54	0.55	4.90	1	0.60	0.54	0.58	0.64
Vapor Frac	1	1	1	1	1	0.36	1	1	0	0	1	0	0	0.02	1	1	0.03	0	1	0.86	1	1	0
Liquid Frac	0	0	0	0	0	0.64	0	0	1	1	0	1	1	0.98	0	0	0.97	1	0	0.14	0	0	1
Enthalpy, Watt	-4.12E+06	-2.81E+06	-2.57E+06	1.24E+07	-1.11E+06	-1.57E+06	-1.93E+05	-29398.37	-1.14E+06	-7.29E+05	-2.70E+05	-1.75E+06	-1.59E+06	-1.75E+06	-3.84E+06	-3.57E+06	-1.14E+06	-1.03E+06	1.01E+05	-3.67E+06	-2061.84	-233.85	-1.13E+06

Appendix 2 Simulation Results of the Cryogenic Air Distillation Process

	1	3	AIRDIST	BLADCOOL	CMBSTRIN	CMPR	FBMIX	FDG	FGTOTURB	FRESHAIR	HRSGIN	NGAS	TRBIN	TRBOUT	TURBMX
Temperature C	431.4	30	30	431.4	500	431.4	16.4	274.8	30	30	601.8	30	1289	666.8	662.6
Pressure, atm	15.199	1.013	1.013	15.199	15.199	15.199	1.013	15.199	5.066	1.013	1.013	1.013	15.199	1.013	1.013
Vapor Frac	1	1	1	1	1	1	1	1	0.918	1	1	1	1	1	1
Mass Flow, tonne/hr	92.598	92.598	6.047	1.852	90.746	90.746	1.858	1.858	0.11	86.551	94.456	1.748	92.604	92.604	94.456
Enthalpy, MMkcal/hr	9.342	0.106	0.007	0.187	10.782	9.155	-2.1	-1.788	-0.165	0.099	-9.953	-1.935	8.794	-8.514	-8.327
Mass Flow, ton/hr															
N2	69.748	69.748	3.356	1.395	68.353	68.353	0	0	0	66.392	69.748	0	68.353	68.353	69.748
O2	22.85	22.85	2.691	0.457	22.393	22.393	0	0	0	20.159	15.456	0	14.999	14.999	15.456
CH4	0	0	0	0	0	0	1.811	1.811	0.063	0	0	1.748	0	0	0
CO	0	0	0	0	0	0	0	0	0	0	0	0	0	0	0
CO2	0	0	0	0	0	0	0	0	0	0	4.969	0	4.969	4.969	4.969
H2	0	0	0	0	0	0	0.021	0.021	0.021	0	0	0	0	0	0
H2O	0	0	0	0	0	0	0.025	0.025	0.025	0	4.283	0	4.283	4.283	4.283
Mole Flow, kmol/hr															
N2	2489.8	2489.8	119.8	49.796	2440.004	2440.004	0	0	0	2370	2489.8	0	2440.004	2440.004	2489.8
O2	714.1	714.1	84.1	14.282	699.818	699.818	0	0	0	630	483.031	0	468.749	468.749	483.031
CH4	0	0	0	0	0	0	112.91	112.91	3.946	0	0	108.964	0	0	0
CO	0	0	0	0	0	0	0	0	0	0	0.001	0	0.001	0.001	0.001
CO2	0	0	0	0	0	0	0	0	0	0	112.909	0	112.909	112.909	112.909
H2	0	0	0	0	0	0	10.498	10.498	10.498	0	0.001	0	0.001	0.001	0.001
H2O	0	0	0	0	0	0	1.406	1.406	1.406	0	237.724	0	237.724	237.724	237.724
	WFGCMPR	AIRCOMPR	WGASTURB												
WORK, kw	370.78	10961.18	-19726.85												

Appendix 3 Simulation Results of the Gas Turbine Process

	G01	G02	G03	G04	G05	G06	G07	G08	G09	G10	HRSGIN	STMHPEX	STMHPSAT	STMHPSPI	STMHPSUP	STMIPEX	STMIPIN	STMIPSTR
Temperature, °C	593.2	558.6	526.9	456.4	438.7	410.1	397.9	368.7	165.2	100	601.8	395.7	313.9	475.6	537.8	307.9	357.2	251.9
Pressure, atm	1.013	1.013	1.013	1.013	1.013	1.013	1.013	1.013	1.013	1.013	1.013	40.7	104	103.7	103.4	6.2	40.7	41
Vapor Frac	1	1	1	1	1	1	1	1	1	0.977	1	1	1	1	1	1	1	1
Mole Flow, kmol/hr	3323	3323	3323	3323	3323	3323	3323	3323	3323	3323	3323	330	330	330	330	430	430	100
Mass Flow, kg/hr	94456	94456	94456	94456	94456	94456	94456	94456	94456	94456	94456	5942	5942	5942	5942	7747	7747	1805
Enthalpy, MMkcal/hr	-10.194	-11.11	-11.944	-13.777	-14.232	-14.966	-15.278	-16.018	-21.089	-23.472	-9.965	-18.12	-18.808	-17.974	-17.744	-23.855	-23.798	-5.678
Mole Flow, kmol/hr																		
H_2O	237.7	237.7	237.7	237.7	237.7	237.7	237.7	237.7	237.7	237.7	237.7	329.8	329.8	329.8	329.8	430.0	430.0	100.2
N_2	2489.8	2489.8	2489.8	2489.8	2489.8	2489.8	2489.8	2489.8	2489.8	2489.8	2489.8	0.0	0.0	0.0	0.0	0.0	0.0	0.0
O_2	483.0	483.0	483.0	483.0	483.0	483.0	483.0	483.0	483.0	483.0	483.0	0.0	0.0	0.0	0.0	0.0	0.0	0.0
CO_2	112.9	112.9	112.9	112.9	112.9	112.9	112.9	112.9	112.9	112.9	112.9	0.0	0.0	0.0	0.0	0.0	0.0	0.0
	STMIPSUP	STMLPEX	STMLPIN	STMLPSAT	STMLPSTR	STMLPSUP	STMTOREF	WATER	WH1	WH2	WI1	WI2	WI3	WI4	WL1	WL2	WL3	WL4
Temperature, °C	569.2	32.9	322.7	162	162	360.1	162	32.9	254.2	314.1	164.3	252.3	252.3	252.3	32.9	163.8	163.8	163.8
Pressure, atm	40.4	0.05	6.2	6.5	6.5	6.2	6.5	0.05	104.6	104.3	41.6	41.3	41.3	41.3	7.1	6.8	6.8	6.8
Vapor Frac	1	0.914	1	1	1	1	1	0	0	0	0	0	0	0	0	0	0	0
Mole Flow, kmol/hr	430	600	600	570	170	170	400	1000	330	330	430	430	100	330	1000	1000	570	430
Mass Flow, kg/hr	7747	10809	10809	10269	3063	3063	7206	18015	5942	5942	7747	7747	1805	5942	18015	18015	10269	7747
Enthalpy, MMkcal/hr	-22.882	-35.159	-33.207	-32.4	-9.663	-9.352	-22.737	-68.126	-21.095	-20.641	-28.26	-27.52	-6.412	-21.108	-68.123	-65.74	-37.472	-28.268
Mole Flow, kmol/hr																		
H_2O	430.0	600.0	600.0	570.0	170.0	170.0	400.0	1000.0	329.8	329.8	430.0	430.0	100.2	329.8	1000.0	1000.0	570.0	430.0
N_2	0.0	0.0	0.0	0.0	0.0	0.0	0.0	0.0	0.0	0.0	0.0	0.0	0.0	0.0	0.0	0.0	0.0	0.0
O_2	0.0	0.0	0.0	0.0	0.0	0.0	0.0	0.0	0.0	0.0	0.0	0.0	0.0	0.0	0.0	0.0	0.0	0.0
CO_2	0.0	0.0	0.0	0.0	0.0	0.0	0.0	0.0	0.0	0.0	0.0	0.0	0.0	0.0	0.0	0.0	0.0	0.0
	OUTPUT	WRKPCND	WRKPHP	WRKPIP	WRKTHP	WRKTIP	WRKTLP											
POWER, kW	-3762.3	4.0	14.9	9.4	-428.1	-1109.4	-2224.8											

Appendix 4 Simulation Results of the Heat Recovery Steam Generation Process

VITA

The author was born in Tianjin, China, in 1972. He obtained the degree of Bachelor of Engineering from Tianjin University in 1995. He came to the United States in 2000 to study at Louisiana State University. He will receive the degree of Master of Science in Chemical Engineering at the 2003 December commencement.